IDENTIFICATION OF DRUG COMBINATIONS EXHIBITING SYNERGISTIC LETHALITY IN PEDIATRIC HIGH-GRADE GLIOMA PDOX CELL LINES

A Dissertation

by

CAN LI

Submitted to the Office of Graduate and Professional Studies of
Texas A&M University
in partial fulfillment of the requirements for the degree of

DOCTOR OF PHILOSOPHY

Chair of Committee,	Peter Davies
Committee Members,	Xianan Li
	Clifford Stephan
	Yun Huang
	Guang Peng
Head of Department,	Carol Vargas

December 2019

Major Subject: Medical Sciences

ABSTRACT

Pediatric high-grade glioma (pHGG) accounts for 3-15% of all primary pediatric central nervous system tumors and is the most aggressive pediatric brain tumor. The standard therapy for pHGG includes maximal safe tumor resection followed by radiation therapy and intensive chemotherapy using oral temozolomide (TMZ). Despite aggressive therapy, the prognosis is still poor and the five-year survival rate is dismal (< 5%). Thus, there is an urgent need to identify effective and efficient combination therapies for treatment of pHGG.

The objective of this study is to develop an unbiased, target-based approach to the discovery of novel combination therapies for pHGG. We are using pHGG cell lines from patient-derived orthotopic xenografts (PDOX) growing both as 3D neurospheres and 2D monolayers. The neurospheres are thought to represent predominantly cancer-based stem cells. For drug screening, we use 2-step strategy, first carrying out a single agent screen with a library of cancer-related therapeutics. We use the single agent screen to identify classes of pharmacologic agents with growth inhibitory/cytotoxic activity against the PDOX pHGG cells. Combinations of prototypic agents from the major classes of active drugs are then tested for synergistic activity in the second stage of combinatorial screening studies. The first stage single agent screening studies, carried out with 1863 well-characterized cancer therapeutics, identified several classes of active compounds including HDAC inhibitors, proteasome inhibitors, HSP90 inhibitors, PI3K/mTOR/Akt inhibitors and cell cycle inhibitors as the most active classes. We selected a minimum of 2 representatives of each of these classes for combinatorial screens and discovered that combinations of proteasome inhibitors (CEP-18770, MLN 2238) and HDAC inhibitors (Panobinostat, JNJ-26481585) and also a Wee1 inhibitor (MK-1775) and combined Chk1 inhibitors (AZD7762, MK-8776) exhibited the greatest synergistic lethality activity. Both of

these sets of combinations exhibited selective activity, inhibiting the viability of pHGG cells much more than normal astrocytes. Because of their profound synergistic activity and their targeted molecular activity, we focused subsequent mechanistic studies on the combination of Wee1 and Chk1 inhibitors. In pHGG cells, the combination of these two classes of drugs not only selectively suppressed cell growth in the pHGG tumor cells, but it also promoted genomic instability, induced the G2/M cell cycle arrest, slowed down the speed of DNA replication during DNA replication and caused mitotic catastrophe. These effects were selective for pHGG tumor cells and were not detected in normal astrocyte cells. In addition, Wee1 and Chk1 inhibitors had a selective effect on the down-regulation ATP production from mitochondrial respiration in tumor cells but not in astrocytes. In conclusion, these studies have identified the combination of Wee1 and Chk1 inhibitors as selective inducers of lethality in pediatric high-grade glioma cells by a mechanism that includes their combined effects on metabolic inhibition and the induction of mitotic catastrophe.

DEDICATION

I would like to dedicate this dissertation to my parents, husband and my kids whose unyielding love, support and encouragement have enriched my soul and inspired me to pursue and complete this research.

ACKNOWLEDGEMENTS

This will be a long list of acknowledgements. There are a lot of people whose help and support I would like to acknowledge. Over the course of my graduate training, I received help, kindness, care and encouragement from many people. Without this support, I would never been able to make this all happen.

I would like to begin by thanking my mentor, Dr. Peter Davies, as he has been instrumental in guiding my graduate development. Dr. Davies has provided me with constant support and guidance while allowing me the independence that is needed for me to become a successful researcher. He has always been nice, kind, patient and encouraging. He is not only an amazing advisor but has also served as a life coach for me. We have had many wonderful conversations not only about science but also about life. He has cared not only about how much data I produced but also whether I was receiving good graduate training. At every meeting he not only asked me about my project but also about how my life was going and he gave me valuable advice at those times when I was experiencing difficulties. I really appreciate his support and confidence in me.

I would also like to thank my committee members for advising me throughout my graduate training. Dr. Xiao-Nan Li, thank you for permitting me to join your PHGG PDOX project. You not only introduced me this amazing tumor model but also provided me with insightful discussions of my results and their implications during our meetings. Dr. Cliff Stephan, thank you for letting me join your lab. I have always greatly appreciated your kind and patient advice, your friendly smiles in the hallway and your great comments during the lab meetings. You always provided encouraging comments when I finish my presentations that helped to guide me in the right direction. Dr. Yun Huang, thank you so much for serving as a

member of my Advisory Committee. You have provided me with a role model not only for my career development as a woman scientist but also in my life. Dr. Huang has showed me that as women scientist it is possible to balance work and personal life. She has also helped me to learn about experimental design and trouble shooting and her questions during my committee meetings helped me to think of my project as a whole rather than an assembly of bits and pieces. Her comments helped me focus on the future application of my project to clinic research. I want to thank Dr. Guang Peng for her guidance in the direction of my project. Her great expertise has been very valuable for the design and interpretation of the mechanistic studies and, at the same time, we have become good friends. I look forward to future collaboration and friendship based on our similar backgrounds, similar research interests and similar experiences.

I want to extend a special thanks to all my friends at the IBT, my time at the IBT would be totally not the same without my amazing group of friends and colleagues.

CONTRIBUTORS AND FUNDING SOURCES

Contributors

This work was supervised by a dissertation committee consisting of Professor Peter Davies (advisor) from the Center for Translational Cancer Research in Texas A&M Institute of Biosciences and Technology, Professor Xiao-Nan Li (co-advisor) from Ann & Robert H. Lurie Children's Hospital of Chicago in Northwestern University Feinberg School of Medicine, Professor Clifford Stephan from the Center for Translational Cancer Research in Texas A&M Institute of Biosciences and Technology, Professor Yun Huang from the Center for Epigenetics & Disease Prevention in Texas A&M Institute of Biosciences and Technology, Professor Guang Peng from Department of Clinical Cancer Prevention in The University of Texas MD Anderson Cancer Center.

The patient-derived orthotopic xenograft cell lines were provided by Dr. Lin Qi and Dr. Yuchen Du from Dr. Xiao-Nan Li's lab. The development of Pharmacological Relationship Trees in Chapter II was conducted by Dr. Reid Powell of from Center for Translational Cancer Research in Texas A&M Institute of Biosciences and Technology. The statistical analyses for cytotoxic activities in single agent screen in Chapter II were conducted by Dr. David Brunell.

Funding Sources

This work was supported by the CPRIT grant (23-465094-00001, Developing New Combinatory Therapies for Pediatric High-Grade Glioma).

NOMENCLATURE

AUC	Area Under Curve
BBB	Blood-Brian-Barrier
CCR5	CC-chemokine receptor 5
CNS	Central Nervous System
CSC	Cancer Stem Cells
CTG	CellTiter-Glo
ECAR	Extracellular Acidification Rate
EGFR	Epithelial Growth Factor Receptor
ER	Endoplasmic reticulum
FBS	Fetal bovine serum
FDA	US Food and Drug Administration
GBM	Glioblastoma Multiforme
HER-2	Human Epidermal Growth Factor Receptor 2
HTS	High-Throughput Screen
IDH	Isocitrate Dehydrogenase
MB	Medulloblastoma
MGMT	O-6-Methylguanine-DNA Methyltransferase
NOD	Nonbese Diabetic
NSCLC	Non-Small Cell Lung Cancer
NSG	NOD DCID gamma
OCR	Oxygen Consumption Rate
PER	Proton Efflux Rate

PFA	Paraformaldehyde
pHGG	Pediatric High-Grade Glioma
PDOX	Patient-derived Orthotopic Xenograft
ROS	Reactive Oxygen Species
RPA	Replication Protein A
RT	Radiotherapy
SAR	Structure-activity Relationship
SCID	Severely Compromised Immune Deficient
TMZ	Temozolomide
VEGF	Vascular Endothelial Growth Factor

TABLE OF CONTENTS

Page

ABSTRACT ii

DEDICATION iv

ACKNOWLEDGEMENTS v

CONTRIBUTORS AND FUNDING SOURCES vii

NOMENCLATURE viii

LIST OF FIGURES xiii

LIST OF TABLES xv

CHAPTER I INTRODUCTION 1

- Pediatric High-Grade Gliomas 1
  - Molecular Biology 1
  - Strategies of Therapy 3
  - Challenges of Chemotherapy in pHGG 4
  - New Strategies for the Treatment of Pediatric Brain Tumors 5
  - Conclusion 6
- Use of Patient-Derived Orthotopic Xenograft Model System for Oncology Drug Discovery 6
  - The Process of Generating PDOX Models 6
  - Application of PDOX Models for Cancer Research 8
  - The Limitations of PDOX Models 10
  - Conclusion 11
- High Throughput Screening for Accelerating the Drug Discovery 11
  - Examples of the Use of HTS in Drug Discovery 12
  - Other Benefits of HTS 13
  - Conclusion 13
- Targeted Cancer Therapies 14
- Rationale for this Dissertation 17

CHAPTER II DISCOVERY OF DRUG COMBINATIONS THAT EXHIBIT SYNERGISTIC LETHALITY ACTIVITY AGAINST PEDIATRIC HGG TUMOR CELLS 20

- Materials and Methods 20
  - Reagents/Solutions 20

Page

Patient-Derived Xenografts Models and Tumor Cells Preparation 20
Tumor Cell and Normal Cell Culture 21
Cell Staining and Imaging 22
Cell Viability and Proliferation Assay 22
Drug Selection 23
Single-Agent High-Throughput Drug Screening 24
Mechanism Annotated Pharmacological Tree 26
High-Throughput Drug Combination Screening 29
Cytotoxicity Screening 32
Statistical Analyses 33
Results 33
PDOX Model and High Throughput Screen 33
High Throughput Screen for Small Molecules that Inhibit the Growth and/or Survival of pHGG Tumor Cell Lines 37
Reproducibility of High Throughput Single-Agent Screens 39
Identification of Drug Combinations Exhibiting Synergistic Effect in Killing pHGG Tumor Cell lines 42
Cytotoxicity of Drug Combinatorial Pairs in Normal Astrocyte Cell line 48
Discussion 49

CHAPTER III WEE1 AND CHK1 ANTAGONISTS COOPERATE TO INDUCE SYNERGISTIC LETHALITY IN PEDIATRIC HIGH-GRADE GLIOMA PDOX CELL LINES 54

Introduction 54
Materials and Methods 56
Reagents/Solutions 56
Cell Culture and Treatment 56
Cell Staining, Imaging, and Viability Assay 56
Cell Viability Assay 57
DNA Damage Marker Stain 57
Cell Cycle Profile 57
DNA Fiber Assay 58
Metabolic Extracellular Flux Analysis 59
Results 61
The Combination of a Wee1 Inhibitor and Chk1 Inhibitors Promoted DNA Damage During DNA Replication in High-Grade Glioma PDOX Cells 61
Effect of Combined Wee1 and Chk1 Inhibitors on the Replication Speed and Replication Fork Stability During DNA Replication in High-Grade Glioma PDOX Cells 65
The Combination of a Wee1 Inhibitor and Chk1 Inhibitor Induced Mitotic Catastrophe in pHGG Tumor Cells 69
Effect of Wee1 and Chk1 Inhibitors on ATP Metabolism in High-Grade Glioma PDOX Cells 72

Page

Discussion 77

CHAPTER IV SUMMARY AND DISCUSSION 80

REFERENCES 88

LIST OF FIGURES

Page

Figure 1. Patient-Derived Orthotopic Xenograft Mouse Model. 21

Figure 2. Drugs Selected for High Throughput Single-Agent Screen. 24

Figure 3. High Throughput Drug Screening System. 25

Figure 4. Visualization of the Pharmacological Tree of the 1836 Annotated Compounds. 29

Figure 5. Overall Research Strategy for Selecting Drugs and Developing Synergistic Lethality. 31

Figure 6.Dose Response Curve of Normalized Growth Rate. 33

Figure 7. pHGG PDOX Model Systems. 34

Figure 8. Cell Growth of pHGG Tumor Cells. 35

Figure 9. Positive Control Selection for the High Throughput Screening Assays. 37

Figure 10. High Throughput Single-Agent Screen of pHGG Cells. 39

Figure 11. Assay Optimization and Reproducibility Analysis. 40

Figure 12. Combinatorial Screens of Combinations of Classes of Pan-Active Compounds in the Inhibition of Growth of pHGG Cells. 44

Figure 13. Combinatorial Screen of Pan-Active Compounds Combined with Representative Drugs from Classes of Compounds Exhibiting Selective Activity for pHGG Cells Grown in Monolayer Culture. 45

Figure 14. Combinatorial Activity of Combination of a Wee1 Inhibitor and Chk1 Inhibitors for pHGG R0315 Cells in Monolayer Culture. 47

Figure 15. Combinatorial Activity of Combination of a Wee1 Inhibitor and Chk1 Inhibitors for pHGG R0315 Cells in Neurosphere Culture. 48

Figure 16. Cytotoxic Effect of a Wee1 Inhibitor and Chk1 Inhibitors on the Normal Astrocyte Cells and pHGG Tumor Cells. 49

Figure 17. DNA Fiber Assay. 59

Figure 18. Effect of Combinations of a Wee1 Inhibitor and Chk1 Inhibitors on DNA Damage in pHGG Tumor Cells and Normal Astrocyte Cells. 63

Page

Figure 19. Effect Wee1 and Chk1 Inhibitors on Cell Cycle Profile of pHGG PDOX Tumor Cells and Normal Astrocyte Cells. 65

Figure 20. Effect of Combination of Wee1i and Chk1i is on the Replication Forks in pHGG PDOX Monolayer Cells..... 68

Figure 21. Effect of Wee1 and Chk1 Antagonist on Mitotic Cells in pHGG Tumor Cells..... 71

Figure 22. Effect of Wee1 and Chk1 Antagonist on Mitotic Catastrophe in pHGG Monolayer Cells. 72

Figure 23. Effect Wee1 and Chk1 Inhibitors on ATP Levels in pHGG PDOX Monolayer Cells. 73

Figure 24. Time Course for the Effect of Wee1 and Chk1 Inhibitors and Chemotherapy Drugs on the ATP Level in pHGG PDOX Cells. 74

Figure 25. Effect of Wee1 and Chk1 Inhibitors on Mitochondrial and Glycolytic ATP Production in pHGG Monolayer Cells. 76

Figure 26. Different Endogenous Replicative Stress in Normal Cells and Tumor Cells. 78

Figure 27. Model of Different Replicative Stress Level Causing Selective Cytotoxic Activities in pHGG Tumor Cells and Normal Cells. 85

LIST OF TABLES

Page

Table 1. Examples of Classification of 1836 Compounds by Features. 27

Table 2. Assay Variability by Minimum Significant Ratio (MSR) and Z' Primer. 41

Table 3. Effect of Treatment of Wee1i and Chk1is on the Replication Forks in pHGG PDOX Monolayer Cells. 67

CHAPTER I

INTRODUCTION

Pediatric High-Grade Gliomas

Pediatric high-grade gliomas (pHGG) account for 3-15% of primary central nervous system (CNS) tumors in children [1]. These tumors represent a devasting disease in children with dismal outcomes in terms of both morbidity and mortality. The average survival is less than two years and the five-year survival rate is less than 10% [2, 3]. Current standard of care treatment for pHGG [4] includes maximal safe tumor resection followed by radiotherapy and/or chemotherapy using oral Temozolomide (TMZ). Even though the available evidence supports the benefit of maximal surgical excision [5], the complications of applying radiotherapy to the developing brain and the relatively ineffective results obtained with various forms of chemotherapy make the treatment of pHGG in children both difficult and associated with multiple complications. In addition, relative resistance to chemotherapy also contributes to frequent treatment failures [6, 7]. Thus, there is an urgent need to identify improved chemotherapies for use in children with HGG. Although both basic and translational research has led to an improved understanding of the basic tumor biology of pHGG the success of the translating these findings into new effective targeted therapies has been relatively disappointing.

Molecular Biology

Based on the results of extensive laboratory research into the biology of pHGG, in 2016, the WHO developed an updated classification scheme for these tumors [8]. Adult glioblastoma (GBM) are now classified based on the Isocitrate Dehydrogenase (IDH) gene status (i.e. mutant or wild-type). However, pHGG, including pediatric GBMs, are different exhibiting a very low

incidence of IDH mutation, particularly in younger children [9, 10] so that the majority of pHGG are IDH wild-type.

Compared to adult GBM, pHGG have a higher incidence of p53 mutation/overexpression and a much lower frequency of depletion of phosphatase and tensin homologue (PTEN) or epithelial growth factor receptor (EGFR). p53 mutations are particularly common in young children (<3 years) [10, 11]. Interestingly, even when there are no p53 mutations per se, pHGG may still exhibit overexpression of the p53 gene and/or protein. Some pHGG cases of pHGG, particularly in older children may exhibit ATRX mutations. This genotype is usually associated with a better prognosis [12]. Histone mutations (H3.3) have recently been identified as a common finding in pHGG patients [13-15]. These mutations include the H3F27M variant (lysine is replaced by methionine at 27 positions) that is unique to pHGG [14] as well mutations resulting in the replacement of glycine by valine or arginine at amino acid 34 of H3.3 nucleic acid (G34V/R). The H3K27M variant is associated with a poor prognosis whereas the outcome of G34V/R is relatively better [13].

The methylation status of the O6-Methylguanine-DNA Methyltransferase (MGMT) promoter has prognostic significance in adult GBMs with inactivation of MGMT highly correlated with sensitivity to TMZ. Overexpression of MGMT has been reported in some pHGG [16] which may explain why the efficacy of TMZ in pHGG is much less than adult GBM.

Vascular endothelial growth factor (VEGF) is commonly overexpressed in adult GBM so anti-VEGF (bevacizumab) therapy is frequently used in the treatment of adult GBMs. However, VEGF expression is relatively low in pHGG and anti-VEGF therapy has proved to be much less effective than in adult GBM [17]. Mutations of PDGFRA have also been recently reported in the

pHGG [18, 19] suggesting that anti-PDGFRA therapies with drugs such as imatinib may be possible treatments for some pHGG tumors.

Strategies of Therapy

Currently maximal surgical resection followed by radiotherapy and chemotherapy are the best treatment for adult GBMs [4, 20]. Maximal surgical excision is also beneficial in pHGG but the value of the resection is also dependent on the location of the tumor [21]. Midline supratentorial tumors, and brainstem tumors are often difficult to remove completely without causing major neurologic deficits.

Radiotherapy (RT) is another therapeutic modality used frequently for the treatment of pHGG. Doses of 50-60 Gy over 5-6 weeks [22, 23], are used routinely in children more than 3 years old. RT is not used before 3 years of age because of the potential for damage to the developing brain. However, recent advances in technology, involving accurate delineation of tumor margins by MRI, have made the use of RT in pHGG safer and more effective.

Chemotherapy is also an important component in the comprehensive treatment of pHGG. Sposto et al. were the first to demonstrate the effectiveness of chemotherapy in pediatric GBM using an adjuvant regimen that included 8 cycles of PCV (procarbazine, CCNU, and vincristine) [24, 25]. This regimen resulted in a significant improvement in the outcome of pediatric GBM patients compared to RT alone. However, this result has been hard to reproduce in other studies possibly because the Sposto study included many patients with low grade gliomas. A landmark trial by Stupp et al showed that the addition of both concomitant and adjuvant TMZ improved the five-year survival in adult patients with GBMs [4]. This trial established the current standard-of-care for the use of TMZ in adult GBM. However, this trial did not include any pediatric patients with pHGG. Most studies have suggested that TMZ does not improve survival figures in

pHGG patients. It has been suggested that the overexpression of MGMT in pHGG which may be one of the reasons why the efficacy of TMZ is not as good as in adult patients with GBM [26]. In conclusion, these studies demonstrated the uncertainty that exists on the routine of use of chemotherapy in patients with pHGG.

Recent insights into the molecular biology of pHGG have led to interest in the evaluation of drugs directed specifically against these molecular targets. These include bevacizumab (anti-VEGF), imatinib (anti-PDGFR), erlotinib and others [18, 27]. Many of these have advanced to Phase I/II clinical trials and none have met expectations. While the widespread failure of targeted agents to provide effective therapies for pHGG is not well understood. The lack of success could be due to the fact that the biological features of pHGG include not only genetic mutations but also epigenetic changes and the activation of biologic pathways that allow the tumors to easily escape from the effects of many mono-targeted therapies.

Challenges of Chemotherapy in pHGG

The difficulty in developing effective therapies for pHGG may be attributable to the complex biology of these brain tumors and also the fact that they are highly invasive, infiltrating the surrounding brain tissue and complicating complete excision or effective radiation. For this reason, recurrence is common [28]. In addition, chemotherapy drugs may fail to impact brain tumors because of their inability to cross the blood-brain-barrier (BBB). In addition, genetic mutations, epigenetic changes and the activation of multiple biologic pathways in brain tumors allows them to easily escape many forms of targeted therapies [29]. Upon regrowth and recurrence, the pHGG tumors often acquire new genetic abnormalities, making them resistant to treatments that might have previously worked. Moreover, there is considerable evidence that pHGG tumors contain cancer stem cells that contribute to resistance. These stem cells must be

eliminated to obtain a durable cure [30]. It is likely that different components of the tumor will need to be targeted, complicating the process of drug discovery for pediatric brain tumors. The presence of extensive intra- and inter-tumoral heterogeneity may be a major reason for why the results of chemotherapy trials have been disappointing [31]. Like many other types of cancers, pHGG can be grouped into multiple subtypes based on their pattern of genetic mutation, epigenetic changes, patient age etc, a diversity that requires multiple strategies for effective therapy. For example, Histone 3 F3A mutations are the most frequent mutations in pHGG [13], but this mutation is only found in 36% of pHGG and it is rarely found in adult GBM. In addition, not all cells within a specific tumor carry the same mutations, and quite often patients' tumors don't carry even the most "frequent" mutations. Because of these complexities new treatment strategies of treatment are needed to create progress in the treatment of pediatric brain tumors.

New Strategies for the Treatment of Pediatric Brain Tumors

A number of new types drugs and therapeutic modalities including integrin inhibitors (cilengitide), EGFR inhibitors, novel antiangiogenic agents, histone deacetylase inhibitors and dendritic cell vaccines are currently being tested for potential improvements in the treatment of pHGG.

It is generally accepted that single agent, targeted therapies will not be sufficient to provide effective therapy for pediatric brain tumors. Combination therapies will be necessary to overcome the multiple "escape" and resistance mechanisms that are common in pHGG. Combination therapies, especially those exhibiting synergistic lethality, may give better therapeutic index resulting in safer and less toxic therapies. There are many ways that combination therapies could be developed, combining new targeted drugs with traditional cytotoxic drugs, combinations of multiple targeted agents or combinations with various forms of

immunotherapy and many others. In addition, there are very novel therapies such as Novo-TTF, an FDA-approved low-intensity electromagnetic field therapy approved for the treatment of recurrent GBM [32, 33].

Conclusion

At the moment pHGG is a rare but difficult-to-treat cancer. There are great hope that scientific and technological advances being made in the understanding of the complex biology of the disease will be translated into new targeted combination therapies that will improve the outcomes of this devastating disease.

Use of Patient-Derived Orthotopic Xenograft Model System for Oncology Drug Discovery

In the general field of oncology, recent advances basic research coupled with major advances in the technology of drug discovery research is resulting in new forms of therapy with much higher therapeutic efficiency and greater margins of safety. However, oncology drug discovery remains a challenging field of drug discovery research because of its high failure rates and large costs [34, 35]. Almost 95% of oncology drugs tested in Phase I clinical trials have failed [36]. It is thought that the incorporation of clinically relevant preclinical models such as Patient Derived Orthotopic Xenograft (PDOX) into drug discovery research may improve the probability of success of new drug discovery ventures.

The Process of Generating PDOX Models

The PDOX models are established by the implantation of cancerous tissue from a patient's tumor directly into an immunodeficient mouse, providing a faithful replication of the original tumor. Several types of immunodeficient mice can be used to establish PDOX models: athymic nude mice, severely compromised immune deficient (SCID) mice, nonbese diabetic (NOD)-SCID

mice and recombination-activating gene 2 (Rag2)-knockout mice [37]. In addition, recently NSG (NOD SCID gamma) mice have emerged as the preferred hosts for PDOX establishment since they have a complete null mutation in the gene encoding the interleukin 2 receptor gamma chain. This mutation causes deficiency in multiple cytokine signaling pathway, resulting in dysfunctions of multiple components of innate immunity [38].

There are two different input materials for establishing PDOX models, either single-cell suspension and tissue fragments. The implanted tumor tissues are usually derived from surgical specimens obtained when a patient undergoes surgery. For the single-cell suspension, the tumor tissue is transported in tube filled with the culture media and then the tumor is digested to generate a single cell suspension. The tissue fragments have an advantage in that they retain cell-cell interaction as well as some of the tissue architecture of original tumor, preserving components of the tumor microenvironment [39]. In orthotopic transplants, the tumor tissue is transplanted into the corresponding anatomical organ. Orthotopic models may be difficult to generate, depending on the organ being transplanted, but it has the advantage of mimicking the natural environment of primary tumor. In general, orthotopic transplants are thought to be among the best model systems even though sometimes cell viability is not good [40, 41].

After PDOX tumor is harvested, it can be cut into small pieces, washed and then placed in freezing media and stored in -80 ℃. These stock tumor fragments can be used later for re-transplantation into other mice. For drug discovery studies, 3 generations of PDOX's are often used. Care is taken to ensure that the PDOX has not diverged genetically or histologically from the origin tumor. The success rate of individual PDOX models is influenced by several factors including characteristics of the primary tumor, the process used for the generation of PDOX, the size and number of tissues implanted and the location of the implantation [42, 43].

Staining with the hematoxylin and eosin or important immunohistochemical markers are used to confirm that the gross of histology of the PDOX is conserved with respect to the original tumor. Whole genome sequencing, RNA sequencing and/or real time PCR are used to confirm that the expression of specific genes is preserved between the PDOX and the original tumor [43].

Application of PDOX Models for Cancer Research

Use of PDOX Models for Target Identification and Validation

Better understanding of basic cancer biology and the emergence of new classes of targeted therapies have changed the landscape of cancer treatment and management. One of the keys to these successes has been identification and validation of molecular targets in cancer cells which distinguish the tumor tissue from normal tissues [44]. Advances in transcriptomics, genomics, functional genomics, proteomics, epigenomics and metabolomics have significantly expanded the scope of tumor target identification [45, 46]. Once a potential target is identified, it must be functionally validated using compounds, antibodies, RNA interference or other methods that inhibit or inactivate the target. Collections of large panels of tumor samples and PDOX's are important resources the development of validated and clinically relevant targets [47].

Established cancer cell lines are widely used for drug discovery research because they are readily available and easy to maintain. In contrast, samples derived directly from patients (tumor explants) are much closer to the tumor as it existed in the patient. However, one of the big limitations of primary tumor explants is the poor quality of the tissue and the limited life of the cells. Compared to the either established cell lines or primary tumor explants, PDOX models provide a practical solution by preserving the clinical characteristics of the original tumor and by providing enough tumor tissue and cells to permit target identification and validation and also for drug discovery screening studies [47].

Use of PDOX Models for Drug and Biomarker Discovery Studies

PDOX models are frequently used in drug discovery research because multiple PDOX models of breast cancer, non-small cell lung cancer (NSCLC), head and neck cancers and colorectal cancer have been shown to have drug response profiles that correlated with the responses observed in the clinic [43]. For example, in renal cell cancer, PDOX model respond to sirolimus and sunitinib, but not erlotinib, which matches the clinical data [48].

Recently, the use of PDOX models as potential screening platforms for pre-clinical drug development has shown promise for the development of new drugs for the treatment of cancer. For example, in preclinical PDOX test, metformin failed to inhibit the growth of pancreatic cancers. When metformin was evaluated in the clinical trials, it showed no benefit when combined with standard therapies in both local and metastatic pancreatic cancer [49]. The use of PDOX models for preclinical testing may save time and resources required for clinical trials.

For the discovery of biomarker, the concordance between the results obtained in PDOX models and clinical trials has helped in the discovery of new biomarker for drug efficacy and drug resistance. The relationship between drug efficacy or drug resistance and molecular characteristics can be easily studied using PDOX models. Similarly, PDOX models can be used for the comparisons of the proteomic or genetic profiles between sensitive and resistant models. These studies can be used to identify prognostic biomarkers for clinical studies [50, 51].

Use of PDOX Models for Precision Medicine

Improved understanding of the relationship between cancer genotype and phenotype is leading to a new era of precision medicine in oncology research [52]. Precision medicine combines an individual patient's characteristics such as the genomic profile of their tumor with the selection of targeted therapies or immunotherapies to maximize the effectiveness of the

treatment and to minimize the side effects [52]. Precision medicine is designed to group patients into sub-population based on the genomic profiling of their tumors and then to use specific strategies tailored to the vulnerabilities of that subgroup of tumors [45]. In this context, PDOX models are very useful because they retain the genomic characteristics of the tumor from which they were derived. PDOX's can be used for the identification and validation of the effectiveness and safety of therapies selected based on precision medicine. For example, it has been reported that integrated PDOX models can be used to identify the individualized therapeutic vulnerabilities of pancreatic cancer [53]. In this study, exon sequencing of patient-derived tumors revealed multiple conserved genetic changes that were then used in PDOX models to identify the sensitivity of the tumors to single and combination drug therapies. Similar efforts have been used to apply the principles of personalized medicine to PDOX models derived from multiple different types of cancers [53].

The Limitations of PDOX Models

Although PDOX models have the potential to improve preclinical and translational research and studies, their use is associated with several limitations. PDOX models require the use of severely immune-compromised mice. The lack of a functional immune system in these PDOX models limits their use in studies which required and intact immune response [37, 38]. For example, immunotherapies cannot be studied in conventional PDOX models established in immune-deficient mice. In addition, different tumor types and different tumor subtypes have varying take rates in terms of the success achieved in establishing them as xenografts [54, 55]. These differences can contribute to an imbalanced representation of tumor types/subtypes that is determined more by their take rate than their clinical incidence rate [55]. Moreover, compared to

established cell lines, PDOX models are much more difficult to manipulate genetically making it difficult to genetically modify the tumors or to introduce detection biomarkers [56].

Conclusion

In conclusion, PDOX models retain the characteristics of their tumor of origin as reflected in: 1) similar histopathological features as compared to the original tumors [29, 40]; 2) faithfully replication of the gene expression profiles of the source tumor [29, 57]; 3) maintenance of cancer stem cell pools in vivo [58, 59]; 4) preservation of most of the broad spectrum of gene mutations found in the source tumors. PDOX models have particular value in pre-clinical studies for drug screening, biomarker development and precision medicine [40, 43].

High Throughput Screening for Accelerating the Drug Discovery

The process of developing a new drug and advancing it to the market is a very complex and slow process that can take more than 15 year and cost of more than $1 Billion [60]. Increasing the efficiency of both drug discovery and drug development, driving down the cost and bringing better drugs to market more quickly is greatly needed [61]. The widespread use of high throughput screen (HTS) to facilitate and accelerate the process of the new drug discovery is an important component of pharmaceutical drug discovery. In current best practices, HTS platforms are capable of testing 10,000 to 100,000 compounds per day [62, 63].

Laboratory automation has been critical to the development of the HTS. The reduction in number of repetitive manual tasks has greatly decrease the potential for errors, saving time and allowing scientists to focus on the research rather than repetition. Currently 384-well and 1536-well plates are industry standards for HTS [64]. In addition, particularly when combined acoustic liquid handling technology [65] such as the Echo system from LabCyte are capable of

accurately dispending volumes as small as 2.5 nL, decreasing the volumes of compounds and reagents required and increasing the accuracy of the system by reducing the use of pipette tips.

The quality of the experimental processes is particularly in programs with large data sets because proper data analysis requires high quality results. The quality of the data can be measured using several tools such as number of negative and positive controls, signal/noise ratios and Z factors [66]. However, the sensitivity of the assay must also be taken in to consideration when optimizing a specific assay. Optimizing a particular HTS screening system requires consideration of the time, cost and the experimental processes [62].

Examples of the Use of HTS in Drug Discovery

Maraviroc (Selzentry/Celsentri; Pfizer) is an example of the use of the power of HTS to optimize the pharmacological and pharmacokinetic properties of a specific drug [67]. The project began with HTS in 1997 and Maraviroc was approved by the US Food and Drug Administration (FDA) in 2007. The compound library selected in this program was screened using a CC-chemokine receptor 5 (CCR5, MIP1) radioligand binding assay which was used to identify agonist hits that had no cellular antiviral activity [68]. One of these weak agonist hits provided a lead that led to optimization of the structure of the agonist hit. The researchers then synthesized more than 4000 compounds that were assembled as a compound library they could be used to screen for antiviral activity due to antagonist activity of CCR5. The final drug candidate, Maraviroc, identified by this screen showed nanomolar efficacy in a clinical trial of antiviral activity with prolonged CCR5 receptor occupancy [68].

A significant advantage of HTS is its ability to identify compound that modulate biological activities such as cell viability, protein translocation and other phenotypic features without information on a specific mechanism of action or a specific molecular target [67]. For the

program to identify Hepatitis C inhibitors, researchers used HTS to first discover compounds that inhibited Hepatitis C virus replication [69]. After subsequent optimization the approach yielded clinically efficacious drug candidates. The selection of an optimized compounds required a series of minor chemical changes that resulted in improvements potency and therapeutic index [69, 70]. The integration of compound identification, hit assessment and lead optimization using HTS provides a reasonable path for the progression of chemical compound into a clinically useful drug [67].

Other Benefits of HTS

In many pharmaceutical and biotech companies, the technology of HTS screening laboratories is now integrated into downstream drug development processes [67]. Laboratories are now using low-volume assays to drive both structure and activity data generation (SAR) and high-throughput absorption, distribution, metabolism, excretion and toxicity screening [71, 72]. This drive for cost-effectiveness, parallel data generation and low-volume assays through the use of HTS has allowed engineers and scientists to refine procedures and reduce the timelines for drug discovery and development [73]. Because phenotypic cellular assays are more physiologically relevant there is a growing trend to use them to perform hit identification and lead optimization [74, 75]. This is particularly true for the use of primary, tumor-derived human cells rather than established cancer cell lines in HTS screening studies.

HTS technologies have also improved upstream drug discovery activities such as target identification and validation. In addition, many research technologies such as RNA interference screening, chemo-genomic and crystallography have benefited from the automation and microplate assay formats originally developed for HTS platforms [73, 76].

Conclusion

HTS has matured to become an important part of pharmaceutical research and a useful tool in expansion of biomedical knowledge. HTS has provided automation tools that are enhancing basic scientific research and increasing the quality of chemical compounds, improvements that are resulting in improved pharmaceutical products [62]. In summary, HTS is proving to be one of the most successful strategies in modern drug discovery research [62, 67].

Targeted Cancer Therapies

Targeted cancer therapeutics are drugs or other substances that interfere with the activity of specific molecules that play important roles in cancer cell proliferation, metastasis, invasion and other properties of malignant cells. Targeted therapies differ from conventional chemotherapies are in several ways including: 1) targeted therapies impact specific molecular targets associated with cancer whereas the traditional chemotherapies act on the general properties of cancer cells such as their rapid rate of cell division (this effect may impact some types of normal cells as well); 2) targeted therapies are designed and selected to interact with their specific targets whereas traditional chemotherapies are selected to kill many different types of cancer cells; 3) many targeted therapies are cytostatic while most traditional chemotherapies are cytotoxic. Many targeted cancer therapies have already been approved by FDA for the treatment of specific types of cancer and many more are being tested in the both clinical trials and preclinical studies.

The first step in the development of a new targeted therapy is the identification of a molecular target. This is often accomplished by the discovery of different levels of expression of a protein between cancer and normal cells. Differential expression is particularly significant if the protein is known to involved in cancer cell growth and / metastasis. For instance the human

epidermal growth factor receptor 2 (HER-2) [77] is expressed at high levels in some types of cancer. HER-2 targeted therapies such as trastuzumab are FDA approved for the treatment of HER-2 overexpressing breast and gastric cancers. Some targets are identified when it is determined that mutant or altered forms of the protein in cancer cells can cause cancer progression. For example, the protein BRAF is mutated in many melanomas [78]. Vemurafenib, a kinase inhibitor that targets BRAF mutated protein is approved for the treatment of metastatic melanomas that have altered BRAF protein. Chromosomal abnormalities in cancer cells can also serve as guides for the detection of molecular targets that can be targeted for therapy. These chromosomal abnormalities include gene fusions can drive cancer development. Many of these mutations caused fusion proteins can serve as potential targets for the targeted therapies. The targeted cancer therapeutic Imatinib mesylate targets the BCR-ABL fusion protein, an abnormal protein that is present in some leukemia cells and promotes leukemia cells growth [79, 80]. By targeting the BCR-ABL fusion protein, Imatinib is a very effective treatment for BCR-ABL positive leukemias.

Both small molecules and monoclonal antibodies are used for targeted therapies. Small molecule compounds are most effective for the targeting of intracellular while monoclonal antibodies are most useful for targets on the cell surface [81]. Small molecule compounds are frequently identified by the high throughput screening studies. Large libraries of diverse chemicals are assembled and tested for their effects on cells with the goal of identifying active compounds “hits”. Monoclonal antibodies are generated by injecting the purified targeted proteins into the animals, causing the animals to produce the antibodies to those targeted proteins.

There are many different types of targeted therapies available for cancer treatment based on their function and biological the biological processes targeted. Examples include hormone therapies, gene expression modulators, signal transduction inhibitors, apoptosis inducers, angiogenesis inhibitors, immunotherapies and many others. Cancer vaccines and gene therapy are also considered targeted therapies because they are directed at specific properties or targets within the cancer cells.

Targeted therapies do have some limitations including the fact that cancer cells often develop resistance to a specific form of targeted therapy [78, 82]. Cancer cells undergo frequent mutations that can result in the failure of the targeted therapy. In addition, the cancer cells can use alternative pathways to support tumor growth and progression. A third problem is that it is sometimes difficult to identify the "driver/survival critical mutations" that are critical for survival in a specific cancer [83]. Extensive intra- and inter-tumoral heterogeneity is another reason why targeted therapies may be directed toward an non-critical target [31]. Another factor that can limit the effectiveness of targeted therapies can be the difficulty in developing inhibitory drugs for some classes of targets even though they have been found to be critical factors in the survival of a particular cancer [84]. For example, the Ras signaling protein is highly mutated in many different types of cancer, but to date no inhibitors of Ras protein have been developed in spite of many different types of drug discovery efforts. Finally, off-target activities may limit their usefulness as therapies for patients with cancer.

To overcome the limitations to the development of effective targeted therapies such as the use of combination to overcome drug resistance. For example, targeting different parts of a particular cell signaling pathway that is altered in cancer may delay the development of resistance and disease progression [85]. Another benefit of using combination therapies is that

combination can exhibit synergistic lethality providing a wider therapeutic index for the therapy making it safer to use. Combination therapies could be limited to two targeted therapies, they can also combine a targeted therapy with a traditional chemotherapy drug. In the future there will be many new opportunities for new combination therapies based both on the rapid increase in the number of targeted therapies and the increased understanding of tumor biology that is coming from advances in genome wide sequencing, bioinformatics and system biology [47].

Cancer is a multifactorial and complicated disease. Multiple risk factors lead to the accumulation of molecular changes and mutations inside the cancer cell that contribute to the initiation of carcinogenesis. Targeted therapy are becoming increasingly useful because of their selectivity for cancer cells [81]. By focusing on the specific molecular changes which are unique to a particular cancer, targeted cancer therapies increase the therapeutic for many types of cancer. Multiple clinical trials of both FDA-approved and experimental targeted therapies are exploring this possibility for multiple types of cancer [86, 87].

Rationale for this Dissertation

Pediatric high-grade glioma (pHGG) accounts for 6-12% of all primary pediatric central nervous system tumors and is the most aggressive pediatric brain tumor [1]. Current standard-of-care treatment consists of tumor resection followed by radiation and chemotherapy. This regimen has been shown to improve patient survival, but the average survival remains less than two years and the five-year survival rate is less than 10% [2, 3]. Resistance to chemotherapy is an important cause of treatment failure [6, 7]. There is an urgent need to identify new safe and effective therapies for use in children with HGG.

The goal of this project is to establish a preclinical rationale for clinical trials of new combinatorial targeted-therapies in children with HGG. The objective is to use an unbiased approach to discover new target-based novel combination therapies for pHGG. We hypothesize that a high throughput combinatorial screening paradigm in both cancer stem cells (as found in 3D neurospheres) and monolayer cultures of tumor cells derived from patient-derived orthotopic xenograft (PDOX) models of pHGG will facilitate the discovery of novel synergistic drug combinations that are effective and selective for pHGG. Dr. Li, a leading expert in PDOX model establishment, has developed a large panel of PDOX mouse models of pHGG [88, 89]. These PDOX models replicate the histology, invasive growth properties, and gene expression profiles of the patients' original tumors and also have maintained cancer stem cell pools during *in vivo* sub-transplantation. Our lab has expertise in high throughput screening technologies. We will screen combinations of FDA-approved and investigational drugs in specialized High Through Screening (HTS) assays that measures the concentration dependence of the combinatorial activity (synergy, additivity or antagonism) across a range of concentrations of both components of the combinatorial pair. With these two experimental platforms, we are now uniquely positioned to address the challenge of discovering effective combinatorial therapies for children with HGG.

To test the hypothesis, we propose the following Specific Aims:

Aim 1: Establish an Effective and Efficient Strategy to Discover Drug Combinations that Exhibit Synergistic Lethality Activity against Pediatric High-Grade Gliomas.

- Select a mechanistically annotated set of compounds for profiling for single agent activity against a panel of pHGG PDOX cells.

- Conduct in vitro combinatorial screens of selected pairs of single-agent active compounds against 3D neurospheres and 2D monolayers from pHGG PDOX cell lines and normal cell types.

Aim 2: Establish the Cellular and Molecular Mechanisms Responsible for the Synergistic Cytotoxic Activity of Selected Drug Combinations with Potential Application as Therapeutic Regimens for the Treatment of pHGG

- Analyze the temporal and spatial effects of drug combinations on apoptosis and cell proliferation in PDOX cell lines
- Examine alterations in the expression and/or activity of the targeted genes and pathways and establish the mechanisms of synergistic tumor cell killing

CHAPTER II

DISCOVERY OF DRUG COMBINATIONS THAT EXHIBIT SYNERGISTIC LETHALITY ACTIVITY AGAINST PEDIATRIC HGG TUMOR CELLS

Materials and Methods

Reagents/Solutions

DMEM/F12 medium (Life Technologies/Gibco), N2 supplement (Life Technologies/Gibco), B27 supplement (Life Technologies/Gibco), rhEGF (Life Technologies/Gibco) and rhFGF (Life Technologies/Gibco), FBS (Life Technologies/Gibco), glutamine (Life Technologies/Gibco), sodium pyruvate (Life Technologies/Gibco), Draq5 (Invitrogen, 65-0880-92), Trypsin 0.25% (Life Technologies/Gibco), 384-well plates (Corning), CellTiter-Glo Cell Viability Assay (Promega, G7573), DAPI (Invitrogen, D1306).

Patient-Derived Xenografts Models and Tumor Cells Preparation

Rag2/severe complex immune deficiency (SCID) mice, normally ages from 8 to 12 weeks are used as the hosts for PDX implantation. Patient tumor cells from Texas Children's Hospital were obtained and cultured in cancer stem cell medium (CSC medium, DMEM/F12 supplemented with N27, B2, rhEGF and rhFGF), and were made into a single cell suspension followed by culturing in 37 °C for 6 hours. Tumor cells were then inoculated intracerebrally into Rag2/SCID mice at $2x10^5$ cells per mouse via injection (Described in Figure1). The animals were maintained in the animal facilities at Texas Children's Hospital. Mice are monitored daily until they developed signs of neurological deficit or became moribund, at which time they were euthanized. All experiments were performed in accordance with national guidelines and

regulations and with approval of the animal care and use committee at Texas Children's Hospital and Baylor College of Medicine.

Tumor cells from PDOX mice were obtained, dissociated, purified and cultured in both CSC medium and normal medium (with FBS). By serial passaging, we established cell lines which could be cultured either as neurosphere cell lines or monolayer cell lines.

All of these steps are standard in Dr. Xiao-Nan Li's lab in Texas Children's Hospital.

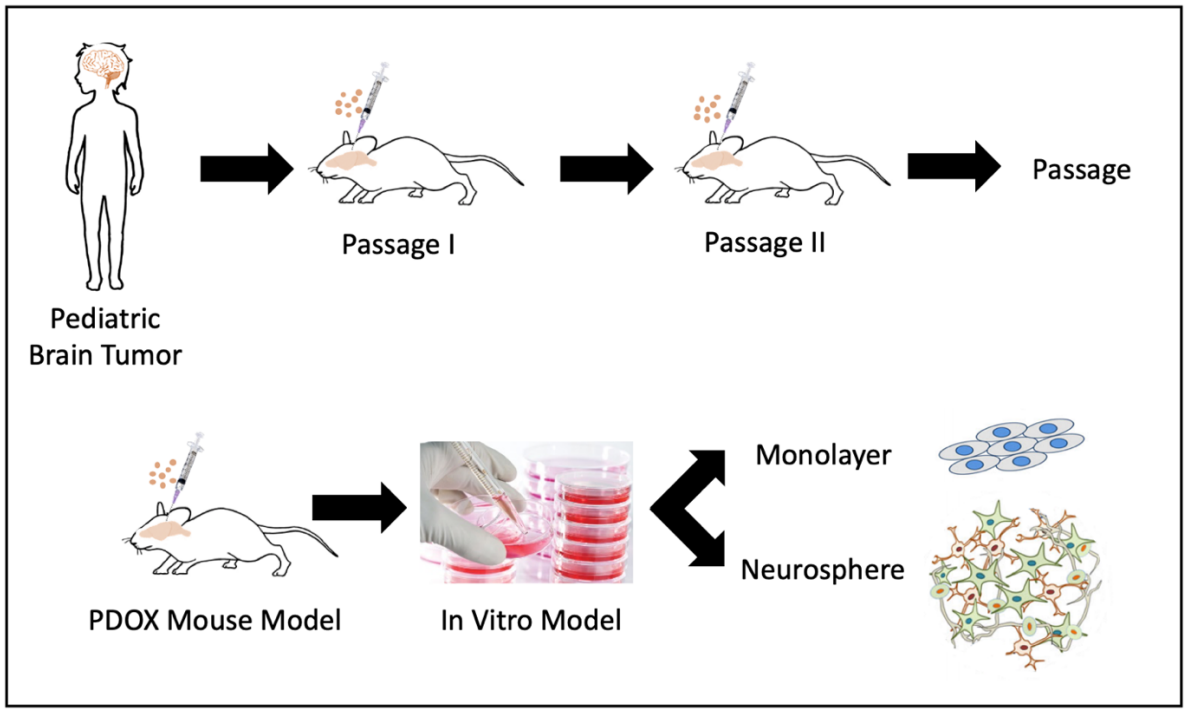

Figure 1. Patient-Derived Orthotopic Xenograft Mouse Model.
Rag2/severe complex SCID mice were used to establish PDX's. Tumor cells were obtained from patients at the time of surgery. The cells were cultured in CSC medium and made into a single cell suspension. Tumor cells were inoculated into SCID mice ($2x10^5$ cells/mouse) via intracerebral injection. The cells from the PDOX tumors were obtained and cultured in both CSC medium and normal medium. Serial passaging established cell lines that could be propagated as either neurosphere or monolayer cell lines.

Tumor Cell and Normal Cell Culture

pHGG tumor cells were provided by Dr. Xiao-Nan Li's lab, Texas Children's Hospital. Neurosphere cells were maintained in DMEM/F12 medium supplemented with B27, N2, 25

ng/ml rhEGF, 25 ng/ml rhFGF, glutamine and sodium pyruvate. Monolayer cells were maintained in DMEM/F12 medium supplemented with 10% fetal bovine serum (FBS), glutamine and sodium pyruvate. A normal astrocyte cell line was purchased from NIH. The normal astrocyte cells were maintained in DMEM/F12 medium supplemented with 10% fetal bovine serum (FBS), glutamine and sodium pyruvate. Cells were cultured in 75 cm^2 flasks or 25 cm^2 flasks in a 37 °C incubator with 5% CO_2 and passaged as needed.

Cell Staining and Imaging

For neurosphere cells, single cells were made by pipetting 20 times and using 40 μm cell strainer to remove big clusters. Single stem-cell like cells were spun down 1200 rpm for 3 minutes and the supernatant was removed. For monolayer cultures, cells were trypsinized by Trypsin 0.25% for 2 minutes and spun down 1200 rpm for 3 min and supernatant was removed. Both of these single cells were seeded into 384-well plate and we tested 5 different cell densities from 250 cells/well to 4000 cells/well to optimize spheroid formation and to establish the doubling time of cells in monolayer culture. Cells were exposed to drugs for 3 or 7 days. Neurosphere cells were stained overnight with Draq5 (Thermo Scientific™). Draq 5 is a far-red DNA stain used to stain both live and dead cells. For monolayer cells, cells were fixed with 4% paraformaldehyde (PFA) for 10 minutes, permeabilized with 0.5% Triton for 10 minutes and the nuclei were stained with DAPI for 5 minutes followed by washing with PBS and imaging. Cells were imaged using an InCell 6000 (GE Healthcare Life Science) with images acquired with 4x magnification and 1 field of view for each well.

Cell Viability and Proliferation Assay

Single cells were seeded into 384-well plate with a total volume of 50 μl and were tested at different cell densities from 250 to 4000 cells/well. Cells were cultured in the absence or

presence of drugs for 7 days. At the end of the treatment, the plates were spun and 35 µl medium per well was aspirated followed by the addition of 15 µl CellTiter-Glo (CTG). After 30 minutes incubation at room temperature, the luminescence of each well was measured on a plate reader. The doubling time was calculated from the value of luminescence or fluorescence at Day 0 and Day 7.

Drug Selection

The GCC Drug Library used for these studies includes 6685 unique FDA-approved and investigational drugs. Of the 6685 drugs available for screening, we selected a subset of 1863 compounds that have well-established mechanisms of action and are clinically relevant for the potential treatment of patients with pediatric cancer. Forty-eight percent (48%) of the 1863 drugs or compounds are targeted kinase inhibitors, 11% are GPCR and G protein inhibitors, 8% are general enzymatic inhibitors, 4% are epigenetic regulators (Described in Figure 2). The collection represents a clinically relevant and a broad range drugs potentially useful for the treatment of cancer. We also cataloged the drugs based on their mechanism of action including the class, the formal target of the drug or the target with the highest affinity, the biological process of the targets and the associated pathway that the drug targeted. These annotations were used to identify clusters of drugs or compounds that affected the proliferation and viability of pediatric HGG cells.

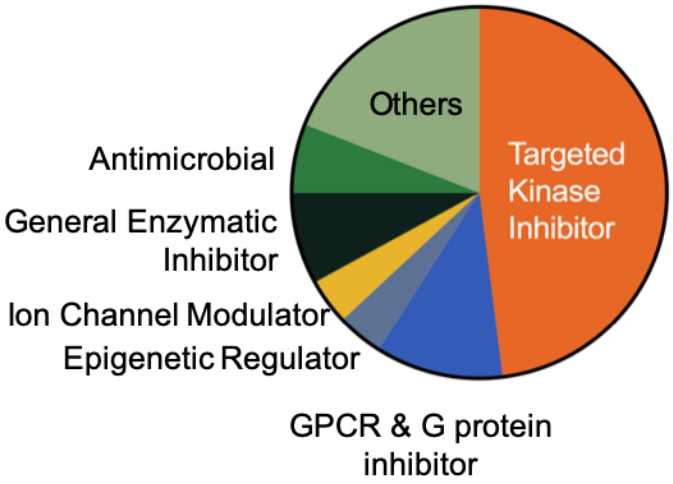

Figure 2. Drugs Selected for High Throughput Single-Agent Screen.
The pie chart indicates the percentage of class of the 1863 drugs used for the screens.

Single-Agent High-Throughput Drug Screening

For the primary single agent screens (Described in Figure 3), 3D neurosphere cells (2000 cells/well) and 2D monolayer cells (1000 cells/well) from pHGG PDX tumors were plated in 50 µl of culture medium in 384-well plates (Corning) using an Multidrop (Thermo). Plates were incubated for 24 hours to allow for neurosphere formation and the attachment of monolayer cells to the bottom of the wells. Drugs were transferred to the wells using a Tecan Freedom Evo 200 and Echo liquid handler. After a 7-day incubation, the viable cell number in each well was determined using the CellTiter-Glo reagent (Promega), read in an automated plate reader (Synergy Neo2 hybrid multi-mode reader, BioTek). The fractional affected cells (fa) was calculated for each drug and each concentration compared to the DMSO control based on the effects on cell viability as measured by CellTiter-Glo. The fa was used in a nonlinear regression analysis using a 4-parameter logistic equation (GraphPad Prism). The dose-response curve was generated and the area-under-the-curve (AUC) for each drug was calculated. AUC values were

normalized and the normalized AUC was used to demonstrate the response of each cell line and each cell culture condition to the drugs being tested.

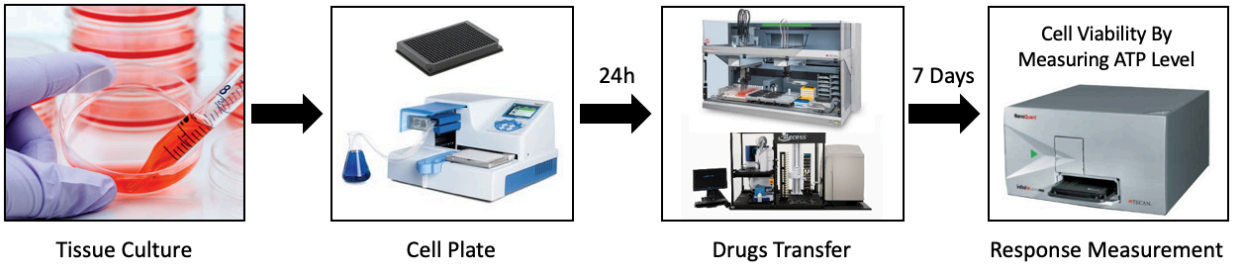

Figure 3. High Throughput Drug Screening System.
Tumor cells were maintained in a humidified incubator. Cells were plated as single cells in 50 µL medium for each well in a 384-well Plate. Plates were incubated for 24h to allow for neurosphere formation and monolayer attachment to the wells. Drugs were transferred and their effects on cell viability were measured at 7 days by using CellTiter-Glo (a measure of ATP).

A subset of drugs were selected for combinatorial screening based on the following properties: 1)Pan-active compounds: Drugs with single agent activity as reflected in a normalized AUC $\geq$ 0.4 of 4 separate models; 2) 3D Neurosphere-selective compounds: drugs displaying cytotoxicity toward neurospheres (AUC $\geq$ 0.4) but with no effect on monolayers (AUC < 0.4) and 3) 2D Monolayer-selective compounds: drugs displaying cytotoxicity to monolayer cultures (AUC $\geq$ 0.4) but having no effect on neurospheres (AUC < 0.4) and 4) Clinically-relevant drugs: drugs with a well-established mechanism of action that are clinically relevant for the treatment of pediatric cancer (Described in Figure 5).

The Z'-factors (Z prime) obtained from the activity of positive and negative controls were used to assess the quality of the assay. The Z' factor is used to determine the reliability of an assay prior to additional quality-control experiments and subsequent screening studies. The closer the Z'-value is to 1, the better the quality of the assay. Z'-factors in the range of 0.5 to 1, are indicative of an excellent assay suitable for the collection of reliable results. The Z-factor is

determined from four parameters: the means (μ) and standard deviations (σ) of both the positive (p) and negative (n) controls (μp, σp, and μn, σn) and is defined as:

$$\text{Z-factor} = 1 - \frac{3(\sigma_p + \sigma_n)}{|\mu_p - \mu_n|}$$

In addition, the concentration-response of a reference compound is run in every screen to determine the stability of the assay over time. The Minimum Signal Ratio (MSR) is a statistical parameter that characterizes the reproducibility of potency estimates based on multiple concentration-response assays. The reference compound MSR can be used to document both between-run and within-run variability. The MSR is calculated as $MSR = 10^{2\sqrt{2}s}$, where the s is the standard deviation of the $\log10(IC_{50})$ values across runs or plates, based on one IC_{50} result per run/plate. A between-run or within-run MSR < 3 criteria is considered to reflect a highly reproducible data set.

Mechanism Annotated Pharmacological Tree

To better visualize the response of cells to different clusters of drugs, we developed a representation, "pharmacological tree", that orders the 1863 compounds based on their mechanisms of action and displays their activity against HGG cell lines. The classification of the 1863 compounds was by features based on their pharmacologic class, their molecular target or their target with the highest affinity, the biologic process that they targeted and the signaling pathway that the drug effected (See Table 1). The distance between drug pairs was calculated based of the similarity in their features. The relationship between all 1836 compounds was then displayed in the form of a pharmacologic tree in which adjacent branches illustrate the most closely associated mechanisms of action. Each branch has multiple circles that represents the activity of one compound. The area of the circle represents the response of cells to the drug

(based on the normalized AUC). The larger the circle, the more active the compound in killing pHGG tumor cells (Described in Figure 4). This pharmacological tree allows one to visualize the patterns of cytotoxic activity based on the various pharmacologic mechanisms of action.

Table 1. Examples of Classification of 1836 Compounds by Features.

Compound	Class	Target	Process	Pathway association
(-)-Blebbistatin	General enzymatic inhibitor	non-muscle myosin II ATPases	ATPase	
(-)-Parthenolide	Epigenetic regulator	HDAC1	Nuclear protein deacetylation	Reader-Writer-Eraser of K-ac
(-)-Terreic acid	Targeted kinase inhibitor	BTK	RTK Inhibitor	PLC/PKC/DAG
(+)-JQ1	Epigenetic regulator	BRD4	Acetylated lysine reader	Reader-Writer-Eraser of K-ac
(+)-Matrine	GPCR & G Protein	Opiate receptor	Opioid Receptor agonist	
(+)-Usniacin	General enzymatic inhibitor	TG synthesis	Metabolic modifier	Cholesterol metabolism
10-Deacetylbaccatin-III	Microtubule poisons	Tubulin/micotubules	Mitotic inhibitor	Cell cycle mitotic progression
10-DEBC hydrochloride	Targeted kinase inhibitor	Akt1	S/T kinase inhibitor	PI3K/AKT/mTOR
17-AAG (Tanespimycin)	Proteotoxic agent	HSP90	Protein folding and repair	Cellular toxicity
17-DMAG (Alvespimycin) HCl	Proteotoxic agent	HSP90	Protein folding and repair	Cellular toxicity
1-Hexadecanol	others	Fatty alcohol	Metabolic modifier	
1L6 (Akt inhibitor)	Targeted kinase inhibitor	Akt	S/T kinase inhibitor	PI3K/AKT/mTOR
1-Naphthyl PP1	Targeted kinase inhibitor	SRC	TK inhibitor	
20-Hydroxyecdysone	Targeted kinase inhibitor	PEPCK	Metabolic modifier	
24BPSAP (MMP2/MMP-9 Inhibitor I)	Migration inhibitors	MMP	Proteases	Invasion~motility
2-Methoxyestradiol (2-MeOE2)	Transcription factor modulation	HIF-2	Oxygen rheostat	Hypoxia
2-Thiouracil	Antihyperthyroid agent		Endocrine and Hormone therapy	

Table 1. Continued

Compound	Class	Target	Process	Pathway association
3-Deazaneplanocin A (DZNeP)	Epigenetic regulator	S-adenosylhomocysteine hydrolase	Histone Methylation writer	Reader-Writer-Eraser of K-me
3-Indolebutyric acid (IBA)	Others		Plant hormone	
3-Methyladenine	Targeted kinase inhibitor	Vps34	S/T kinase inhibitor	PI3K/Akt/mTOR
4-Phenylbutyrate	Epigenetic regulator	Pan-HDAC	Nuclear/cytoplasmic protein deacetylation	Reader-Writer-Eraser of K-ac
5-hydroxymethyl Tolterodine (PNU 200577, 5-HMT, 5-HM)	GPCR & G Protein	mAChR	Ion homeostasis	Acetylcholine signaling
5-hydroxytryptophan (5-HTP)	GPCR & G Protein	5-HT	Seratonin related signaling	PI3K/AKT/mTOR~MAPK
5-Iodotubericidin	GPCR & G Protein	Adenosine receptor	cAMP related signaling	PI3K/AKT/mTOR~MAPK

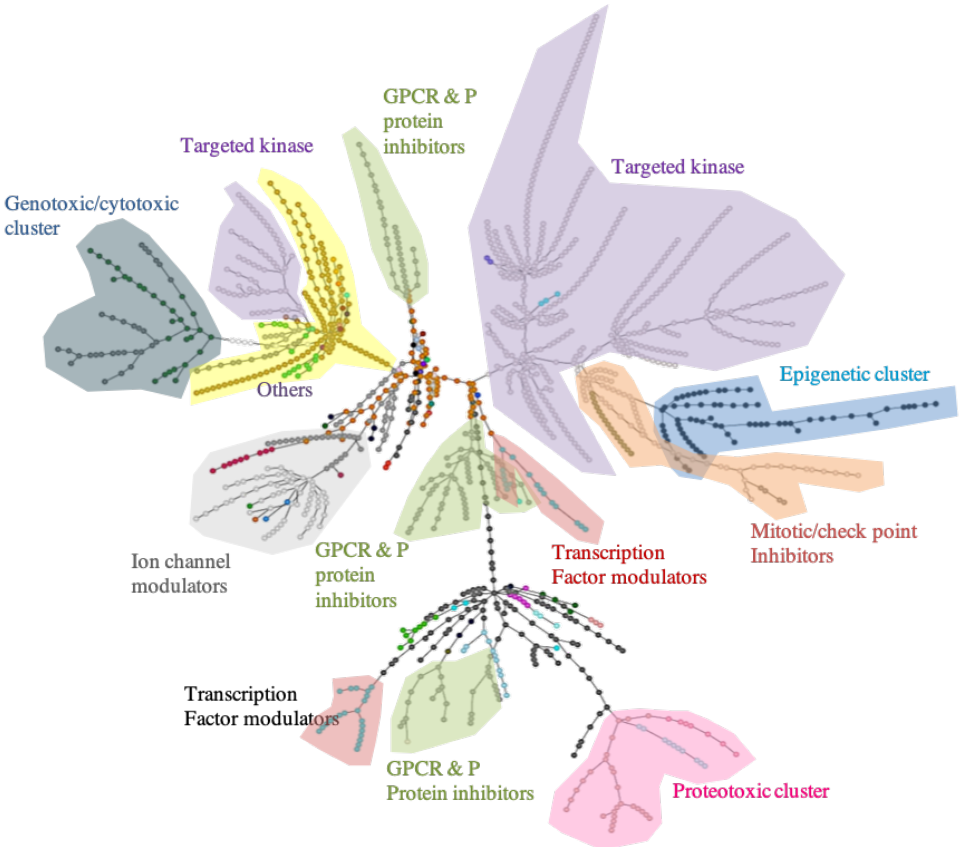

Figure 4. Visualization of the Pharmacological Tree of the 1836 Annotated Compounds.
1863 compounds were classified based on their biological features including class, canonical target, pathway associated with target and cellular or systemic process effected. Gower distances were calculated using the drug annotations table. By using the distance to computer nodes and edges of a minimum spanning tree and enabling it into an interactive network object. Each branch indicates a different class of activity and each circle indicates a compound or drug. The area of each circle indicates the drug response (normalized AUC).

High-Throughput Drug Combination Screening

From the single-agent screens, we selected several diverse classes of active drugs based on their cytotoxic activity in HGG cells (Described in Figure 5). For primary combination screens, we used 6 doses by 6 doses matrix (started with 1μM and half log dilution) of drug concentrations for all pairs (245 pairs). These primary combination screens were carried out in 2D monolayer cultures due to the stability of the system and less variability. Drug combinations to be tested included: 1) Pan-active compounds combined with Pan-active compounds (45 pairs); 2) Pan-active compounds combined with 3D neurosphere-selective compounds (100 pairs); 3)

Pan-active compounds combined with 2D monolayer-selective compounds (100 pairs). Quantitative indices of drug interaction (synergy, additivity or antagonism) were generated by independently varying the concentration of each of the components in the combination. The Bliss independence model for synergy will be applied to all combinations tested. A set of charts graphing relative synergy (excess killing) or antagonism (reduced killing) and a numerical synergy index will be used to define a synergistic interaction. In cases where the two drugs tested in combination are also effective as single agents, the expected Loewe additivity is calculated and the Over-Bliss value is calculated in the Bliss method. Over-Bliss value greater than 0 indicates synergy while the value less than 0 indicates antagonism. An Over-Bliss value of 0.30 or higher and a fa value of greater than 0.40 were used as the criteria for synergistic activity of a specific drug combination.

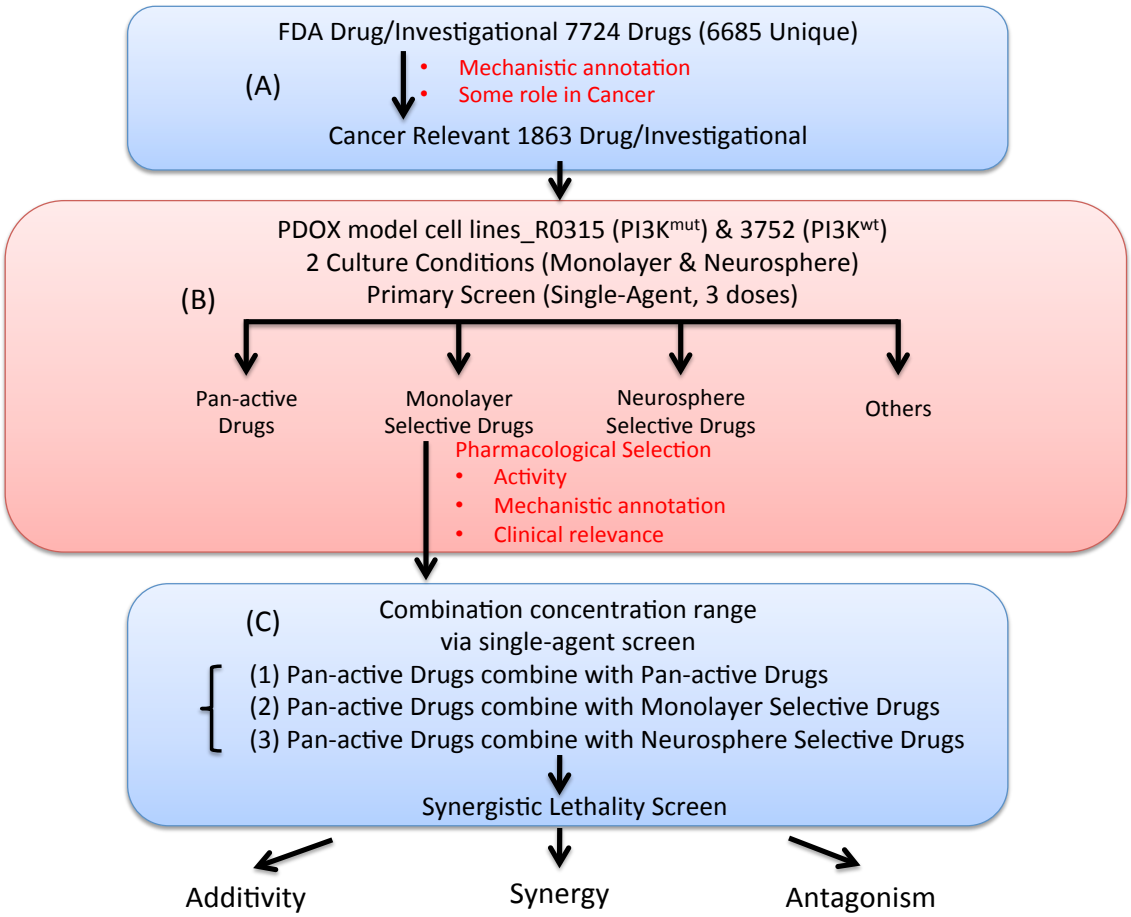

Figure 5. Overall Research Strategy for Selecting Drugs and Developing Synergistic Lethality.
(a) A subset of 1863 drugs were selected from our GCC Library. The 1863 drugs were screened in 2 PDOX model ($PI3K^{mut}$ and $PI3K^{wt}$) in 2 different cell culture. (b) We cataloged 4 levels of activity based on the responses to model systems: Pan-active, neurosphere selectively active, monolayer selectively active and others. And we selected 10 most promising drugs for the first 3 levels. (c) Primary combination screening used a 6x6 matrix of drug concentrations for all pairs in monolayers due to the stability and less variables of monolayers. Quantitative indices of drug interaction (synergy, additivity or antagonism) will be generated based on independently varying concentration of each of the components. Pairs exhibiting additive or synergistic activity in the primary screen were validated using a second 10x10 matrix tailored to the specific pairs against both neurosphere and monolayer cell lines.

Pairs exhibiting synergistic activity in the primary screen were validated using a secondary 10 doses by 10 doses matrix (4 times of IC_{50} and 2 times dilution for each drugs) with dose ranges tailored to the specific pairs. These secondary screens were run against all of the pHGG cell lines in both neurosphere and monolayer culture. The "excess over Bliss" was used as a measurement for synergistic activity. The same as the primary combinatorial screen, an over-

Bliss value of 0.30 or higher and a fa value of greater than 0.40 were used as the criteria for synergistic activity of a specific drug combination.

Cytotoxicity Screening

Normal human astrocytes were used as a control to test for the selectivity of the cytotoxic activity of specific combinations. To address differences in apparent cytotoxic activity based on differences in the baseline proliferative rate of the cells, the normalized growth rate (GR) of both astrocytes and HGG cells were calculated by comparing to the ATP level at Day 0 and Day 7. The Hafner Formula for calculating the normalized GR is:

$$GR(c) = 2^{\frac{\log_2(x(c)/x_0)}{\log_2(x_{neg}/x_0)}} - 1$$

The normalized GR value closer to 1 indicates that the cells grow like untreated cells, the value equal 0 indicates that the cell growth is 100% suppressed and the value closer to -1 indicates the more cells were killed. At the same time the normalized GR was used in a nonlinear regression analysis using a 4-parameter logistic equation (GraphPad Prism) and the dose-response curve of GR was made by GraphPad Prism (Described in Figure 6). By comparing the normalized GR value, we could determine the effect of the combinatorial pair on the proliferation of pHGG tumor cells and normal Astrocytes.

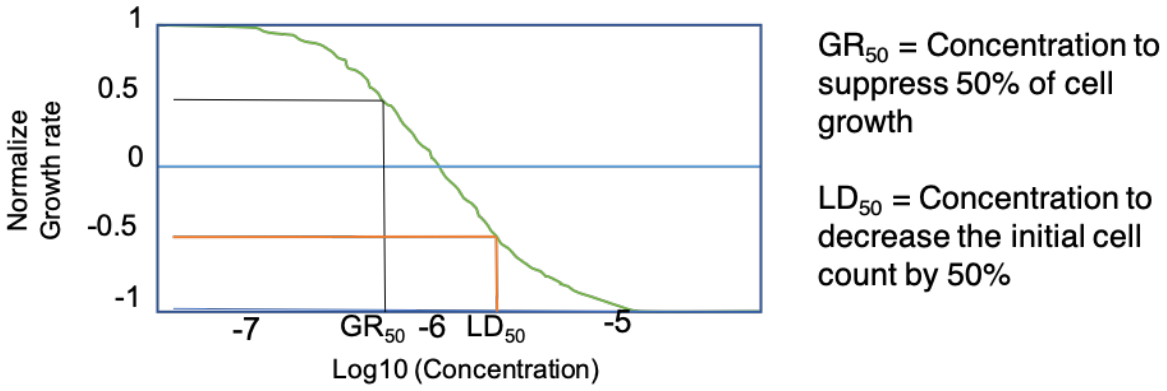

Figure 6.Dose Response Curve of Normalized Growth Rate.
A dose response curve showing the growth of tissue to stimulation by an agonist. Low doses are insufficient to generate a response (GR value is 1), while the high doses generate a maximal response (GR value is -1). GR_{50} indicates the concentration to suppress 50% of cell growth, LD_{50} indicates concentration to decrease the initial cell count by 50%. X axis indicates the concentration of drugs, the Y axis indicates the normalized Growth Rate value.

Statistical Analyses

Statistical analysis was performed using GraphPad Prism software. All data are presented as Means ± SEM unless stated otherwise. Comparisons between different groups were made using Student's t test or ANOVA as appropriate. Dose-response curves were calculated using Prism and the AUC for each drug was calculated. P Values of 0.05 or lower were considered statistically significant for all experiments (*P<0.05; **P<0.01; ***P<0.001). The excess over-Bliss was used as a measurement for a synergistic effect. The over-Bliss value of 0.30 or higher and fa value of 0.40 or higher were considered statistically significant for combinatorial screen.

Results

PDOX Model and High Throughput Screen

To make sure the pHGG PDOX model established successfully, we examined the cerebra of PDOX GBM xenografted mice 10 weeks post tumor injection. As Figure 7a illustrates, there is a large intra-cerebral tumor located in the xenografted mouse brain compared to the normal

brain. Moreover, H&E staining showed histological features typical of GBM (Figure 7b, i and ii), and immunohistochemical staining using human-specific anti-mitochondrial antibodies showed human GBM cells infiltrating deeply into the mouse brains (Figure 7b, iii and iv).

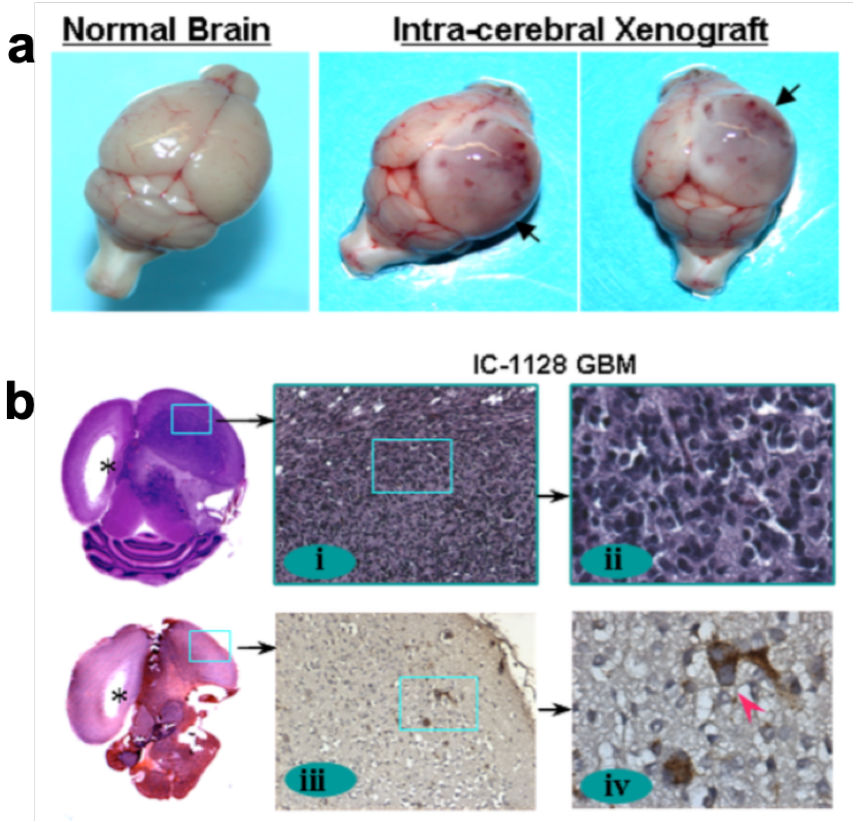

Figure 7. pHGG PDOX Model Systems.
(a) A high intra-cerebral tumor 10 weeks after tumor injection. (b) H&E staining showing histological features of GBM (i, ii) and immune-histochemical staining using human-specific antibodies showing human GBM cell infiltrating into mouse normal brains (iii, iv).

To screen for compounds that inhibit the survival of pHGG tumor cell lines, we chose two PDOX cell lines, R0315, a $PI3K^{mut}$ cell line and 3752, a $PI3K^{wt}$ cell line, cultured in both 3D neurosphere and 2D monolayer cultures. We optimized the high throughput screen system by i) testing an optimal cell density and duration of cell culture, ii) selecting the best endpoint assays for measuring cell viability, iii) identifying the best positive and negative controls for the high

throughput screening systems and the assessment of data quality control. To optimize cell density and the duration of cell cultures, cells were seeded into 384-well plates at 5 different cell densities ranging from 125 cells/well to 2000 cells/well to determine the time to confluence for 2D monolayer cells and the size of the 3D spheroids. We selected a seeding density of 2000 cells/well for 3D neurosphere cells allowing overnight spheroid formation (perimeter of spheroid is 60-100 μm, seen in Figure 8a) and then cultured for 7 days to achieve good-sized spheroids (perimeter of spheroid is 100-350 μm, seen in Figure 8a). For the 2D monolayer cells, a seeding density of 1000 cells/well was selected, the cells were then allowed to attach overnight and then cultured for 7 days to achieve 80% confluence (seen in Figure 8a).

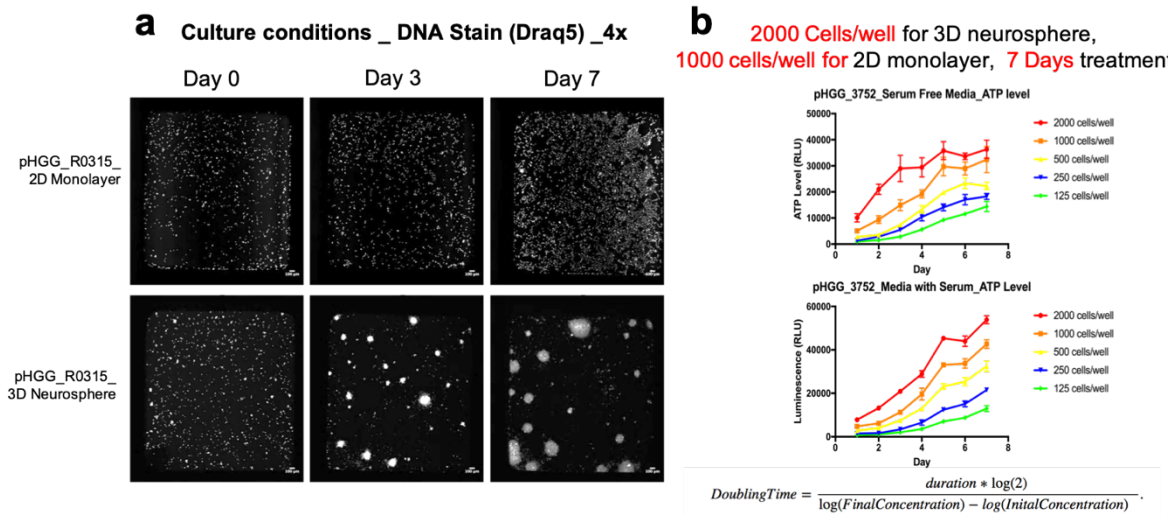

Figure 8. Cell Growth of pHGG Tumor Cells.
(a) Cell growth of 2D monolayer cells and 3D neurosphere cells. Cells labeled with Draq5 (far red) 10 min prior 4x imaging for 2D monolayer cells and 18 hours for 3D neurosphere cells. (b) Time course of cell viability by CellTiter-Glo in different cell density and cell lines and doubling time of cell growth.

Cell viability was measured using the CellTiter-Glo assay (CTG) which measures the ATP levels in living cells as the endpoint assay. The CTG cell viability assay is easy to be

performed and very sensitive specially for 3D neurospheres. We measured the time-course of cell viability by CTG at different cell plating densities and using different cell lines. We used the CTG value to calculate the doubling time of each cell density for each cell line. The results showed (Figure 8b) that for monolayer cultures, seeding 1000 cells/well for the R0315 and 3752 cell lines, the doubling times were 2.34 days and 2.22 days respectively. Seeding the pHGG_R0315 and pHGG_3752 cell lines at 2000 cells/well in serum free medium resulted in doubling times 3.12 days and 3.49 days respectively. The doubling time for the two cell lines in both culture conditions are similar. For this reason, we selected 2000 cells/well for 3D neurosphere and 1000 cells/well for 2D monolayer as the optimal seeding densities.

To identify the proper positive and negative controls for the screening assays, we tested 8 cytotoxic compounds including Doxorubicin, Staurosporine, Dasatinib, Anisomycin, 17-AGG, Etoposide, Vincristine, Vorinostat. Staurosporine, a broad-spectrum protein kinase inhibitor showed the lowest IC_{50} for cytotoxic activity (3nM) compared to the control (DMSO) (Figure 9a). The two pHGG cell lines were treated for 7 days with a wide dose range of test the efficacy of Staurosporine (Figure 9b). For subsequent screening studies, staurosporine was used as a positive control and DMSO 0.1% served as the negative control (Figure 9c). The values obtained with the positive and negative control were used to calculate the Z'-factor (Z prime) that assessed the quality of the assay. For the CTG cell viability assay Z' factor was 0.86, a value that confirms that this assay is reliable enough to be used for additional quality-control experiments and subsequent screening studies.

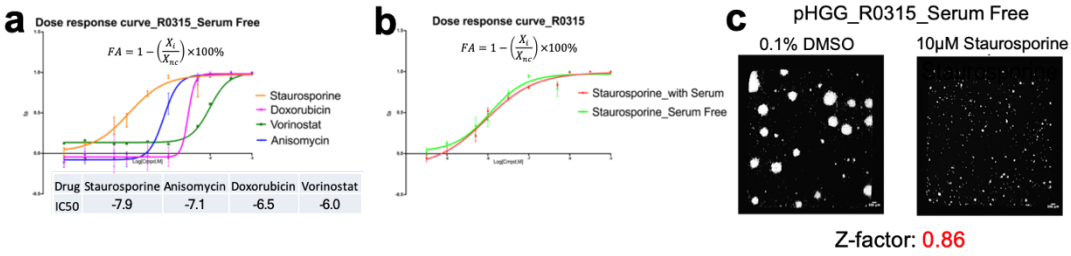

Figure 9. Positive Control Selection for the High Throughput Screening Assays.
(a) Dose response curves and IC_{50} determinations for a panel of cytotoxic compounds tested on pHGG R0315 3D tumor cells in neurosphere culture. Data are mean ± SEM. (b) Dose response curve of Staurosporine for both neurosphere and monolayer culture of pHGG R0315 cells. Data are mean ± SEM. (c) Negative control (DMSO) and positive control (Staurosporine) for high throughput screening assays. pHGG R0315 cells in neurosphere culture were labeled with Draq5 (far red) for 18h prior to imaging (4X).

High Throughput Screen for Small Molecules that Inhibit the Growth and/or Survival of pHGG Tumor Cell Lines

To screen for compounds that inhibit the growth and/or survival of pHGG tumor cell lines, we selected the pHGG R0315 cell line, which is a $PI3K^{mut}$ cell line, and pHGG 3752 which is $PI3K^{wt}$ cell line. Both lines were tested in both 3D neurosphere and 2D monolayer culture. A large panel of cancer-relevant drugs (1863 different agents) were screened for both anti-proliferative and cytotoxic activity in both the pHGG cell lines. All compounds were tested at 10, 1, 0.1 μM and cell viabilities were measure by ATP level as determined by the CellTiter-Glo assay. Dose response curves for each compound were calculated using the CTG values at 72h and the AUC was calculated. As shown in Figure 10a, using an AUC ≥ 0.7 as a criterion for compound activity, only 8.5% of the compounds tested were active. Using an AUC ≥ 0.4 of the tested compounds 17% were active compounds. In order to maximize the possibility of discovering classes of compounds showing synergistic activity, for future studies we used an AUC ≥ 0.4 as the cut-off value for an "active" compound or drug.

We used the responses of both 2 PDOX model cell lines in both 3D neurosphere and 2D

monolayer culture conditions, to subdivide the panel of 1863 test drugs into 4 levels of cytotoxic activity: i) pan-active drugs defined as being active in both cell lines in both neuroshpere and monolayer culture, ii) monolayer-selective drugs active only in cells grown in 2D monolayer culture, iii) neurosphere-selective drugs active only in cells grown in 3D neurosphere culture and iv) inactive drugs that represented all other drugs that were either inactive or showed limited activity in a limited set of experimental models. In this initial single agent screen, there were 224 (12%) pan-active drugs, 40 (2%) 2D monolayer-selective drugs, 17 (1%) 3D neurosphere-selective drugs and 1582 (85%) inactive drugs (Figure 10c). The pharmacological trees (Figure 10b) demonstrated a high degree of similarity in the response of the two different pHGG cell lines, independent of the culture conditions the panel of drugs tested. Five mechanistic clusters: i) genotoxic or cytotoxic drugs, ii) proteotoxic drugs, iii) a subset of targeted kinase inhibitors associated with the PI3K/mTOR pathway, iv) epigenetic regulators and v) checkpoint kinase inhibitors that interfered with mitosis represented the most active groups of compounds (Figure 10b). Among the pan-active compounds (224 drugs) could be grouped into several diverse pharmacologic classes (Described in Figure 10d) including HSP90 inhibitors (11 HSP 90 inhibitors representing 92% of the all the HSP 90 inhibitors tested), proteasome inhibitors (5 proteasome inhibitors representing 83% of all the proteasome inhibitors tested), HDAC inhibitors (18 HDAC inhibitors representing 69% of the HDAC inhibitors tested), PI3K/mTOR/Akt inhibitors (25 PI3K/mTOR/Akt inhibitors representing 32% of the PI3K/mTOR/Akt inhibitors tested) and cell cycle regulators (27 cell cycle regulators representing 57% of the cell cycle regulators tested).

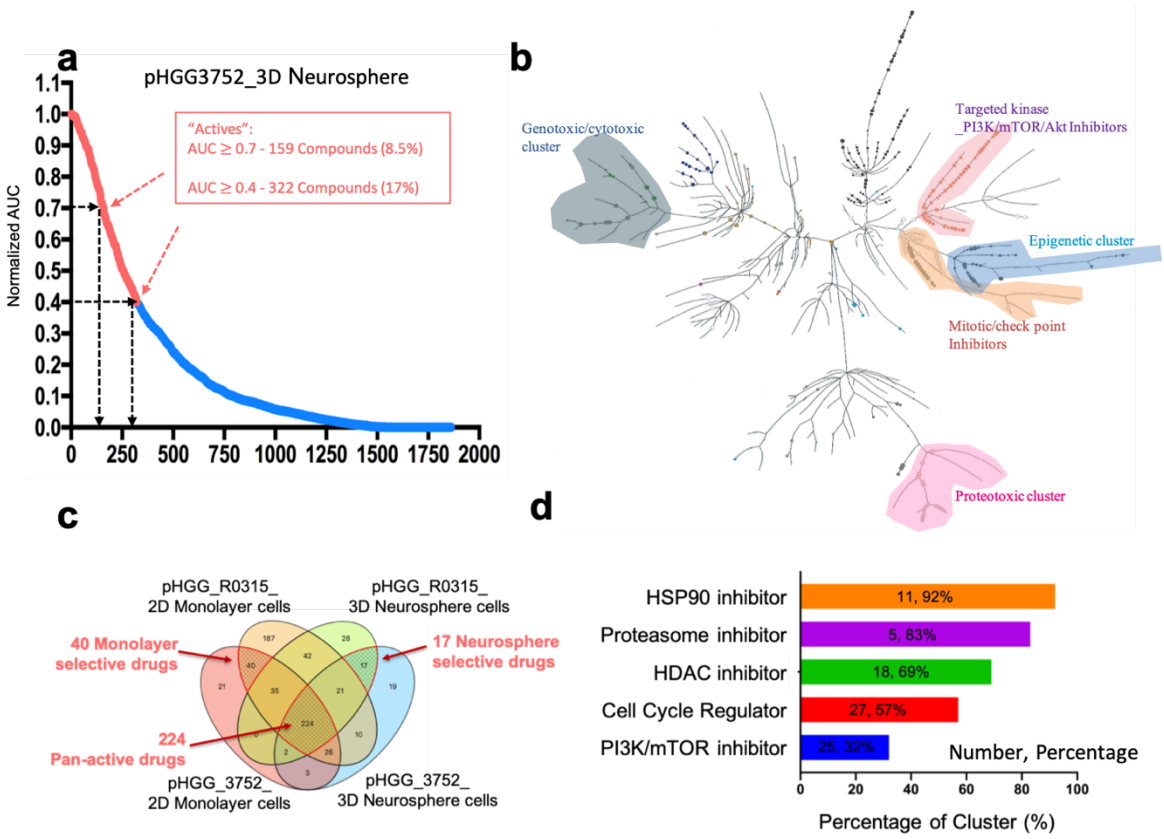

Figure 10. High Throughput Single-Agent Screen of pHGG Cells.
(a) Cell viability. Each column represents a single compound, Normalized AUC were calculated. The red columns indicate AUC is bigger than or equal to 0.4. (b) Effect of mechanistically annotated drugs on cell viability in PDOX pHGG_3752_3D neurosphere cells. Proteotoxic cluster, cytotoxic or genotoxic compounds, HDAC inhibitors, Mitotic or check point include the most active compounds. (c)Venn Diagram of the number of active drugs in the 2 PDOX cell lines in monolayer and neurosphere cell culture condition. (d) The major pharmacologic classes of drugs with the highest representation in the set of pan-active drugs.

Reproducibility of High Throughput Single-Agent Screens

The values obtained with the positive (Staurosporine) and negative control (0.1% DMSO) were used to calculate the Z'-factor (Z prime), a measure of the quality of the assay. The Z primer values for all the 84 plates from 2 different cell lines cultured as both neurospheres and monolayers (21 plates for each cell line in each culture condition) were within the range of 0.5 to 1 with most having Z' prime factors of greater than 0.70 (Figure 11c and Table 2). These determinations indicate that the quality of the data is both consistent and reliable.

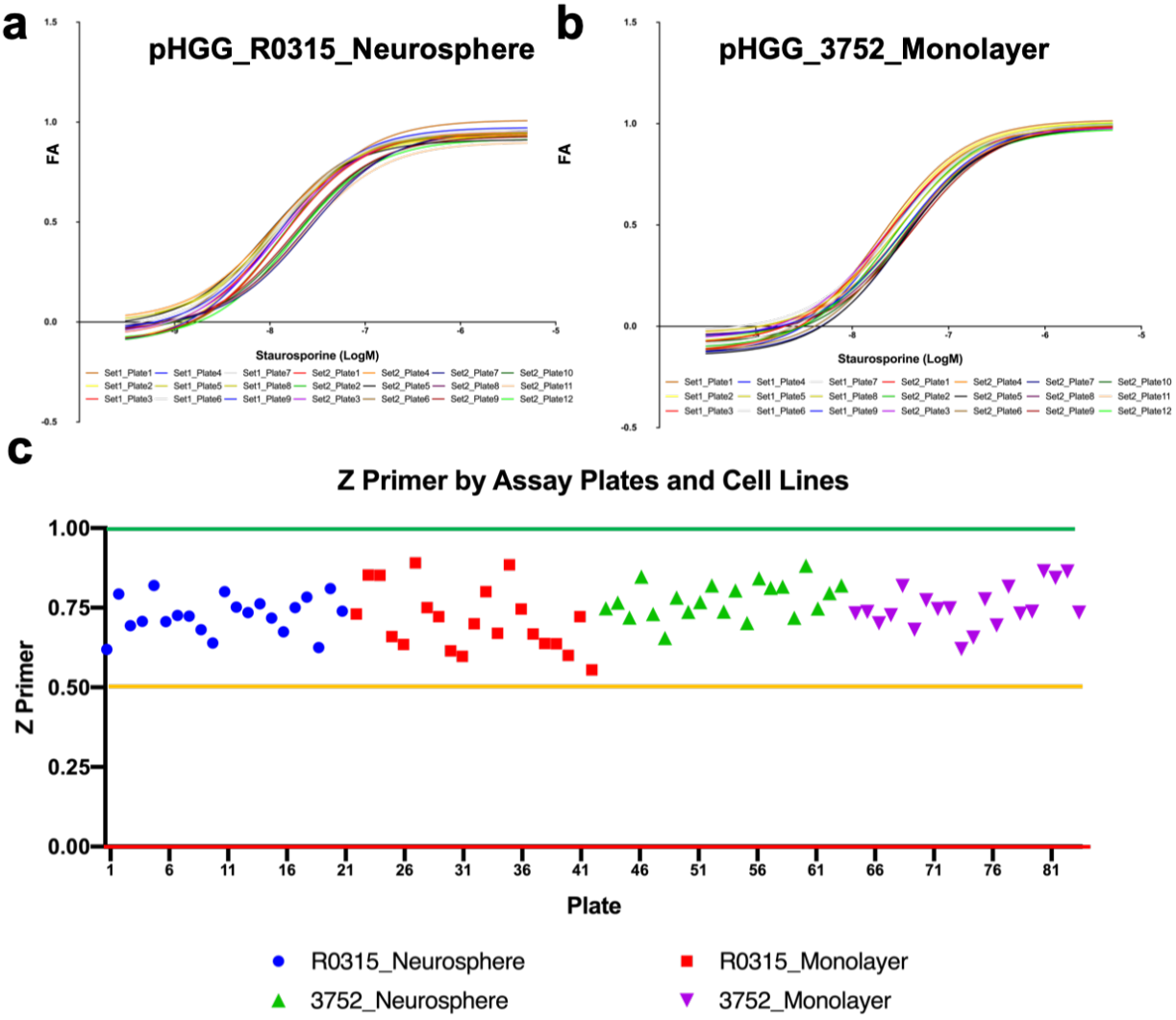

Figure 11. Assay Optimization and Reproducibility Analysis.
(a)(b) Dose-response Curves of Staurosporine (positive control) in different assay plates from 2 sets of independent experiments in pHGG R0315 neurosphere cells (a) and pHGG 3752 monolayer cells (b). X axis indicates the concentration of Staurosporine, and Y axis indicates the fraction affect. Data are from 9 plates from Set1 and 12 plates from Set2. The curves are Nonlin fit curves. (c) Z primer values for total 84 plates from 2 different cell lines cultured in both neurosphere and monolayer (21 plates for each cell line in each culture condition). Z primer between 0 and 0.5 indicates a marginal assay. Z primer between 0.5 and 1.0 indicates an excellent assay.

In addition, the multiple dose-response curves for the positive control (Staurosporine) was used to estimate the reproducibility of the assay using the Minimum Signal Ratio (MSR). As is illustrated in Figure 11a-11b, the dose-response curves of Staurosporine from 21 plates from 2 independent sets of data from 2 different cell lines demonstrated that the curves are highly reproducible with some evidence that the results obtained with monolayer cells are slightly

tighter compared to the neurosphere data. The observation indicated that the reproducibility of the monolayer assays is somewhat better than that of the neurosphere assays. The calculated MSR data (Table 2) demonstrated that most of the MSR data from monolayer assays are less than 3.0, which indicates the screen data are reproducible and stable. While the MSR data from the neurosphere assays were between 3.0-5.0. However, the Log (IC_{50}) is close enough between the two assays to demonstrate that the results obtained can be trusted. The lower reproducibility of the neurosphere cultures compared to the monolayers may be due to the complex biological features of neurosphere cells, including the difficulty in accurately determining the number of cells in neurosphere, heterogeneity between the interior and surface of the neurospheres and other factors.

Table 2. Assay Variability by Minimum Significant Ratio (MSR) and Z' Primer.

	Cell line_Data Set	MSR	Z Primer	Log (IC_{50})
Within-Run	R0315_Neurosphere_Set1	4.44	0.72 ± 0.06	-7.92 ± 0.05
	R0315_Neurosphere_Set2	3.25	0.73 ± 0.06	-7.86 ± 0.03
	R0315_Monolayer_Set1	2.91	0.75 ± 0.10	-7.55± 0.03
	R0315_Monolayer_Set2	3.03	0.68± 0.09	-7.54 ± 0.03
	3752_Neurosphere_Set1	3.67	0.75 ± 0.05	-7.74 ± 0.04
	3752_Neurosphere_Set2	4.85	0.79 ± 0.05	-7.78± 0.06

Table 2. Continued

	Cell line_Data Set	MSR	Z Primer	Log (IC_{50})
	3752_Monolayer_Set1	2.78	0.74 ± 0.04	-7.58 ± 0.02
	3752_Monolayer_Set2	2.40	0.77 ± 0.08	-7.56 ± 0.02
Between-Run	R0315_Neurosphere	4.49	0.73 ± 0.06	-7.89 ± 0.05
	R0315_Monolayer	2.92	0.71 ± 0.10	-7.54 ± 0.03
	3752_Neurosphere	4.68	0.77 ± 0.06	-7.76 ± 0.06
	3752_Monolayer	2.63	0.75 ± 0.07	-7.56 ± 0.02

Identification of Drug Combinations Exhibiting Synergistic Effect in Killing pHGG Tumor Cell lines

The single agent screen identified 224 drugs that were classified as "pan-active drugs, meaning they exhibited cytotoxic activity against both pHGG cell lines independent of whether they were cultured in monolayer of neurosphere culture conditions. Since these pan-active drugs fell in to 5 major pharmacologic classes, we selected 2 prototypic representatives from each of these 5 classes and tested them in pairwise combination for synergistic activity. These combinatorial screens were structured as 6 doses by 6 doses combination screens carried out with 45 pairs of compounds in pHGG 3752 cells grown in monolayer culture. By using the Bliss Independence Model, we set a threshold of the Over-Bliss value $\geq$ 0.3 as indicating synergy and

if associated with a fa value ≥ 0.4 as reflecting "synergistic lethality". Among these 45 combinatorial pairs tested in the primary screen, 14 pairs exhibited synergistic cytotoxic activity in the 3752cell line monolayer cells. This value of synergistic activity reflects 31% of the compounds tested. As is illustrated in Figure 12a, the synergistic combinations were not randomly distributed but were grouped into three specific mechanistic classes including: i) HDAC inhibitors with HSP90 inhibitors, ii) HDAC inhibitors with proteasome inhibitors, iii) HDAC inhibitors with PI3K/mTOR inhibitors. The combinations of classes on pan-active compounds was much more likely than other combinations of drugs to result in synergistic lethal activity. For instance, only 17% of the combinations of drugs in which one component was a pan-active component and the other was selectively active in monolayer cells showed any evidence of synergistic activity. No evidence of synergy was detected in any of the combinations of pan-active compounds with compounds that were selectively active in pHGG cells grown in neurosphere culture conditions.

We carried out secondary combinatorial screens of all combinations found to exhibit synergistic activity in the primary combinatorial screening assays based on the criteria of Over-Bliss greater than 0.3 and the fa greater than 0.4. These secondary combinatorial screens the activity of 10 by 10 doses combinations for each of the active components was tested in both R0315 and 3752 pHGG cell lines cultured as both neurospehere and monolayer cultures. We again used the criteria for "synergistic lethality" as an Over-Bliss value of > 0.3 and a fa value ≥ 0.4. The results of these secondary screens confirmed only 9% of pan-active drugs combinations showed "Synergistic Lethality". Among the combinations of drugs showing the most frequent synergistic lethality activity, combinations of HDAC inhibitors (Panobinostat, JNJ-26481585) and proteasome inhibitors (CEP-18770, MLN 2238) exhibited the most frequent synergistic

activity (seen Figure 12a). Comparison of the dose response curves of the proteasome inhibitor CEP-18770 and HDAC inhibitor JNJ-26481585 alone and in combination (Figure 12b) shows that the addition of the HDAC inhibitor to the proteasome inhibitor results in a half-log left-shift of the IC_{50} compared to the IC_{50} of the proteasome inhibitor only. These results demonstrate that combinations of proteasome inhibitors and HDAC inhibitors synergize to inhibit the growth of pHGG tumor cells.

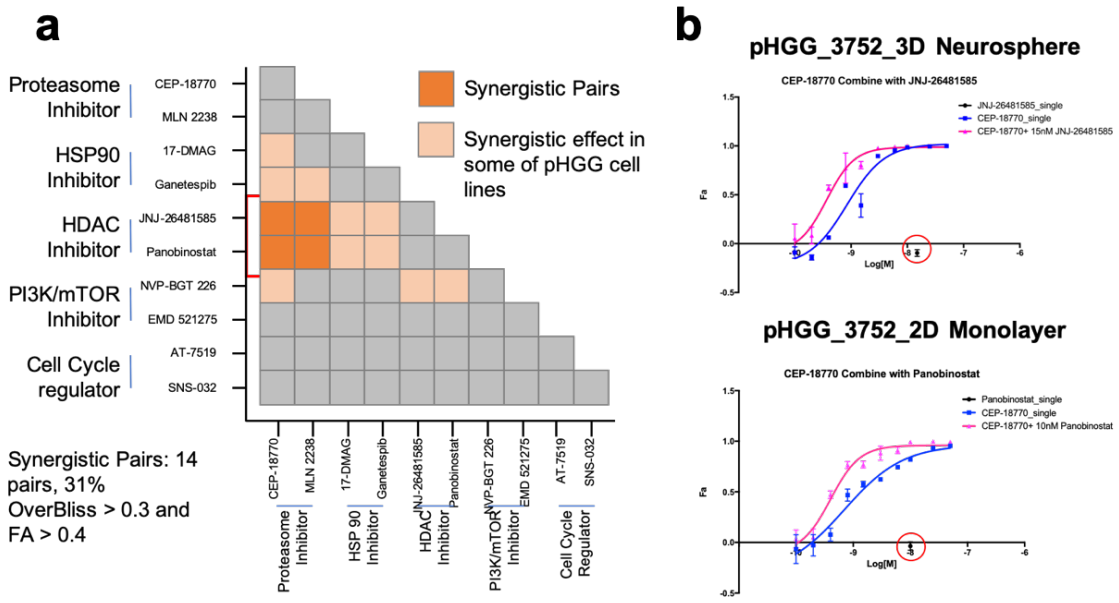

Figure 12. Combinatorial Screens of Combinations of Classes of Pan-Active Compounds in the Inhibition of Growth of pHGG Cells.
(a) Combinatorial matrix of the activity 45 pairs of pan-active compounds combines with pan-active compounds. Two representatives of each of 5 pharmacologic classes of pan-active compounds were combined and tested for cytotoxic activity against pHGG cells in monolayer culture. Quantitative indices of drug interaction (synergy, additivity or antagonism) were calculated based on the Bliss independence model. Dark orange squares indicate significant synergistic activity. Light orange square indicates significant synergistic activity that was selective for the cell line or culture condition tested. Grey squares reflect no evidence of synergy. (b) Dose response curves for the combination of a proteasome inhibitor with or without the addition of an HDAC inhibitor. Data are mean ± SEM.

Secondary screens of the combinations of drugs that included a representative of the classes of pan-active compounds and compounds selective for activity in monolayer (as opposed

to neurosphere) that showed synergistic activity in the pHGG 3752 monolayer assays (the 17% active pairs) demonstrated that none of these combinations showed synergistic activity in both pHGG cell lines and either monolayer or neurosphere culture conditions. All of the synergistic combinatorial pairs were selective for a particular cell type or a particular culture condition (Seen in Figure 13).

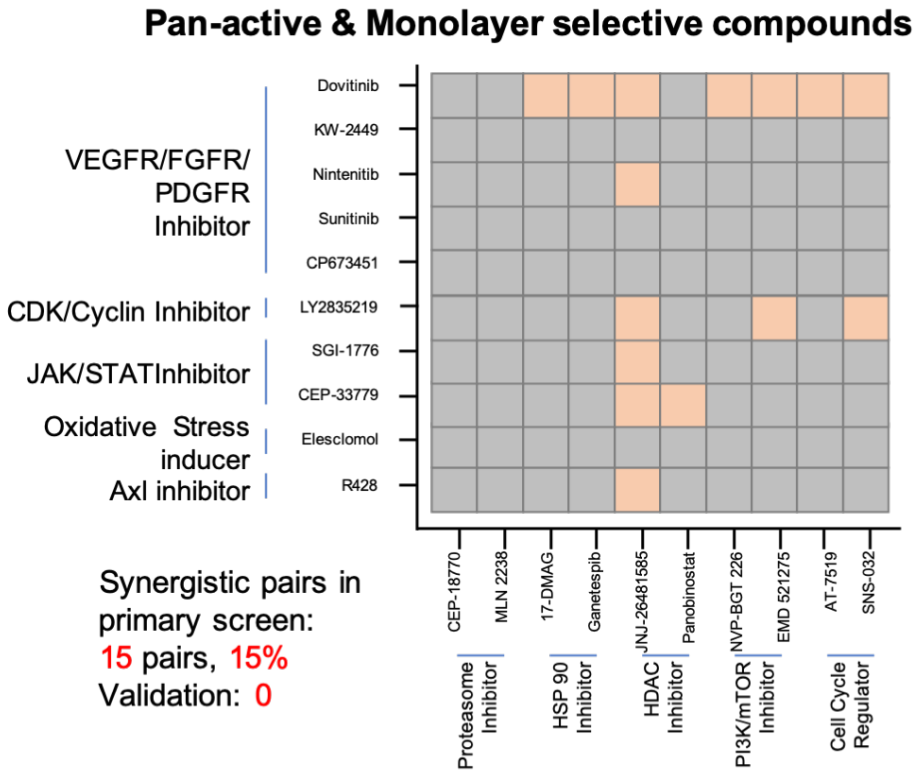

Figure 13. Combinatorial Screen of Pan-Active Compounds Combined with Representative Drugs from Classes of Compounds Exhibiting Selective Activity for pHGG Cells Grown in Monolayer Culture. Combinatorial matrix of synergistic activity of 100 pairs of pan-active compounds combined with representatives of the pharmacologic classes of compounds selectively active in pHGG cells grown in monolayer culture. Quantitative indices of drug interaction (synergy, additivity or antagonism) were generated based on the Bliss independence model. Dark orange square indicates significant synergistic activity in 2 different cell lines in both neurosphere and monolayer cultures. Light orange square indicates significant synergistic activity in only some of the cell lines screened. Grey squares reflect no evidence of synergy.

Although the combination of HDAC and proteasomal inhibitors produced significant synergistic cytotoxic activity in pHGG cells we chose not to pursue a detailed investigation of the mechanism of this synergistic effect because both agents inhibit multiple cell regulatory pathways complicating the development of a clear understanding of their mechanism of action. We chose therefore to review our combinatorial screening results with the goal of identifying synergistic combinations of targeted agents with well-defined mechanisms of action that might provide insides into the molecular mechanisms that accounted for their synergistic activity. One of the most promising pharmacologic classes that had been identified in our initial single agent screening studies was the class of inhibitors that targeted cell cycle activity. Studies by a colleague, Dr. Lei Guo, who was also searching for synergistic combinations of drugs that targeted pediatric brain cancers, in his case ependymomas, had also suggested that the class of cell cycle inhibitors exhibited synergistic activity in PDOX cells from patients with ependymoma. To explore this interaction in the context of pHGG cells, we examined the activity of the Wee1 inhibitor MK-1775 and Chk1 inhibitors (AZD7762 and MK-8776) in both RO315 and 3752 cells in both monolayer and neurosphere culture. The combinatorial screens were carried out with 10 concentrations (2-fold dilutions) of each compound ranging from 1 μM to 2 nM. Cells were cultured for 7 days and survival was assessed using the Cell-Titer Go assay. For the monolayer cultures, both the cell count and ATP level were assessed. For the neurospheres, ATP levels were measured using CellTiter-Glo. As shown in the Figure 14, combinations of the two inhibitors produced a much greater reduction in cell number compared to DMSO control) than either of the drugs alone. As shown in the Figure 15, both the combinations of MK 1775 with AZD 7762 and MK 1775 with MK 8776 exhibited strong synergy in suppressing the survival of pHGG neurosphere cells. For example, MK 1775 alone had an IC_{50} of 1 uM, whereas

the addition of 62 nM AZD7762 lowered the IC_{50} to 33 nM. Similarly, the addition of 125 nM MK8776 resulted in the lowering of the IC_{50} of MK 1775 from 1 uM to 100 nM. Put all together, the combination of Wee1i and Chk1i exhibits significantly synergistic effect on suppressing the tumor growth in pHGG cells in both neurosphere and monolayer culture conditions. The studies on the synergistic effects of dual inhibition of Wee1 and Chk1 were reported in acute myeloid leukemia, lung cancer, prostate cancer and ovarian cancer [90-93] but not in the pediatric high-grade gliomas. This raise up the question that how this synergistic effect happened in pHGG. The next step for us was to identify the mechanism of action of combinations of Wee1 inhibitors and Chk1 inhibitors with the goal of understanding the molecular basis for their synergistic cytotoxic activity in pHGG cells.

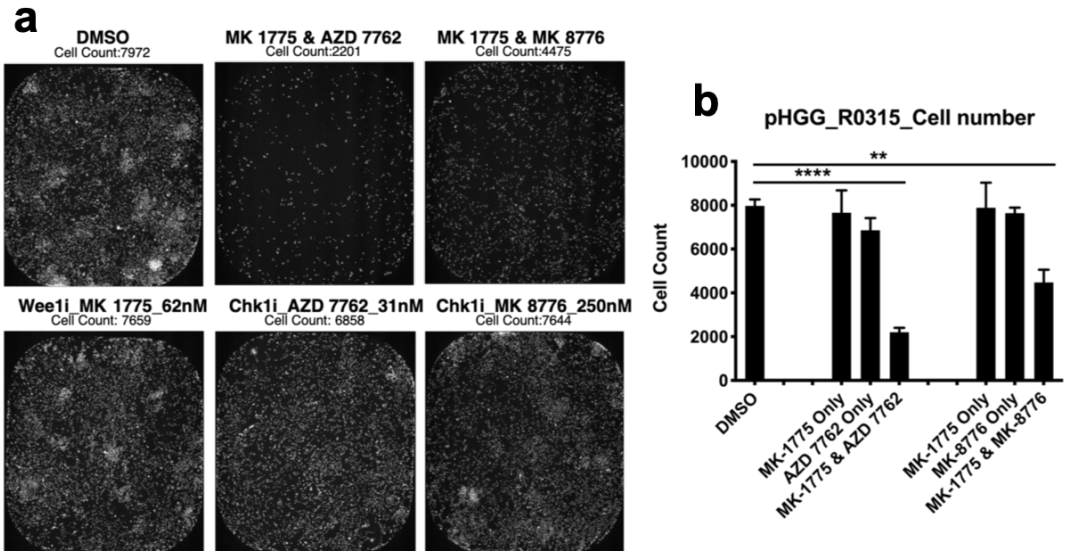

Figure 14. Combinatorial Activity of Combination of a Wee1 Inhibitor and Chk1 Inhibitors for pHGG R0315 Cells in Monolayer Culture.
(a-b) Representative images (a) and cell count (b) by nuclear staining after 7 days treatment of DMSO, MK 1775 (Wee1 inhibitor), AZD 7762 (Chk1 inhibitor), MK 8776 (Chk1 inhibitor), combination of MK 1775 and AZD 7762, combination of MK 1775 and MK 8776 in R0315 2D monolayer cells. Cells were fixed with 4% PFA and nuclei were stained with DAPI. Data are mean ± SEM. *, $P < 0.05$; **, $P < 0.01$; ***, $P < 0.001$; ****, $P < 0.0001$.

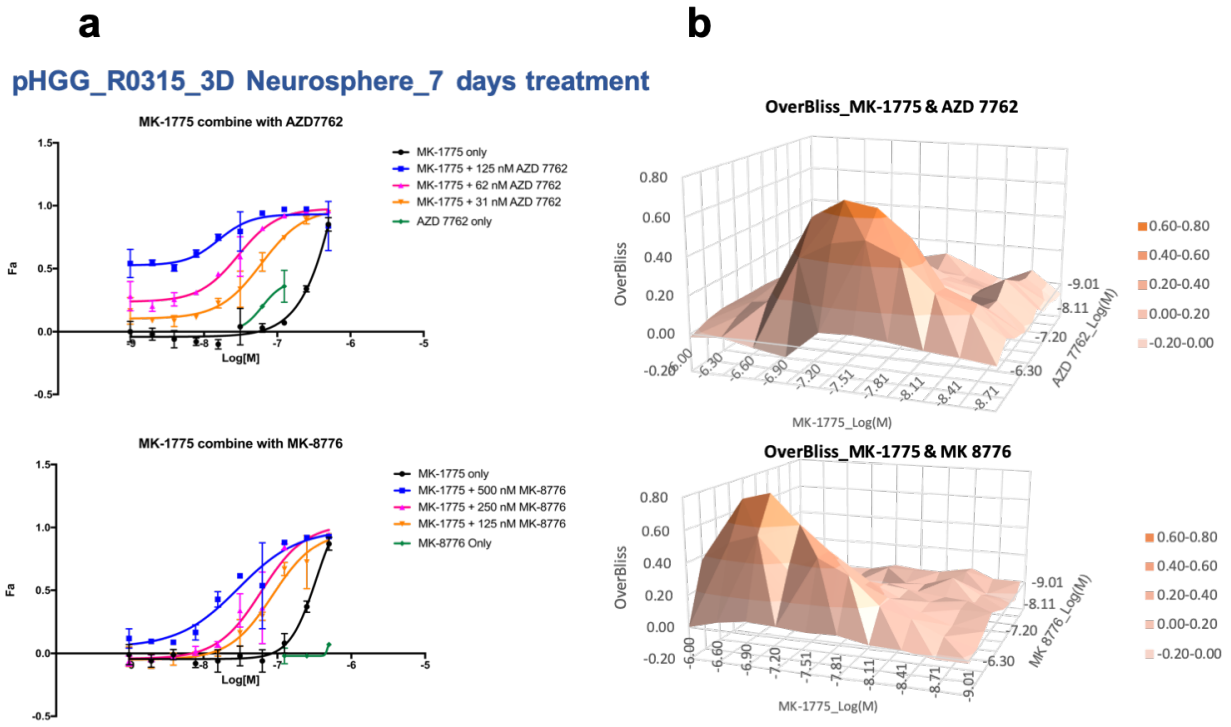

Figure 15. Combinatorial Activity of Combination of a Wee1 Inhibitor and Chk1 Inhibitors for pHGG R0315 Cells in Neurosphere Culture.
(a) Dose Response Curves showing the response to Wee1 inhibitor (MK 1775) combining with different concentrations of Chk1 inhibitors (AZD 7762, MK-8776). The black curves indicated the dose response of single Wee1 inhibitor treatment and the green curves indicated the dose response of single Chk1 inhibitor treatment. The blue, pink and orange curves indicate the response of combining Wee1 inhibitor with different concentration of Chk1 inhibitors. X axis indicates drug concentration and Y axis indicated the drug response (fa). Data are mean ± SEM. (b) Surface chart showing the combinatorial activities of a Wee1 inhibitor combining with 2 Chk1 inhibitors. X and Y axis indicates 10 drug concentrations of drugs used in the specific drug combination, and Z axis is the Calculated Over-Bliss value which indicated the combinatorial activities. The darker the orange is, the more synergistic effect of the combination with specific concentrations of each drug has.

Cytotoxicity of Drug Combinatorial Pairs in Normal Astrocyte Cell line

To determine whether the synergistic cytotoxic activity of Chk1/Wee1 combinations was selective for pHGG cells or was a general property of both normal and malignant neuronal cells, we compared the effect of combinations of the Wee1 and chk1 inhibitors on the viability of the two pHGG cell lines and two normal human astrocyte cell lines by calculating the normalized Growth Rate for each cell line. As seen in Figure 16, the combination of Wee1 inhibitor MK 1775 and the two Chk1 inhibitors inhibited the growth of normal astrocytes at concentrations

much higher than those required to inhibit pHGG tumor cells. For example, the IC_{50} for the inhibition of growth of normal astrocytes by the combination of MK 1775 and 31nM AZD 7762 is 494 nM whereas the IC_{50} for pHGG cells tumor is 100 nM. The IC_{50} for the inhibition of astrocyte growth by MK-1775 and 250 nM MK-8776 is 200 nM, while the IC_{50} pHGG cells is about 60 nM. Concentrations of the enzyme inhibitors that inhibited tumor cell survival by 50% had no effect on astrocytes. For example, 63 nM MK 1775 combined with 31 nM AZD7762 inhibited tumor cell survival by 75% but it had no effect on Astrocyte (the GR value is 1, see Figure 16a, 16c) or 63 nM MK 1775 combined with 250 nM MK 8776 inhibited tumor cell survival by 68% but had no effect on Astrocyte (the GR value is 1, see Figure 16b, 16c). These results demonstrate that the combination of Wee1 and Chk1 inhibitors selectively inhibit survival of pHGG tumor cells when compared to normal astrocytes.

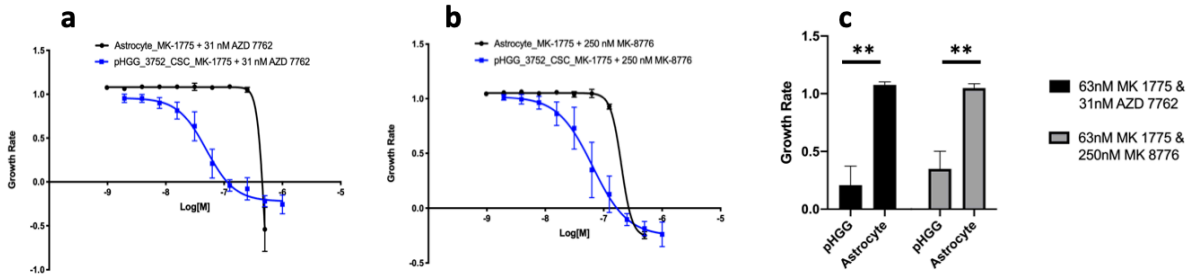

Figure 16. Cytotoxic Effect of a Wee1 Inhibitor and Chk1 Inhibitors on the Normal Astrocyte Cells and pHGG Tumor Cells.

(a) (b) Dose Response Curves of normalized Growth rate for a Wee1 inhibitor (MK-1775) combined with Chk1 inhibitors (AZD 7762, MK-8776) in both pHGG tumor cells and normal Astrocyte cells. Error bars show mean ± SEM, n ≥ 3 independent experiments. (b) Bar chart summarizing the Normalized Growth Rate of combination of a Wee1 inhibitor MK 1775 (63 nM) and Chk1 inhibitor AZD 7762 (31 nM) and Combination of MK 1775 (63 nM) and Chk1 inhibitor MK 8776 (250 nM) in both normal Astrocyte cell line and pHGG 3752 neurosphere cell line. Error bars show mean ± SEM, n ≥ 3 independent experiments; *, $P < 0.05$; **, $P < 0.01$; ***, $P < 0.001$.

Discussion

Despite aggressive multimodal therapy, the prognosis for pediatric patient with high

grade gliomas [2, 3] remains extremely poor. In this study, we developed a strategy to identify more effective therapies for this disease which is using the power of high-throughput targeted combinatorial drug screening, to evaluate the combinatorial activity of large numbers of combinations of therapeutically useful drugs. It is likely that combination therapies that exhibit synergistic lethality may give a wider therapeutic index making them less toxic and safer to use. Although high-throughput screening has been used to search for new therapies for other cancers [45, 84], the approach has not been used extensively for pHGG. By using our PDOX models, we have been able to identify drug combinations that exhibit synergistic lethality and that may provide the basis for the development of new therapies for this extremely aggressive disease.

There are some studies in the literature that have used established cell lines and monolayer cell lines to search for new combinatorial therapies. The model system we have used for our studies take advantage of the availability of patient derived orthotopic xenograft cells that replicate the histology and gene expression profiles of the patients' original tumors. These PDOX models also have maintained the pools of cancer stem cells during their in *vivo* propagation. By using this model, which includes subsets of tumor cells we anticipate being able to identify drugs that would be effective against a large population of tumor cells. Using these PDOX models and high throughput screening technologies, we found 224 active compounds that significantly reduced survival of pHGG cells in both neurosphere and monolayer culture. Based on the pharmacologic classification of the active drugs we observed that the two independent tumor cell models that we used exhibited very specific drug response profiles. This observation suggests that the pattern of response to the drugs is not associated with specific gene mutations or aberrations since the two pHGG cell lines are derived from genetically distinct tumors. Furthermore the 224 pan-active compounds identified by the single agent screen could be

grouped into 5 mechanistically-annotated pharmacologic clusters. The clusters identified by the screening studies, proteasome inhibitors, HDAC inhibitors, cell cycle regulators, HSP 90 inhibitors and PI3K/mTOR pathway inhibitors include many drugs that are active in many other cancers. Many of them are currently in clinical trials for a wide range of cancers and other diseases [74, 94-100]. HDAC inhibitor for example not only act on and modify histones, but also are involved in many other cellular processes including tumor progression, cell cycle control, apoptosis, angiogenesis and cell invasion [95]. Thus, HDAC inhibitors exert multiple cellular effects and their mechanism of action can include cell cycle arrest, the activation of apoptotic pathways, the initiation of DNA damage and repair, the generation of reactive oxygen species (ROS), angiogenesis and proteotoxicity. Some HDAC inhibitors such as Vorinostat (SAHA, Zolina) was FDA approved in 2006 for use in combination with temozolomide and radiotherapy for treating patients with newly diagnosed glioblastoma multiforme (GBM).

By doing the combinatorial screen of these different strategies of combination, we found the multifunctional compounds combining multifunction compounds are more frequently having synergistic effect on inhibiting the cell survival of pHGG tumor cells. For example, combination of Proteasome inhibitors and HDAC inhibitors gave a significant synergistic effect on inhibiting the survival of pHGG tumor cells. Recent studies have demonstrated that the HDAC inhibitors induce synergistic levels of apoptosis when given in combination with the proteasome inhibitor like bortezomib induce synergistic levels of apoptosis. Clinical trials to evaluate the effect of this combination is ongoing [101]. Since both proteasome inhibitor and HDAC inhibitors impact similar pathways such as ER stress and apoptosis, they both induce ROS production and can inhibit angiogenesis. Since these cellular processes play a very important role in the survival, maintenance and metabolism of pediatric HGG, the combined effects of both proteasome and

HDAC inhibitors could be a target for treatment strategies. However, it remains to be established how toxic these combinations may be to normal cells.

Another combination that exhibited synergistic activity was the combination of an HDAC inhibitor combined with PI3K pathway inhibitor. HDAC and PI3K antagonists have been shown to cooperate to inhibit the growth of MYC-driven medulloblastoma (MB) [98]. The HDAC inhibitor induces expression of FOXO1, and the PI3K/AKT signaling pathway regulates the nuclear location of FOXO1, so PI3K pathways inhibitors synergized with HDAC inhibitors to activate FOXO1 and to inhibit the growth of MYC-driven MB [98]. The combination of HDAC and PI3K inhibitors could represent a new avenue for the treatment of pHGG.

In our studies, the combination of pan-active compounds had the highest frequency of exhibiting synergistic lethality. Using this strategy, we expanded our combinatorial screen and found that Wee1 inhibitor and Chk1 inhibitors showed a selectively synergistic effect on inhibiting survival of pHGG tumor cell lines. Wee1 and Chk1 are key regulators of the damage surveillance pathways that maintain genome integrity [102, 103]. They are also involved in cell cycle regulation and DNA damage repair. The combined inhibition of Wee1 and Chk1 has been reported to synergistically enhance therapeutic activity in melanoma, leukemia, lung, prostate and ovarian cancers [90, 91, 104-106]. The combination of inhibition of Wee1 and Chk1 was surprisingly selective, impacting cancer cells to a much greater degree than normal cells. Concentrations of the Wee1 inhibitor and the Chk1 inhibitors have effect on pHGG tumor cells didn't affect the cell growth in normal Astrocyte. Thus, the combination of Wee1 and Chk1 could be a potential treatment for pHGG.

Due to the difficulties in the studying mechanisms responsible for synergistic effect of two multifunctional drugs (HDACi and Proteasome inhibitor) whereas Wee1 and Chk1

inhibitors are targeted therapies, the next step in our studies will be to focus on studying the mechanism of action of combinations of Wee1 inhibitors and Chk1 inhibitors with the goal of understanding the molecular basis for their synergistic cytotoxic activity in pHGG cells.

CHAPTER III

WEE1 AND CHK1 ANTAGONISTS COOPERATE TO INDUCE SYNERGISTIC LETHALITY IN PEDIATRIC HIGH-GRADE GLIOMA PDOX CELL LINES

Introduction

Maintenance of genome integrity is essential for preventing the development of diseases related to genomic instability such as cancer. One of the major threats to genome integrity is DNA damage [102, 107]. To counteract the threats posed by DNA damage, mammalian cells have developed a complex network of DNA damage surveillance pathways that maintain genome integrity. Wee1 and Chk1 are two enzymes that play a key role as regulators of DNA damage surveillance pathways. Chk1 regulates the activity of the S phase and G2 checkpoints [108, 109] of the cell cycle as well as replication initiation and the stability of the replication fork [110-112]. Chk1 also controls the mitotic entry in normal circumstances cells and plays an important role in the function of the mitotic spindle checkpoint [113]. Wee1 has an essential role in regulating the normal cell cycle especially in regulating the G2/M transition [114]. Wee1 is a protein kinase that is involved in checkpoint regulation in response to DNA damage and/or replication stress. It arrests cell cycle progression in S and G2 phase by adding an inhibitory phosphorylation (Tyr15) to cyclin-dependent kinases CDK2 and CDK1, respectively [114, 115]. The biological processes regulated by Wee1 and Chk1 kinases are highly dependent on the activity of CDK's.

Blocking S and G2 DNA damage checkpoints represent a promising antitumor therapeutic strategy. Due to aberrant p53 signaling, which abrogates the G1 checkpoint, many cancer cells demonstrate an increased dependence on S and G2 DNA damage checkpoints. Even

in p53 wild type cells, the inhibition of Chk1 or Wee1 induces high levels of replication stress due to unscheduled initiation of DNA replication an effect that can contribute cell death. Indeed, potent inhibitors of Chk1, Wee1 which are key component of the S and G2 checkpoints, are under clinical evaluation. Not only much greater effect has been seen when combining the Wee1 or Chk1 inhibitors with DNA damage agents, HSP90 inhibitors and or other cell cycle regulatory proteins [103, 116-118], but also the combination of Wee1 and Chk1 inhibition showed significant synergistic effect on some cancer cell lines [117, 119]. Strong rationale exists for combined therapy with Wee1 and Chk1 inhibitors. Wee1 is overexpressed and associated with patient outcomes in many cancer types, including ovarian, glioblastoma and breast cancer. Chk1 has also found to be overexpressed in a variety of human tumors including breast, colon, liver, gastric, some subtype of neuroblastoma, etc. Some research demonstrated enhanced activation of Chk1 may contribute to therapy resistance including cancer stem cells from glioblastoma, prostate and lung NSCLC to chemotherapy or radiotherapy as well as other anticancer therapies, for instance, HDAC inhibitors. At the same time, both of the Wee1i and Chk1i can abrogate G2 arrest, causing cells with unrepaired DNA damage to enter into mitosis and undergo mitotic catastrophe. Wee1i and Chk1i have demonstrated antitumor activity in a number of preclinical models including acute myeloid leukemia, lung cancer, prostate cancer and ovarian cancer [90-93]. However, there is no information available to date on the expression of Wee1 and Chk1 in pediatric high-grade gliomas and the efficacy of combination of Wee1i and Chk1i in pHGG remains to be fully elucidated.

In our study we have investigated the cytotoxic activity in pHGG cell lines (in monolayer or neurosphere culture) achieved by combining a Wee1 inhibitor (MK 1775) with Chk1 inhibitors (AZD7762 or MK-8776). We found that combinations of the two classes of inhibitors

had much greater cytotoxic activity than either agent alone. The goal of the studies described in this Chapter is to identify the underlying molecular mechanisms that contribute to this selective and synergistic activity. Since inhibitors of both Wee1 and Chk1 play important roles in promoting DNA damage, regulating cell cycle progression, and the initiation and stability of replication fork our studies investigated these aspects including cell cycle profile, DNA damage and replication fork stability.

Materials and Methods

Reagents/Solutions

Propidium iodide (Thermo Fisher Scientific, P1304MP), IdU (Sigma-Aldrich, I7125), CIdU (Sigma-Aldrich, C6891), ProLong Gold anti-fade reagent (Thermo Fisher Scientific, Invitrogen, P36935), SDS (Sigma-Aldrich, 436143), Tris-HCl (Promega, H5121), EDTA (Sigma-Aldrich, 1233508), Seahorse XF Real-Time ATP Rate Assay Kit (Agilent, 103592-100).

Antibodies

p-Histone H2A.X (Ser139) antibody conjugated with Alexa Fluor-488 (Cell Signaling, #9719), Mouse anti-BrdU (BD Biosciences,347580), Rat-anti-BrdU (Abcam 6326), Alexa-488 anti-rat antibody, Alexa-594 anti-mouse antibody, phospho-Histone H3 (Ser-10) antibody (Cy5 conjugate, Millopore 16-218), cleaved caspase-3 (BD Bioscience, 559565), Alexa Flour 555 conjugated anti-rabbit (Molecular Probe, Life Technologies).

Cell Culture and Treatment

As described in Material and Methods in the Chapter II.

Cell Staining, Imaging, and Viability Assay

As described in Material and Methods in the Chapter II.

Cell Viability Assay

As described in Material and Methods in the Chapter II.

DNA Damage Marker Stain

Cells were collected by centrifugation and the supernatant was aspirated. The cells were resuspended in 0.5 ml-1 ml PBS and formaldehyde was added to obtain a final concentration of 4%. Cells were fixed for 15 minutes at room temperature and then washed with PBS. Cells were permeabilized by the addition of ice cold 90% methanol for 20 min. Permeabilized cells were stained with a 1:200 dilution of phosphor-Histone H2A.X (Ser139) antibody conjugated with Alexa Fluor-488 (Cell Signaling, #9719) for 1h in 37°C, followed by washing in PBS. Cells were resuspended in PBS and analyzed by flow cytometry with gates created to exclude non-specific staining. Statistical analyses were performed using FlowJo and Prism 6 (GraphPad) software.

Cell Cycle Profile

For neurosphere cells, single cells were made by pipetting 20 times and using 40 μm cell strainer to remove big clusters. Single stem-cell like cells were spun down 1200 rpm for 3 minutes and the supernatant was removed. For monolayer cultures, cells were trypsinized by Trypsin 0.25% for 2 minutes and spun down 1200 rpm for 3 min and supernatant was removed. Single cells were fixed in cold 70% ethanol for at least 30min followed by washing with PBS twice and staining with propidium iodide (Thermo Fisher Scientific, P1304MP)/RNase for 20 minutes at room temperature. Cell cycle analysis was performed on a BD FACS Canto flow cytometer with gates created to exclude cellular debris and cell doublets. The results were quantified as the average of at least three independent experiments ± SEM per time point. Statistical analyses were performed using FlowJo and Prism 6 (GraphPad) software.

DNA Fiber Assay

Cells were plated and treated with DMSO, MK 1775, AZD 7762, MK 8776, a combination of MK 1775 and AZD 7762 or a combination of MK 1775 and MK 8776 for 72h. After the treatment, cells were labeled with IdU (5-Iodo-2′-deoxyuridine, 25 μM, Sigma-Aldrich, I7125) for 30 min, washed 3 times with PBS, labeled with CIdU (5-Chloro-2′-deoxyuridine, 250 μM, Sigma-Aldrich, C6891) for an additional 30 minutes, and then washed with PBS 3 times. DNA fibers were spread as described in Figure 17. Briefly, cells were diluted 1:5 with unlabeled cells, and 2.5 μl of the cells suspended in PBS (cell density: $\sim 10^6$ cell/ml) was spotted onto a glass slide. After briefly drying at room temperature for 4 minutes, 7.5 μl of spreading buffer (0.5% SDS, 200 mM Tris-HCl pH 7.4, 50 mM EDTA) was dropped on the cells and incubated for 6 min. Slides were tilted (∼15°) to spread lysed cells across the slide. Slides were air dried, fixed in methanol: acetic acid (3:1) for 15 min, and then stored at 4°C overnight before staining. IdU and CldU tracks were detected using Mouse anti-BrdU (BD Biosciences,347580) (1:25) and Rat-anti-BrdU (Abcam 6326) (1:200) for 1hr in room temperature, followed by Alexa-488 anti-rat antibody (1:200) and Alexa-594 anti-mouse antibody (1:200) for 1hr at room temperature followed by mounting with ProLong Gold anti-fade reagent (Thermo Fisher Scientific, Invitrogen, P36935). Fibers were imaged at 60x oil with DeltaVision Elite (Deconvolution microscope). Imaging analysis and DNA fiber length measured by ImageJ. At least 500 fibers for each treatment were analyzed. Statistical analyses were performed using a two-tailed Mann-Whitney test with Prism 6 (GraphPad) software.

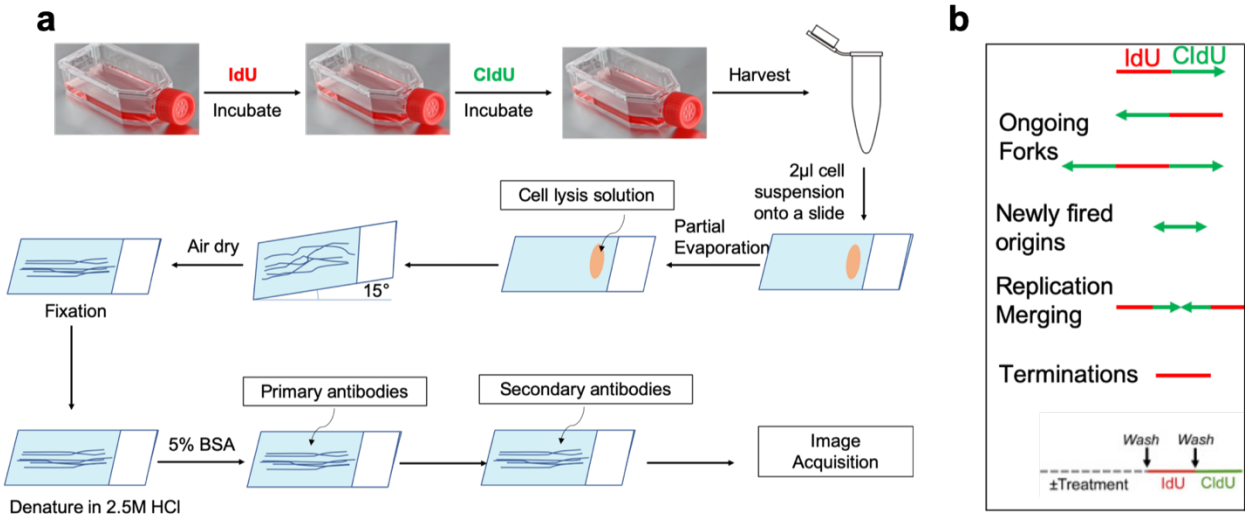

Figure 17. DNA Fiber Assay.
(a) Schematic overview of the protocol (see text for details). (b) Representative kinds of DNA fibers identified by using the protocol. The images showed marked replication structures: ongoing replication; origin of replication fired during first pulse of labelling; origin of replication fired during second pulse of labelling; replication merging; stalled fork or termination during first pulse.

Metabolic Extracellular Flux Analysis

The Seahorse XF96 Analyzer (Seahorse Bioscience, Agilent) was used to measure oxygen consumption rate (OCR), extracellular acidification rate (ECAR) and proton efflux rate (PER) in pHGG tumor cells. Cells were plated at 1.5×10^4/well in 80 µL culture medium in 96-well plates and treated with DMSO, MK 1775, AZD 7762, MK 88776, a combination of MK 1775 and AZD 7765 or a combination of MK 1775 and MK 8776 for 16 hours. For a typical bioenergetic profile, we used oligomycin to block ATP synthase; and then combination of rotenone and antimycin-A to detect non-mitochondrial metabolic activity. Before the measurement, cells were incubated for 1 hour with XF Assay Medium (Seahorse Bioscience) plus glucose, L-glutamine and sodium pyruvate. During the assay, we injected the following at the final concentrations in the injection ports: 1.5 µM oligomycin, 0.5 µM for both rotenone and antimycin A. OCR, ECAR and PER were calculated by plotting the O_2 tension of media as a function of time (pmol/min) and lactic acid production (measured by acidification) as a function

time (pmol/min), All data was normalized by the cell number measured in each individual well. Based on the alteration of OCR, ECAR and PER, the analyzer software calculated the rate of mitochondrial respiration and glycolysis. The results were quantified as the average of 4-6 wells ± SEM per time point in at least three independent experiments.

Immunofluorescence Assay for Mitotic Catastrophe cells

pHGG monolayer cells were seeded in 384-well plates and were treated with DMSO, the Wee1 inhibitor MK 1775 (63 nM), the Chk1 inhibitors AZD 7762 (31 nM), MK 8776 (250 nM) or the combinations of the Wee1 inhibitor and Chk1 inhibitors for 3 days. After treatment, cells were fixed with 4% PFA, incubated with 0.5% Triton X-100 for 10 minutes followed by washing with ice-cold PBS and blocking in PBS + 5% BSA + 2% FBS + 0.1% Triton X for 60 minutes at room temperature. Cells were stained with specific antibodies against phospho-Histone H3 (Ser-10) (1:200, clone 3H10, Cy5 conjugate, Millipore 16-218), γ-H2AX (Ser-139) (1:200, Alexa Flour 488 conjugate, clone 20E2, Cell Signaling #9719) and cleaved caspase-3 (1:500, BD Bioscience, 559565) at 4°C overnight followed by incubation with Alexa Flour 555-conjugated anti-rabbit (1:500, Molecular Probe, Life Technologies) antibodies for 2 hours at room temperature. Cell nuclei were counterstained with DAPI. Cells were imaged on ImageXpress Micro Confocal High Content System. MetaXpress® PowerCore™ software was used for image analysis for analyzing the intensity of these 3 different channels of single cells in each well. For quantification, all the cells in 384-well plates were counted in 7 independent wells. We set a threshold of the intensity of FITC channel > 800 as indicating γ-H2AX positive cells, a threshold of the intensity of Cy5 channel > 600 as indicating pHH3 positive cells and intensity of TexasRed channel > 550 as indicating cleaved-caspase 3 positive cells. By using these thresholds, triple positive cells indicated the mitotic catastrophe cells. The results were quantified

as the average of 7 wells ± SEM. Statistical analyses were performed using a two-tailed Mann-Whitney test with Prism 6 (GraphPad) software.

Results

The Combination of a Wee1 Inhibitor and Chk1 Inhibitors Promoted DNA Damage During DNA Replication in High-Grade Glioma PDOX Cells

The accumulation of DNA damage is a common consequence of loss of Wee1 or Chk1 activity. In order to measure the effect of inhibitors of both Wee1 and Chk1 on DNA damage we used a biochemical marker, the phosphorylation of the histone variant H2A.X on serine-139, to quantitate the extent of damaged DNA in inhibitor-treated cells. We treated the both neurosphere and monolayer cultures of pHGG PDOX cells with MK 1775, AZD 7762, MK 8776, or a combination of MK 1775 and AZD 7762, or a combination of MK 1775 and MK 8776 for 12h, 24h, 48h and 72h. Cells were then stained with an antibody to phosphorylated histone variant H2A.X and the extent of antibody binding, a marker for DNA damage was quantitated by flow cytometry. Quantitative analysis of DNA damage using flow cytometry demonstrated a significant increase in the γ-H2A-postive cell population following combined Wee1 inhibitor and Chk1 inhibitor treatment compared to either DMSO (control) or treatment with the individual inhibitors alone (Figure18). For example, in neurosphere cells (Figure 18 a, 18d), the average of γ-H2AX-postive cell population in the cells treated with the combination of MK1775 and AZD 7762 was 18.47% while that in control DMSO group was only 1.13%. The averages of γ-H2AX-postive cell populations in the single treatment groups, MK 1775, AZD 7762 or MK 8776 were 2.46%, 3.14%, 1.28% respectively, a set of values not significantly different from control. These results showed that the combination of MK 1775 and AZD 7762 corporately promoted

significant DNA damage for pHGG tumor cells. Similar results were obtained when the Wee1 inhibitor was combined with a second Chk1 inhibitor (MK 8776). Comparison of the results obtained with neurosphere and monolayer cultures demonstrated that the effect on DNA damage occurred earlier in the neurosphere cultures (24h) than in cells growing in monolayer culture (72h) (Figure 18b, 18e).

To test whether the effect of the combination of Wee1 and Chk1 inhibitors on DNA damage in pHGG cells was selective for the tumor cells, we compared the activity of the inhibitors in normal astrocytes with their activity in pHGG cells. Comparison of the results obtained with the pHGG cells (Figure 18a, b, d, e) with that obtained with normal astrocytes (Figure 18c, f) demonstrated a much greater effect of the combinations of inhibitors on the tumor cells compared to the normal cells. While the optimal concentration of both inhibitors increased the indices of DNA damage by 16-fold, compared to control DMSO in tumor cells, the same concentrations of drugs increased damage in the normal astrocytes by less than 2-fold (a statistically non-significant effect). While the effect of the combinations on damage to the tumor cells was clearly synergistic, it was at best additive in the normal astrocytes.

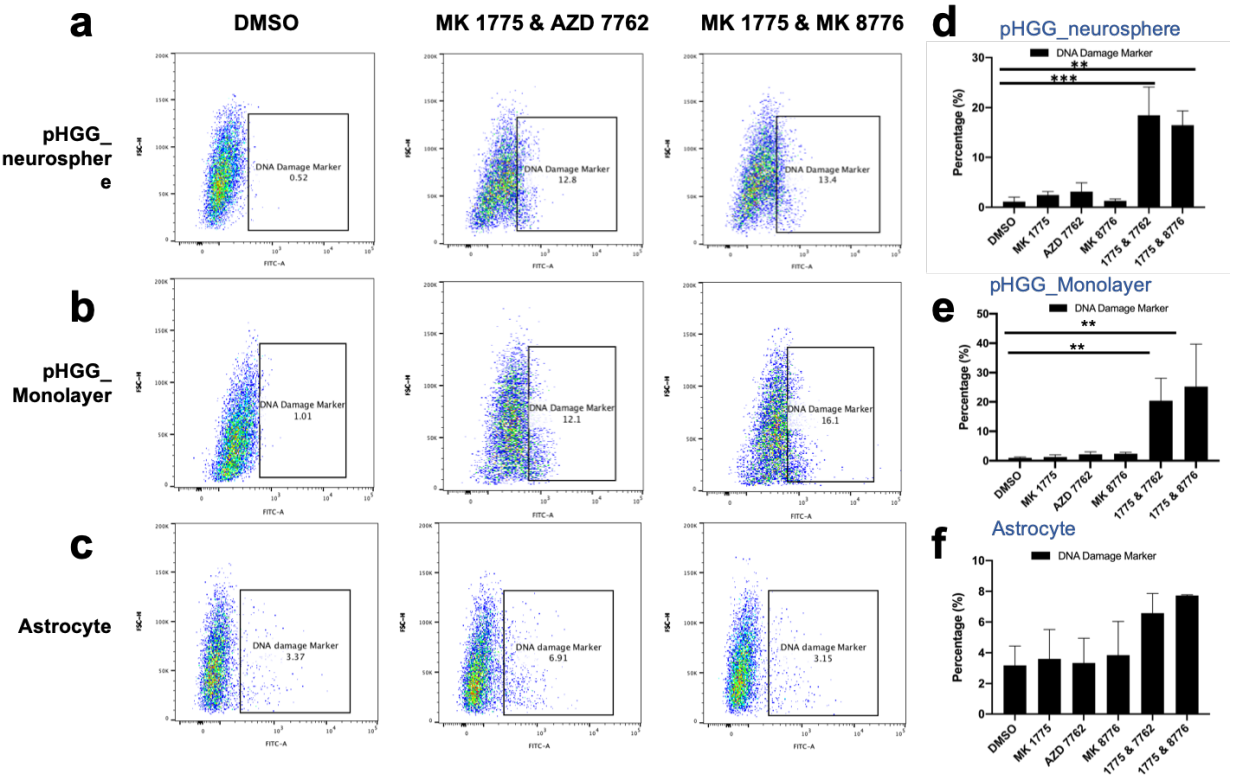

Figure 18. Effect of Combinations of a Wee1 Inhibitor and Chk1 Inhibitors on DNA Damage in pHGG Tumor Cells and Normal Astrocyte Cells.
(a-c) Representative flow cytometric plots showing the total percentage of γ-H2AX-postive cells after treatment of DMSO, combination of MK 1775 (63 nM) and AZD 7762 (31 nM), MK 8776 (250 nM) in (a) pHGG neurosphere cells (24h), (b) monolayer cells (72h) and (c) normal Astrocyte cells (72h). After treatment, the cells were incubated with γ-H2AX -Alexa Flour-488 for 1 hour and then stained with 1ug/ml PI. After gating on single cells via PI-width and area parameters cells were gated for γ-H2AX positive cells against DNA content. X axis indicates the intensity of channel of with Alexa Flour-488. Y axis indicates FSC-H used for identify single cells based on the cell size. (d-f) Bar chart summarizing the percentage of total γ-H2AX-postive cells after treatment of DMSO, combination of MK 1775 (63 nM) and AZD 7762 (31 nM), MK 8776 (250 nM) in (d) pHGG neurosphere cells (24h), (e) monolayer cells (72h, middle) and (f) normal Astrocyte cells (72h, bottom). Error bars show mean ± SEM, n ≥ 3 independent experiments; *, $P < 0.05$; **, $P < 0.01$; ***, $P < 0.001$.

The Combination of Wee1 and Chk1 Inhibitors Induced G2/M Arrest in High-Grade Glioma PDOX Cells

To examine the effects of combinations of Wee1 and Chk1 inhibitors on the distribution of cell cycle phases in pHGG cells, we used flow cytometry to quantitate the distribution of pHGG R0315 cells in neurosphere and monolayer cultures following treatment with the checkpoint inhibitors alone or in combination. Both neurosphere and monolayer cultures were

treated with the Wee1 inhibitor MK 1775 (63 nM), the Chk1 inhibitors AZD 7762 (31 nM) or MK 8776 (250 nM), or a combination of MK 1775 and AZD 7762, or a combination of MK 1775 and MK 8776 for 12, 24, 48, 72h. The results we obtained (Figure 19) clearly demonstrate that combined Wee1/Chk1 inhibition promotes mitotic entry decreasing the fraction of cells in the G1 phase of the cell cycle and increasing the fraction of cells in G2/M phase. The fraction of cells in the S phase was not changed significantly. For example, after 24 hours of treatment with the combination of MK 1775 and AZD 7762, the average of fraction of cells in G1 was lowered from 33.6% (DMSO control) to 8.4%, and the average of fraction of cells in G2/M was increased from 14.1% (DMSO control) to 22.8% (Figure 19a, 19d). This effect on mitotic entry developed early after exposure to the drug combination, being detectable within 24 hours of the addition of the drugs and persisting until at least 72h. The results obtained with monolayer cells, was similar to the results obtained with neurospheres (Fig 19b, 19e). Treatment of cells with the combination of inhibitors increased mitotic entry. For instance, treatment of cells with the combination of MK 1775 and AZD 7762 for 72hrs lowered the average of fraction of the cells in G1 phase from 40.8% (DMSO control) to 18.3% and increased the cells in G2/M phase from 14.3% (DMSO control) to 25.4%. It is noteworthy that the effect of the combination treatment on the monolayers was delayed with respect to the neurospheres. As shown in the time course study, the effect of the combination treatment of cell cycle was not detected until 48 hours after the addition of the drug and then persisted until at least 72h after the initiation of the treatment.

In contrast, to the tumor cell lines, treatment of normal astrocytes with either the individual checkpoint inhibitors or the combinations had no effect on their cell cycle (Figure 19c, 19f). This difference in cell cycle dynamics mirrors the fact the combination of inhibitors has no

effect on normal cell proliferation while significantly inhibiting the proliferation of the pHGG tumor cells.

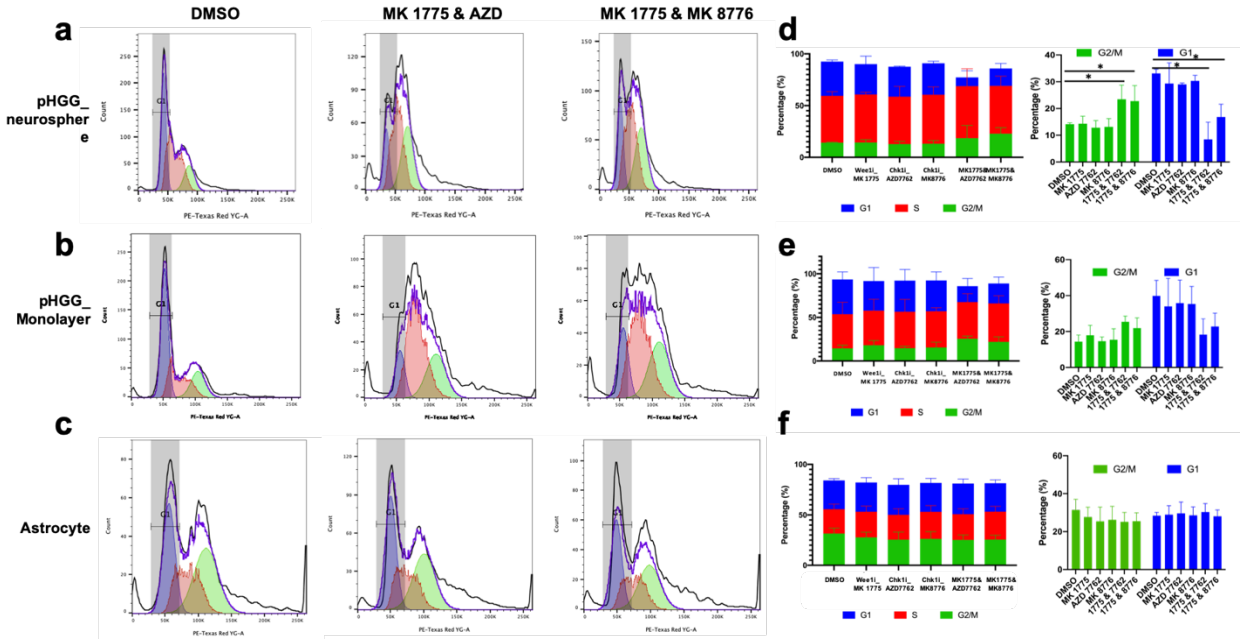

Figure 19. Effect Wee1 and Chk1 Inhibitors on Cell Cycle Profile of pHGG PDOX Tumor Cells and Normal Astrocyte Cells.
(a-c) Representative flow cytometric plots showing cell cycle profiles after treatment of DMSO, combination of MK 1775 (63 nM) and AZD 7762 (31 nM), MK 8776 (250 nM) in (a) pHGG neurosphere cells (24h), (b) monolayer cells (72h) and (c) normal Astrocyte cells (72h). After treatment, the cells were stained with 1ug/ml PI for 30 min. Cell cycle analysis calculated G1, S Phase and G2/M from a PI-area histogram. (c-f) Bar chart summarizing quantitation of cell cycle after treatment of DMSO, combination of MK 1775 (63 nM) and AZD 7762 (31 nM), MK 8776 (250 nM) in (d) pHGG neurosphere cells (24h), (e) monolayer cells (72h) and (f) normal Astrocyte cells (72h). Error bars show mean ± SEM, n ≥ 3 independent experiments; *, $P < 0.05$; **, $P < 0.01$; ***, $P < 0.001$.

Effect of Combined Wee1 and Chk1 Inhibitors on the Replication Speed and Replication Fork Stability During DNA Replication in High-Grade Glioma PDOX Cells

To evaluate the effect of combinations of the Wee1 inhibitor MK1775 and Chk1 inhibitors AZD 7762 and MK 8776 on genomic integrity during DNA replication, we performed a DNA fiber assay. This assay uses sequential pulse labelling of replicating DNA with IdU and

CIdU to estimate the replication fork velocity and the frequency of replication fork initiation. pHGG cells in both monolayer and neurosphere cultures were treated with 0.1% DMSO, 63nM MK 1775, 31 nM AZD 7762, 250 nM MK 8776, or a combination of MK 1775 and AZD 7762, or a combination of MK 1775 and MK 8776 for 72h. At the end of the incubation, cells were pulse labelled sequentially with IdU and CIdU under conditions described in detail in the Methods section. After pulse labelling, cells were lysed, DNA fibers were spread onto a glass slide and labelled with fluorescent antibodies specific for either IdU or CldU (under conditions described in detail in the Methods section). Inspection of the isolated stained DNA fibers using fluorescent imaging allows for the calculation of replication fork velocities (1 μm roughly corresponds to 2.59 kb). The longer both labeled tracts are, the faster of the replications rate. Slower replication, which may be due to slower DNA polymerization or increased fork stalling, is reflected in shorter tracts. The results from this study (Figure 20) demonstrated that both the IdU and CldU - labeled tracts (red and green respectively in the combination group) were much shorter than the comparable tracks in the DMSO controls. Quantitation of the length of the labelled tracks (in Figure 20b) in the combination-treated cells showed that length of green tracts (CldU) were 3.88 ± 3.93 μm and 5.63 ± 4.28 μm separately in both checkpoint inhibitor combination groups compared to 11.84 ± 4.21μm ($P < 0.0001$) in the DMSO control. Quantitation of the speed of the replication forks (in Figure 20c) in DMSO control group was 1.02 ± 0.36 kb/min, while the replication rates in the combination groups were 0.44 ± 0.34 and 0.49 ± 0.37 kb/min (both of the p value vs DMSO < 0.0001). Cells treated with the two Chk1 inhibitors, AZD 7762 and MK 8776, as single agents had median lengths of the labelled DNA tracks that were comparable to the DMSO controls (9.61± 5.05, 8.25 ± 5.14 μm respectively). The replications rates for the Chk1 inhibitor-treated cells were also similar to controls (0.83±

0.44, 0.71± 0.44 kb/min respectively). The Wee1 inhibitor MK 1775 caused shorter fiber length (5.92 ± 3.72 μm) and a slower speed of replication (0.51± 0.32 kb/min) than the two Chk1 inhibitors or the DMSO control (P value <0.0001). The effect of Wee1 inhibitor was similar to the effect of the combination treatment. The results obtained demonstrate that the combination of the Wee1 and Chk1 inhibitors slowed the replication speed during the DNA replication and suggest that the Wee1 inhibitor plays a dominant role in this effect. The reduction in the DNA replication rate is likely to contribute to the ability of combinations of Wee1 and Chk1 inhibitors to synergistically suppress the growth of pHGG tumor cells.

Table 3. Effect of Treatment of Wee1i and Chk1is on the Replication Forks in pHGG PDOX Monolayer Cells.

Treatment	Fiber Length (Green, μm)	Replication Fork Speed (kb/min)
DMSO	11.84 ± 4.21	1.02 ± 0.36
Wee1i_MK 1775	5.92 ± 3.72	0.51 ± 0.32
Chk1i_AZD 7762	9.61± 5.05	0.83 ± 0.44
Chk1i_MK 8776	8.25± 5.14	0.71 ± 0.44
MK 1775 & AZD 7762	3.88 ± 3.93	0.44 ± 0.34
MK 1775 & MK 8776	5.63 ± 4.28	0.49 ± 0.37

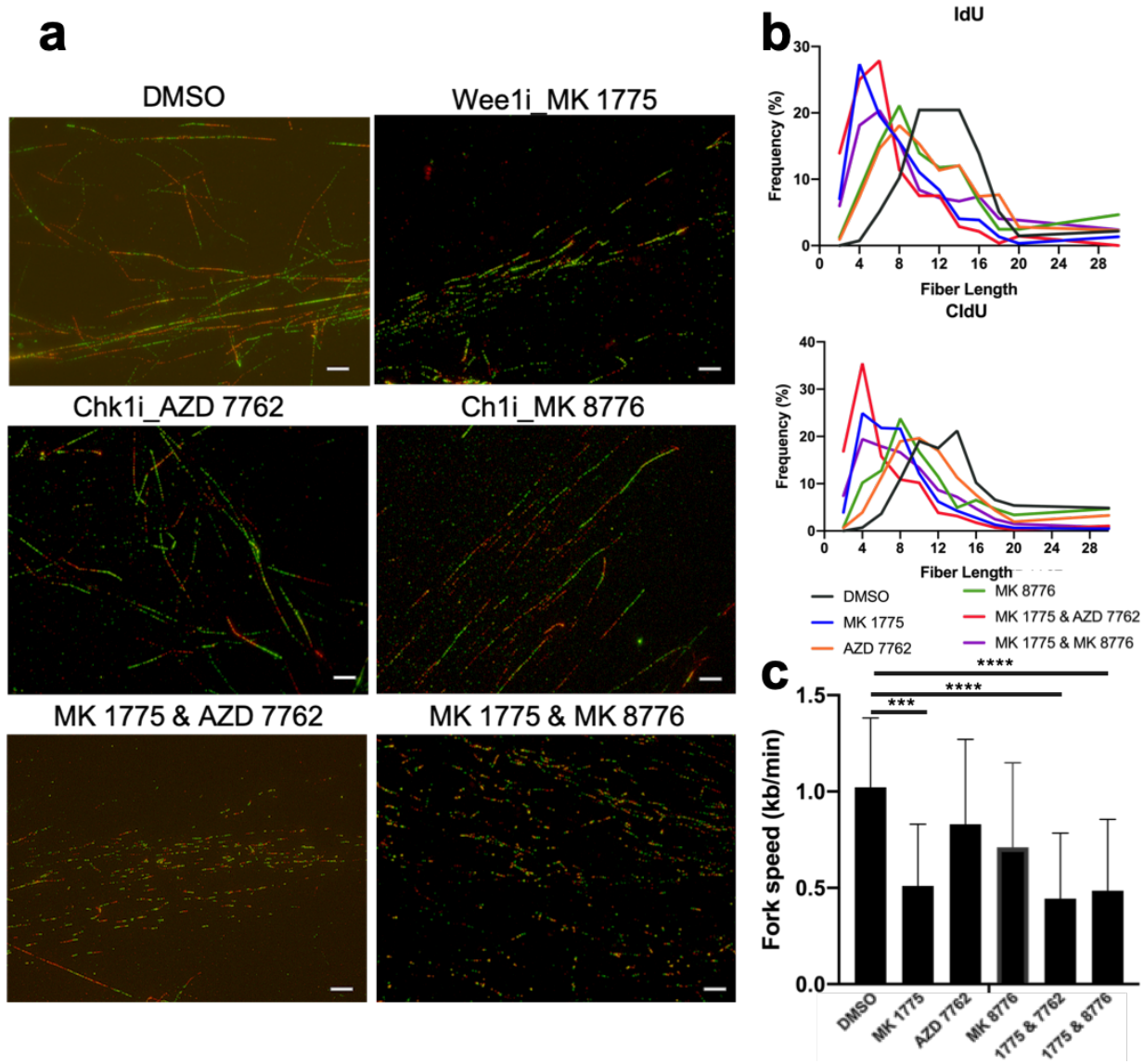

Figure 20. Effect of Combination of Wee1i and Chk1i is on the Replication Forks in pHGG PDOX Monolayer Cells.
(a) Representative immunofluorescent images showing the replication forks at 72 hours following treatment with DMSO, Wee1 inhibitor MK 1775 (63 nM), Chk1 inhibitor AZD 7762 (31 nM) and MK 8776 (250 nM), combination of MK 1775 AZD 7762 and combination of MK 1775 and MK 8776 in monolayer culture condition. Scale bar, 10µm. (b) Frequency distribution of fiber length of IdU and CIdU. The shift of curves of IdU and CIdU to the left in monolayer culture condition upon combination of Wee1i and Chk1is. (c) Bar chart summarizing quantitation of replication fork speed after treatment of DMSO, combination of MK 1775 (63 nM) and AZD 7762 (31 nM), combination of MK 1775 (63 nM) and MK 8776 (250 nM). Median replication fork speed (kb/min) is indicated. Data are median ± SEM, *, $P < 0.05$; **, $P < 0.01$; ***, $P < 0.001$. ****, $P < 0.0001$.

In addition to providing information on the speed of DNA replication, DNA fiber analysis also provides information initiation of DNA replication forks (origin of firing) and the

stability of replication forks. Comparison of the DNA fibers from the inhibitor combination-treated cells compared to DMSO controls reveals many fewer pulse labelled fibers (Figure 20a). This result indicates a decrease in extent of the initiation of DNA replication during the pulse-labelling interval. In addition, there were many more replications forks visible in the combination-treated cells compared to controls, with an increase in the number of green only tracts (origins that fired during the second labeling periods) indicative of an increase in the number of replication forks that initiated during the second labeling periods and an increase in the number of red only tracts (origins that fired during the first labeling periods but terminated) indicative of an increase in the number of replication forks that terminated. Taken together, the results of the DNA fiber assays showed that the combination of Wee1 inhibitor and Chk1 inhibitors caused a slowing replication speed and an increase in replication forks instability.

The Combination of a Wee1 Inhibitor and Chk1 Inhibitor Induced Mitotic Catastrophe in pHGG Tumor Cells

Mitotic catastrophe is induced when cells enter into mitosis in the presence of damaged DNA. The resulting disruption in the replicative machinery results in the induction of apoptosis. Since our previous studies have demonstrated the combined effect of a Wee1and Chk1 inhibitor is to both stimulate mitotic entry and increase DNA damage in the pHGG tumor cells, we hypothesized that mitotic catastrophe might result. If this is the case then the induction of mitotic catastrophe could be the underlying mechanism leading to the death in pHGG cells in induced by combined Wee1/Chk1 inhibition.

To address this possibility, we investigated the distribution of genotoxic lesions, caused by combined Wee1 inhibitor and Chk1 inhibitors in pHGG tumor cells. Both monolayer and

neurosphere cultures were treated with DMSO, MK 1775 (63 nM), AZD 7762 (31 nM), MK 8776 (250 nM) or a combination of MK 1775 and AZD 7762, or a combination of MK 1775 and MK 8776 for 0,12, 24, 48 and 72h. These Wee1/Chk1 abrogation in the pHGG tumor cells lead to the accumulation of mitotic cells carrying DNA lesions, as evidenced by the appearance of a substantial γ-H2A-postive cell populations in G2/M phase after 24h for the 3D neurosphere cells (Described in Figure21a, b) and 72h for the 2D monolayer cells (Described in Figure21a, c). The combination of MK 1775 and AZD 7762 significantly increased of γ-H2A-postive cell populations in G2/M phase to 20.85 ± 2.47 vs DMSO 1.04 ± 0.71 (P value is 0.0024) after 24 hours in neurosphere culture and 13.13 ± 1.42 vs DMSO 0.25 ± 0.04 (P value is 0.0049) after 72 hours in monolayer culture. Similarly, the combination of MK 1775 and MK 8776 also induced significant increase of γ-H2A-postive cell populations in G2/M phase to 20.55 ± 5.16 vs DMSO 1.04 ± 0.71 (P value was 0.016) after 24 hours in neurosphere culture and 13.86 ± 2.72 vs DMSO 0.25 ± 0.04 (P value was 0.030). While none of the single treatments of MK 1775, AZD 7762 and MK 8776 change the γ-H2A-postive cell populations in G2/M phase (Figure 21b, 21c). Thus, these Wee1/Chk1 dual inhibition in the pHGG tumor cells result in the accumulation of mitotic cells carrying DNA damage.

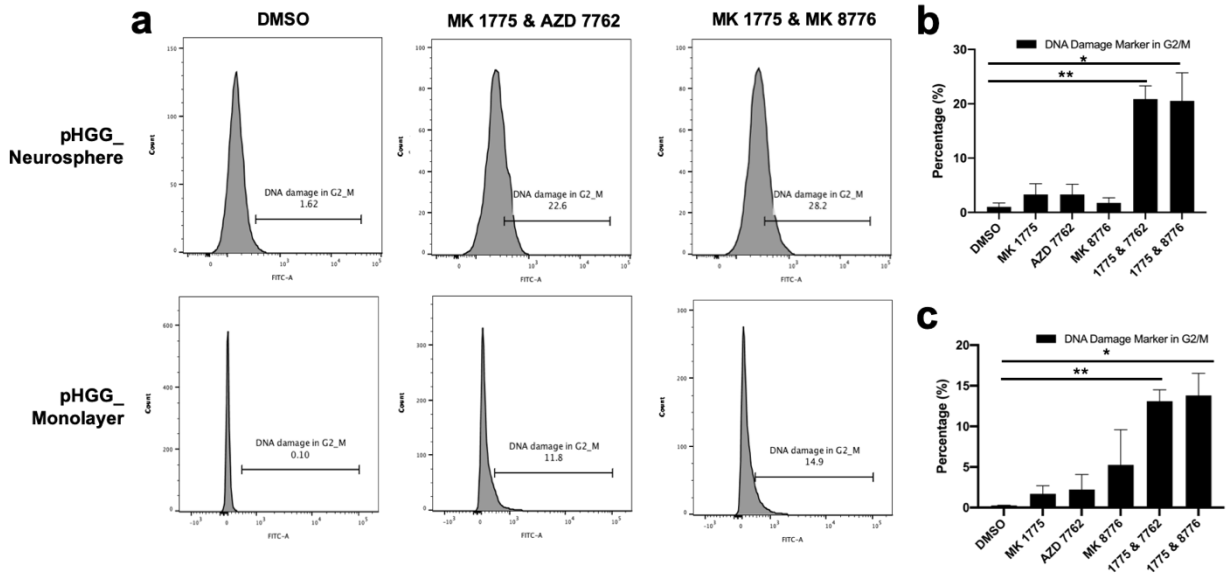

Figure 21. Effect of Wee1 and Chk1 Antagonist on Mitotic Cells in pHGG Tumor Cells.
(a) Representative flow cytometric plots showing the DNA damage cell populations in G2/M phase after treatment of DMSO, combination of MK 1775 (63 nM) and AZD 7762 (31 nM), MK 8776 (250 nM) in (top) pHGG neurosphere cells (24h), (bottom) monolayer cells (72h). (b-c) Bar chart summarizing quantitation of the DNA damage cell populations in G2/M phase after treatment indicated in (b) neurosphere cells (24h) and (c) monolayer cells (72h). Error bars show mean ± SEM, n ≥ 3 independent experiments; *, $P < 0.05$; **, $P < 0.01$; ***, $P < 0.001$.

To prove that the pHGG cells exposed to dual Wee1/Chk1 inhibition indeed undergo mitotic catastrophe, we stained the 2D monolayer cells with antibodies against pHH3, γH2AX, and cleaved caspase-3, a marker of apoptosis. Triple-positive cells were scored as undergoing mitotic catastrophe. As we see in the bar graph (Figure 22), the DMSO, mono-Wee1 inhibitor and mono-Chk1 inhibitors, the population of cells undergoing mitotic catastrophe were similar which were about 3% while that of the combination of Wee1 and Chk1 inhibitors were about 12-13% which is 4 times as the DMSO and single treatments. Together, our data suggest that the cell death in pHGG tumors results from mitotic catastrophe.

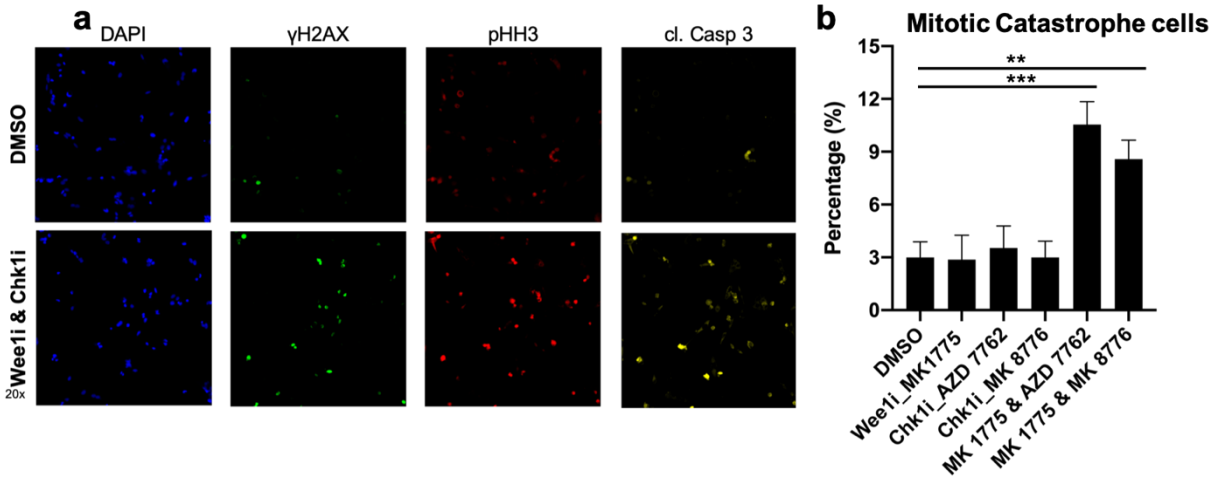

Figure 22. Effect of Wee1 and Chk1 Antagonist on Mitotic Catastrophe in pHGG Monolayer Cells.
(a) Representative images of pHGG 2D monolayer cells treated with DMSO and combination of Wee1 and Chk1 dual inhibition for 72 hours. (b) Quantification of mitotic catastrophe cell populations following treatment of DMSO, MK 1775 (63 nM), AZD 7762 (31 nM), MK 8776 (250 nM), combination of MK 1775 and AZD 7762, combination of MK 1775 and MK 8776 for 72 hours in monolayer cells. Data are Mean ± SEM. *, $P < 0.05$; **, $P < 0.01$; ***, $P < 0.001$.

Effect of Wee1 and Chk1 Inhibitors on ATP Metabolism in High-Grade Glioma PDOX Cells

One of the potential mechanisms to account for the slowing of the replication speed during the DNA replication in cells treated with combinations on checkpoint inhibitors could be a lowering of the endogenous levels of ATP. To address this question, we measured the effect on cellular ATP levels of 72 hours exposure of pHGG cells (in monolayer culture) to either the individual inhibitors alone or in combination (Figure 23a, 23b). The cellular content of ATP as measured by CellTiter-Glo and was normalized to total cell number, as determined by the counting of DAPI stained nuclei. The results of this experiment, Figure 23 showed that both the Wee1 and Chk1 inhibitors alone induced a modest but significant decrease in intracellular ATP content but the combination treatment resulted in a much greater (30%-50%) decrease in cellular ATP levels.

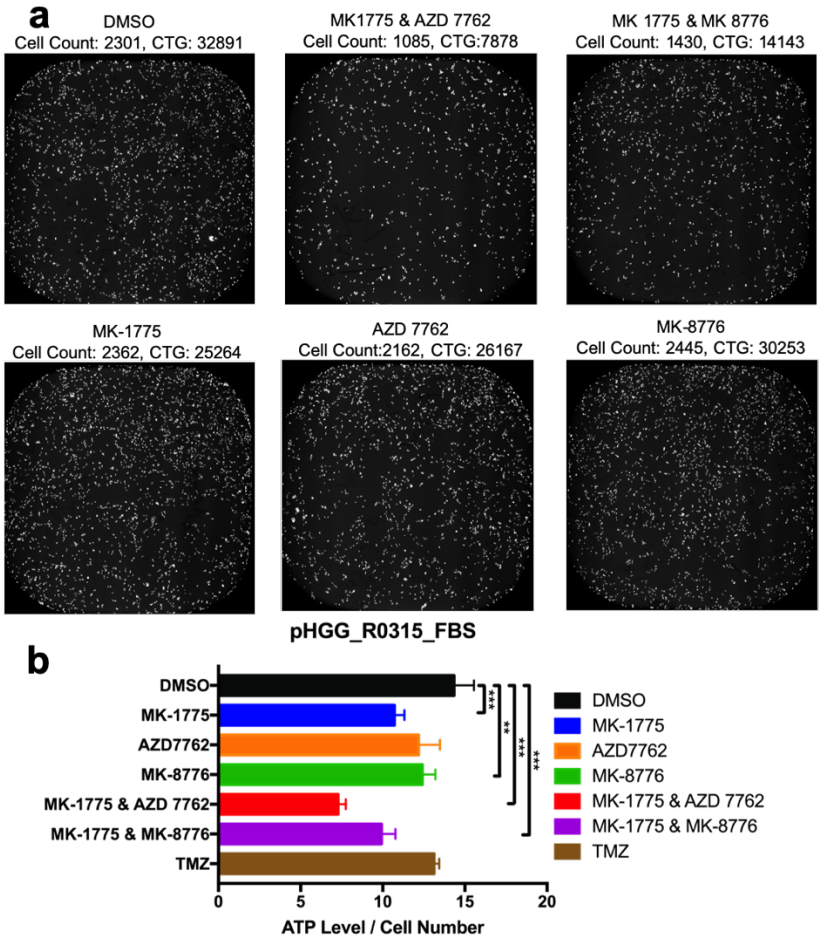

Figure 23. Effect Wee1 and Chk1 Inhibitors on ATP Levels in pHGG PDOX Monolayer Cells.
(a) Representative nuclei staining images of nuclei stain after 72 hours treatment following treatment with DMSO, Wee1 inhibitor MK 1775 (63 nM), Chk1 inhibitor AZD 7762 (31 nM) and MK 8776 (250 nM), combination of MK 1775 AZD 7762, combination of MK 1775 and MK 8776 in monolayer culture condition. (b) Bar chart summarizing quantitation of ATP level normalized to the cell count after treatment of DMSO, combination of MK 1775 (63 nM) and AZD 7762 (31 nM), combination of MK 1775 (63 nM) and MK 8776 (250 nM). Data are Mean ± SEM, n ≥ 3 independent experiments; *, $P < 0.05$; **, $P < 0.01$; ***, $P < 0.001$. ****, $P < 0.0001$.

To establish the optimal treatment time to detect metabolic changes in ATP levels in pHGG cells we carried out a series of time course studies that measure ATP (by CTG assay) in cells treated with the checkpoint inhibitors alone or in combination and some standard chemotherapy (doxorubicin and temozolomide) or apoptosis-inducing drugs (staurosporine). The results obtained (Figure 24) showed that after 12 hours of treatment with a combination of Wee1 inhibitor and Chk1 inhibitors, the ATP levels started to decline while the single agent treatment

with Wee1 inhibitor and the two Chk1 inhibitors did not (as compared to the DMSO control) In addition, at 12hrs the cell number was not significantly reduced compared to the control group. Based on these results, we selected 16 hours as the optimal treatment time for subsequent metabolic profiling (Seahorse) studies.

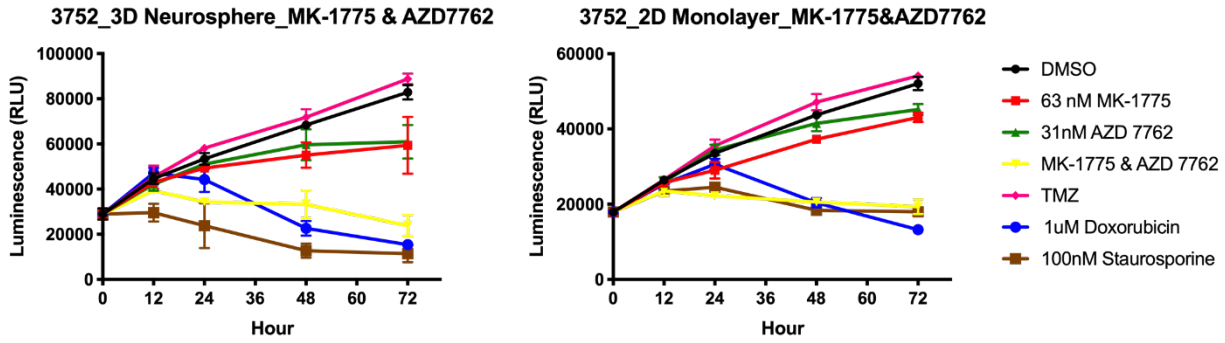

Figure 24. Time Course for the Effect of Wee1 and Chk1 Inhibitors and Chemotherapy Drugs on the ATP Level in pHGG PDOX Cells.
Time course of ATP level of 0,12,24,36,48 and 72 hours following treatment with DMSO, Wee1 inhibitor MK 1775 (63 nM), Chk1 inhibitor AZD 7762 (31 nM), combination of MK 1775 AZD 7762, Doxorubicin (1 μM) and Staurosporine (100 nM) in both neurosphere (left) and monolayer (right) culture conditions. Data are mean ± SEM; n ≥ 3 replicates.

We used a Seahorse XF Analyzer to obtain quantitative information on the Oxygen Consumption Rate (OCR – a measure of mitochondrial metabolism) and the Extracellular Acidification Rate (ECAR - a measure of glycolytic activity) of pHGG cells treated with checkpoint inhibitors either alone or in combination. Cells were plated and treated with drugs (or a DMSO control) for 16 hours and the basal metabolic rate and its components were measured by serial injections of metabolic inhibitors such as Oligomycin (1.5 μM), Rotenone (0.5 μM) and Antimycin A (0.5 μM). Alterations of OCR and ECAR in response to drug treatment and metabolic inhibitors were measured by Seahorse and the metabolic parameters were calculated. The results of these studies (Figure 25b) showed that neither the individual checkpoint inhibitors

or the combinations of inhibitors had any effect on the ECAR. However, analysis of the OCR curves (Figure 25a) showed exposure of the cells to the one of Chk1 inhibitors AZD 7762 decreased the OCR significantly compared to the DMSO control in the basal line, the average of OCR value was dropped to 27.5 pmol/min compared to the DMSO control of 34.8 pmol/min (P value was 0.039). While the other Chk1 inhibitor MK 8776, the average of OCR value was 28.6 pmol/min but showed no significant change compared to DMSO-treatment. The Wee1 inhibitor MK1775 also had a minimal and non-significant effect of OCR compared to DMSO control. The combination of each of the Chk1 inhibitors with the Wee1 inhibitor showed significantly reduce on the OCR value (P value were 0.018 and 0.021 respectively) while the combination of MK 1775 and AZD 7762 was no more effective than the Chk1 inhibitor AZD 7762 alone (P value was 0.46) in the basal line. These results demonstrate that the two Chk1 inhibitors specially AZD 7762 reduce the OCR to a significantly greater extent than the Wee1 inhibitor MK 1775.

By comparing basal OCR with the OCR following the abolition of all mitochondrial metabolism by Oligomycin it is possible to calculate the rate of mitochondrial ATP production in the basal state. Comparison of the effect of the effect of the checkpoint inhibitors on ATP production from glycolysis and mitochondrial metabolism (Figure 25d) reveals that ATP production from glycolysis doesn't change after the treatment with the inhibitors either alone or in combination whereas ATP production from mitochondrial respiration (Figure 25d) is significantly suppressed by the combinations of the Chk1 and Wee1 inhibitors (P value were 0.014 and 0.017). Moreover, one of the Chk1 inhibitors used, AZD 7762 also showed the effect of reducing ATP production from mitochondrial respiration (P value was 0.032) while the other Chk1 inhibitor MK 8776 (P value was 0.18) and Wee1 inhibitor alone MK 1775 (P value was 0.18) show no-significant effect on that. Comparing AZD 7762 (Chk1 inhibitor) alone with the 2

combinatorial pairs, the effect of decreasing ATP production from mitochondrial respiration had no significant difference (P values were 0.46, 0.26 respectively). Our data suggest that the combination of Wee1 inhibitor and Chk1 inhibitor showed inhibitory effects of on mitochondrial energy production. However, the inhibitory effects of the combination of MK 1775 and Chk1 inhibitor AZD 7762 on mitochondrial energy production is due to the activity of the Chk1 inhibitor AZD 7762. While effects of the other pair MK 1775 and MK 8776 on the energy production is due to additivity or minimal synergistic effect. The Chk1 inhibitor may play a dominant role in this inhibitory effect on ATP production.

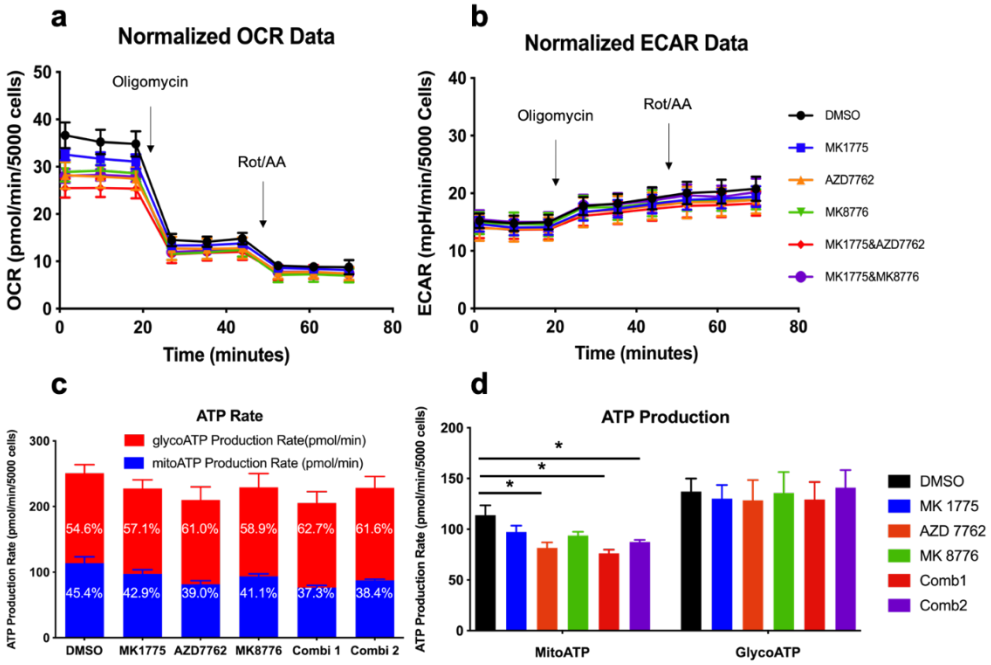

Figure 25. Effect of Wee1 and Chk1 Inhibitors on Mitochondrial and Glycolytic ATP Production in pHGG Monolayer Cells.

(a-b) Metabolic profile of normalized OCR(a) and normalized ECAR(b) after 17 hours treatment with DMSO, Wee1 inhibitor MK 1775 (63 nM), Chk1 inhibitor AZD 7762 (31 nM) and MK 8776 (250 nM), combination of MK 1775 AZD 7762, combination of MK 1775 and MK 8776 in monolayer culture condition by Seahorse ATP rate assay. n ≥ 3-6 replicates from 3 independent experiments. (c) A comparison of ATP rates from mitochondrial respiration and glycolysis after treated in (a) are indicated. Data are mean ± SEM. n ≥ 3-6 replicates from 3 independent experiments. (d) A comparison of ATP production from mitochondrial respiration and glycolysis after treatment are indicated. n ≥ 3-6 replicates from 3 independent experiments. Data are mean ± SEM. *, $P < 0.05$; **, $P < 0.01$.

Discussion

In the previous chapter, we demonstrated that the combination of a Wee1 inhibitor and Chk1 inhibitors have selective synergistic effect on decreasing cell viability in pHGG tumor cells in both of monolayer and neurosphere cultures. To further understand the molecular mechanisms involved how these mechanism-annotated combination pairs effect on the cell viability of the pHGG tumor cells, we have in the present study combined a Wee1 inhibitor MK 1775 with Chk1 inhibitors AZD 7762 and MK 8776. Our hypothesis is that simultaneous inhibition of two cell cycle control proteins will introduce a high degree of DNA damage incompatible with cell viability. The combination of these 2 inhibitors leads to an increased anti- tumor effect both in 2D monolayer and 3D neurosphere culture conditions. Furthermore, our studies showed that co-treatment synergistically decreased viability, along with DNA damage, premature mitosis, slower replication speed and mitotic catastrophe. Moreover, the combination of Wee1 and Chk1 also have effect on the metabolic changes which is reduction of ATP production from mitochondrial respiration. Our results provide a rationale for testing the Wee1/Chk1 inhibition as a strategy for the pHGG tumors.

Combinations of MK1775 and AZD 7762 as well as MK1775 and MK 8776 led to a synergistic reduction of viability in our studies of pHGG tumor cells in both neurosphere and monolayer cultures but the synergistic effect was not present in normal cells. The reason for this selective effect could be different levels of replicative stress between cancer cells and astrocyte cells (Figure 26). Cancer cells are highly proliferative cells indicating that the replicative stress inside the cancer cells may be much higher compared to the relative slow proliferative activity normal cells. The DNA damage caused by the combination of Wee1 and Chk1 inhibition in astrocytes was much less than in the tumor cells. There may still be some

degree of genomic protection threshold because of the moderate replication stress and limited DNA damage caused by the combination. In the normal astrocytes there is very limited DNA damage, no cell cycle changes, no mitotic catastrophe and no cell death. The tumor cells on the other hand have high replication stress that is increased after the inhibition of Wee1 and chk1, resulting in massive DNA damage, forced G2/M phase entry and the induction of mitotic catastrophe and tumor cell death. This could be one of the explanations for why combined Wee1/Chk1 inhibition was much more cytotoxic than single agent treatment and had such a selective anti-tumor effect on the pHGG tumor cells.

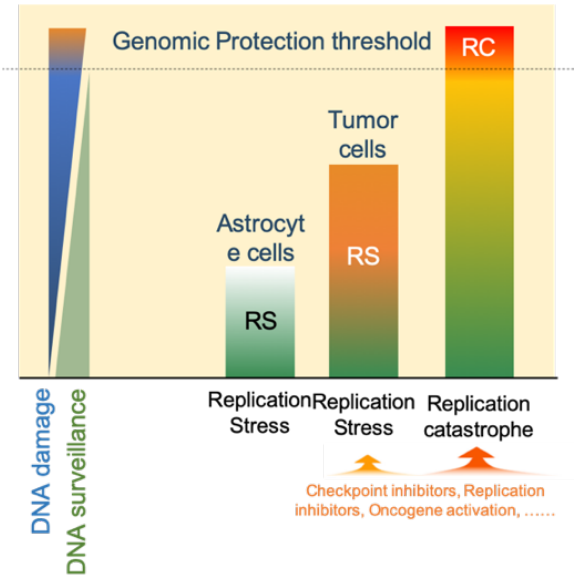

Figure 26. Different Endogenous Replicative Stress in Normal Cells and Tumor Cells.
All forms of DNA require DNA surveillance pathways protection. The DNA surveillance pathways provide a safe dynamic range to support multiple reactions involving DNA production and conditions of low to moderate replication stress (RS) in normal situation. Different perturbations that can induce large quantities of DNA damage in the cell (orange), and may cause RC (replicative catastrophe) in human cells (above the dashed line).

In addition, we found that the combination of Wee1i and Chk1i could reduce the ATP

production from mitochondrial respiration selectively in pHGG tumor cells. Tumor cells have a high energy demand in order to support the critical cell processes such as cell growth, proliferation, migration and invasion. Some studies have shown that multiple catabolic pathways are used for energy production within glioma cells and these pathways are critical for supporting cellular function [122]. In addition, other studies have demonstrated that inhibition of the metabolic pathways critical for the support of DNA replication may lead to increased replication stress and synergy with checkpoint kinase inhibitors such as Chk1 inhibitors [123]. Altered metabolic activity could be one of the mechanisms responsible for the selectively synergistic activity of the Wee1/Chk1 combination. The targeting of tumor cell metabolism could be a novel strategy for the treatment of pHGG tumors.

In conclusion, our data provide a strong rationale for the evaluation of checkpoint abrogation through the use of Wee1 and Chk1 inhibitors as a basis for the development of new therapies for pHGG tumors.

CHAPTER IV

SUMMARY AND DISCUSSION

Pediatric high-grade glioma (pHGG) is one of the most aggressive brain tumors in children [124]. The goal of this study has been to establish a preclinical rationale for clinical trials of novel combinatorial targeted therapies for pHGG. We developed the target-based novel combination therapies for pHGG to provide a rationale for the evaluation of new combinatorial therapies in children with HGG. In this study, we developed a high throughput combinatorial screening paradigm in both cancer stem cell (based on 3D neutrosphere) and monolayer cultures of tumor cells generated from patient-derived orthotopic xenograft (PDOX) model to identify the novel synergistic drugs combinations that were most effective and selective for pHGG.

In the first part of this study, we implemented a high throughput screening strategy using 1863 mechanism-annotated cancer relevant drugs and compounds to identify the most active drugs which exhibit cytotoxicity in pHGG tumor cells. Instead of just selecting the most cytotoxic drugs for pHGG tumor cells as the basis for combinatorial screening, we developed a method using a "pharmacological relationship tree" to identify the most effective mechanism-annotated drug classes. The single agent screen result in the demonstration that HDAC inhibitors, proteasome inhibitors, HSP90 inhibitors, PI3K/mTOR inhibitors and cell cycle regulators were the five most active pharmacologic classes.

By combining Pan-active compounds with Pan-active compounds, we found that combinations of a Wee1 inhibitor (MK-1775) combined Chk1 inhibitors (AZD7762, MK-8776) or an HDAC inhibitors (Panobinostat, JNJ-26481585) combined with Proteasome

inhibitors (CEP-18770, MLN 2238) exhibited the strongest synergistic lethality in pHGG tumor cells. By using the high throughput combinatorial screening paradigm in both cancer stem cell (based on 3D neurosphere) and monolayer cultures of tumor cells generated from patient derived orthotopic xenograft (PDOX) model, we were successfully in identifying novel combinations with potential to serve as the basis for new therapies for children with HGG.

During the single agent screening studies, we found that even for cells with different genotypes, such as R0315 which is $PI3K^{mut}$ and 3752 which is $PI3K^{wt}$, there was a remarkably similar response of the tumor cells to drugs tested. The five most active drug classes are HDAC inhibitors, proteasome inhibitors, HSP90 inhibitors, PI3K/mTOR inhibitors and cell cycle regulators in both cell types tested. The explanation for this could be: i) most of the pHGG cancers are highly dependent on similar targets, cell processes or signaling pathways that are being targeted by the drugs being tested; ii) some of these drugs such as HDAC inhibitors, proteasome inhibitor, HSP 90 inhibitors, have multiple functional which could interfere with multiple proteins and therefore affect multiple cell processes, resulting cell death. In our study, by combining the active and most effective drug classes from the single agent screen, we were successful in identifying combinatorial pairs that exhibited synergistic lethality. The strategy of combining the most effective drugs may be one of the strategies for discovering for more synergistic pairs for pHGG in the future.

Moreover, the combination of Wee1 inhibitor and Chk1 inhibitors showed selective synergistic lethality in the pHGG tumor cell rather than in normal Astrocyte cells. All of these data indicated that Wee1/Chk1 inhibition could selectively inhibit the viability in pHGG tumor cells and could be a potential novel combinatorial strategy for management of

pHGG. Due to the difficulties in studying the mechanisms responsible for the synergistic effects of two multifunctional drugs (HDACi and Proteasome inhibitor) we decided to focus on the mechanisms of combination of the targeted agents Wee1i and Chk1 inhibitors since they showed selective synergistic lethality in pHGG.

The second part of this study has been to identify the molecular mechanisms responsible for the selectively synergistic cytotoxic activity of Wee1/Chk1 inhibition in pHGG. The combinatorial screening of Wee1i/Chk1i dual inhibition demonstrated a rapid decrease in ATP level (used for measuring the cell viability) between 12 to 24 hours after the initiation of treatment. This decline in ATP preceded and changes in cell number. This observation raised the question of whether the dual inhibition of Wee1 and Chk1 could cause a deficiency in energy supply. To address this question, we used the Seahorse metabolic assay system to measure the effect of Wee1i and Chk1i on ATP production. Our Seahorse Metabolic Assay results demonstrated that the combination of Wee1i and Chk1i reduced the ATP production from mitochondrial respiration and didn't affect the function of glycolysis. The combination of Wee1i and Chk1i had no effect on ATP production in normal astrocyte cells. ATP production provides the energy necessary to drive almost all cell biological process in all normal cells, even more so in tumor cells that have a high demand for metabolic energy. Tumor cell growth signaling and gene activation require ATP for protein phosphorylation, and cellular machineries that include the enzymes for DNA/RNA synthesis. Biomolecules cannot be produced without adequate supplies of metabolic energy. If the supply of ATP is deficient, almost all of cell processes will be impacted. The high energy requirements for the synthesis of dNTP and DNA repair may also contribute to the energetic stress in Wee1i and Chk1-treated pHGG cell. There is no information currently available on

the metabolic profile in pHGG or whether the energy deficiency is a metabolic vulnerability of pHGG. However, there are studies that have shown that tissues with a high dependence on aerobic respiration, such as the central nervous system and heart, are particularly vulnerable to treatment with ATP synthesis inhibitors. ADDA, 5(1-[2-(1-adamantyl) ethoxy]-3-(3, 4-dihydro-2(1*H*)- isoquinolinyl)-2-propanol hydrochloride]), was found to possess a significant anti-glioblastoma multiforme activity both in vitro and in a mouse xenograft model [120] (nude mouse, rear flank). This activity was due to a specific noncompetitively inhibition of mitochondrial complex IV activity. Chemo-resistance to temozolomide in glioblastoma multiforme is associated with an increased level of complex IV activity [120]. It is possible that the effect of reducing ATP production from mitochondrial respiration may contribute to the efficacy of dual inhibition of Wee1 and Chk1 in pHGG. Exploiting the metabolic vulnerability of pHGG cells could be one of the strategies for the management of pHGG in the future. The dependence of pHGG cells ATP production from mitochondrial respiration could be due to the reduced quantity of mitochondrial or deficiencies in their function. Future studies to quantify mitochondrial based on mitochondrial DNA and tracing the metabolic function of mitochondria by using $U^{13}C$-Glucose Metabolic Flux Assay could be used to address this question. Using these methods, we could quantify pHGG cell metabolism after different treatments as well as the differences in metabolic activity between tumor cells and normal cells.

The effect of reducing ATP production from mitochondrial respiration is probably not the only reason for the efficacy of combinations of Wee1 and Chk1 antagonists. The Seahorse metabolic data demonstrated that the ATP production also significant reduced after mono-treatment of Chk1 inhibitor AZD 7762 whereas the cell viability and cell count data

showed that cells could still survive after 3 or 7 days. These results indicate that there are additional mechanisms responsible for the synergistic effect of combination of Wee1 inhibitor and Chk1 inhibitors.

Similar to the findings from other studies, we found that the combination of Wee1 and Chk1 inhibition selectively cooperated to induce DNA damage and G2/M phase arrest, increased replication initiation and slowed down the replication fork speed. The consequence of these effects may be that the dual Wee1 and Chk1 inhibition selectively induces mitotic catastrophe and cell death in pHGG tumor cells. Our data are compatible with a model (Figure 27) in which, due to high endogenous replicative stress in cancer cells, with the combinatorial therapy with Wee1i and Chk1i increase replicative stress and resulted in massive DNA damage and cell death. In the normal astrocyte cells that have low endogenous DNA damage and replicative stress, the combinatorial therapy of Wee1 and Chk1i induced minimal increases in replicative stress and the cells survived. Together, these data indicate that endogenous replicative stress in tumor cells may underlie the efficacy of combinatorial Wee1 and Chk1 therapy in the tumor cells. Moreover, the replicative stress may be one of biomarker for the efficacy of therapy of combination of Wee1i and Chk1i. To test this hypothesis, in the future study, we will need to elevate the replicative stress in the normal cells to levels and then test the efficacy of combined inhibition of Wee1 and Chk1 in the higher stressed normal cells. These studies could provide insights as to whether the level of endogenous replicative stress predicts the efficacy of therapy of combination of Wee1i and Chk1i.

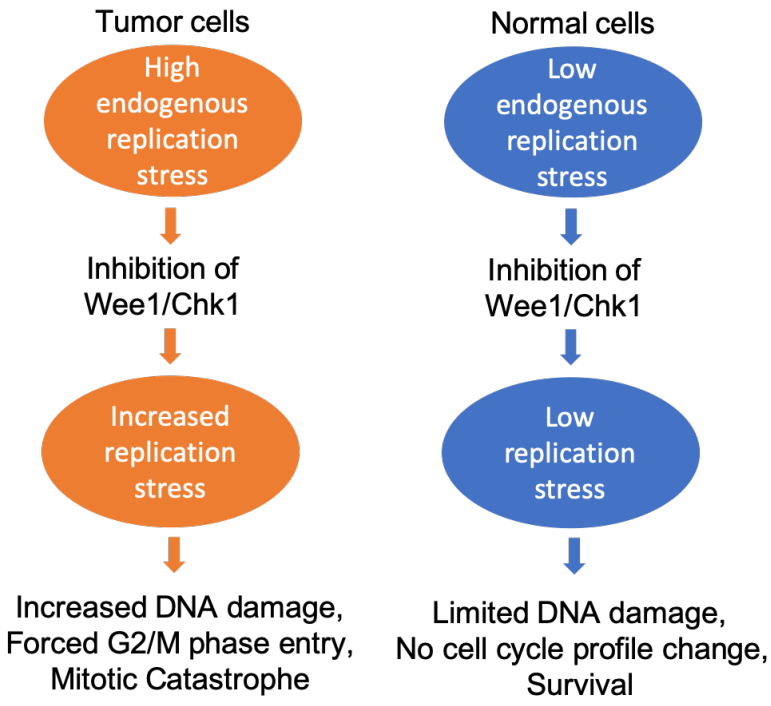

Figure 27. Model of Different Replicative Stress Level Causing Selective Cytotoxic Activities in pHGG Tumor Cells and Normal Cells.
High endogenous replicative stress in cancer cells, with the combinatorial therapy with Wee1 and Chk1i further increased the replicative stress with massive DNA damage and cell death. In the normal astrocyte cells with low endogenous DNA damage and replicative stress, the combinatorial therapy of Wee1 and Chk1i induced minimal increases in replicative stress and cells survived.

Lack of cellular energy and energy metabolites and high replicative stress are the two of the mechanisms we have identified that may account for the synergistic effect of combined Wee1 and Chk1 inhibition in pHGG tumor cells. In addition, the lack of energy may cause the tumor cells to be particularly sensitive to the higher replicative stress. To address this possibility, we could elevate the energy supply and then test the efficacy of combination of Wee1 and Chk1 inhibition in tumor cells in the future study.

In summary, our study provides a strategy of the discovery of new drug combinations with potential applications in the treatment of pHGG. Rather than using traditional totally un-biased high throughput screening to discover the drug combinations, we annotated the

mechanisms of the compounds selected for the screen and did then used mechanism-based combinatorial screen and to identify and characterize combinatorial pairs exhibiting synergistic lethality. We not only successfully identified mechanisms that contribute to the synergistic effect of some drugs in pHGG tumor cells but we have also provided a future strategy to identify novel combinations for the treatment of pHGG. From the mechanism studies, we have shown that Wee1i/ Chk1i combination not only resulted in mitotic catastrophe, but also discovered a novel effect of combinatorial treatment on the metabolic activity of pHGG cells. In the future, we will study the mechanisms for this metabolic effect and use it to discover more metabolism-associated interventions for pHGG. Our study suggests that combining drugs that impact cancer metabolism and drugs that impact DNA damage may provide novel effective and efficient treatments for pHGG and other cancers.

Although the results obtained with combined Wee1/Chk1 inhibition in *in vitro* cell viability studies is promising but needs to be validated in the PDOX model *in vivo*. A major challenge to the *in vivo* studies will be the management of toxicity. Future studies will need to address the proper doses, treatment frequency, delivery methods and other experimental pharmacodynamic parameters. Recent studies have reported that sequential therapy with PARP and Wee1 inhibitors can be used to minimize toxicity while maintaining efficacy [121]. The sequential inhibition of PARP and ATR or Wee1 has been shown to have antitumor activity in vivo that is similar to concurrent treatment but exhibits less toxicity on normal cells. Sequential treatments may also be an option for in vivo validation of Wee1 and Chk1 inhibitors in animal models of pHGG. An additional challenge to the use of Wee1/Chk1 inhibitor combinations to treat intracranial tumors is the blood-brain barrier (BBB). Studies have reported that the efficacy of the Wee1 inhibitor MK 1775 is limited by heterogeneous distribution across the BBB in

glioblastoma [122]. The ability of Wee1 and Chk1 inhibitors to by-pass the BBB is not well known and needs to be tested in the PDOX models of pHGG, these studies need to be conducted in the context of pHGG since the ability of drugs to cross the BBB in brains with tumor is not the same as in the normal brain. We need to develop new drugs or new drug delivery systems that can be used to by-pass the BBB and therefore be used for the treatment of pediatric brain cancers.

REFERENCES

1. Kilburn, L.B., et al., *Phase I trial of capecitabine rapidly disintegrating tablets and concomitant radiation therapy in children with newly diagnosed brainstem gliomas and high-grade gliomas.* Neuro Oncol, 2013. 15(6): p. 759-66.
2. Sturm, D., et al., *Paediatric and adult glioblastoma: multiform (epi)genomic culprits emerge.* Nat Rev Cancer, 2014. 14(2): p. 92-107.
3. Braunstein, S., et al., *Pediatric high-grade glioma: current molecular landscape and therapeutic approaches.* J Neurooncol, 2017.
4. Stupp, R., et al., *Radiotherapy plus concomitant and adjuvant temozolomide for glioblastoma.* N Engl J Med, 2005. 352(10): p. 987-96.
5. Mahvash, M., et al., *Glioblastoma multiforme in children: report of 13 cases and review of the literature.* Pediatr Neurol, 2011. 45(3): p. 178-80.
6. Sarkaria, J.N., et al., *Mechanisms of chemoresistance to alkylating agents in malignant glioma.* Clin Cancer Res, 2008. 14(10): p. 2900-8.
7. Valera, E.T., et al., *Pediatric glioblastoma cell line shows different patterns of expression of transmembrane ABC transporters after in vitro exposure to vinblastine.* Childs Nerv Syst, 2009. 25(1): p. 39-45.
8. Yan, H., et al., *IDH1 and IDH2 mutations in gliomas.* N Engl J Med, 2009. 360(8): p. 765-73.
9. Pollack, I.F., et al., *IDH1 mutations are common in malignant gliomas arising in adolescents: a report from the Children's Oncology Group.* Childs Nerv Syst, 2011. 27(1): p. 87-94.

10. Pollack, I.F., et al., *Expression of p53 and prognosis in children with malignant gliomas.* N Engl J Med, 2002. 346(6): p. 420-7.

11. Suri, V., et al., *Pediatric glioblastomas: a histopathological and molecular genetic study.* Neuro Oncol, 2009. 11(3): p. 274-80.

12. Simon, J.A. and R.E. Kingston, *Mechanisms of polycomb gene silencing: knowns and unknowns.* Nat Rev Mol Cell Biol, 2009. 10(10): p. 697-708.

13. Wu, G., et al., *Somatic histone H3 alterations in pediatric diffuse intrinsic pontine gliomas and non-brainstem glioblastomas.* Nat Genet, 2012. 44(3): p. 251-3.

14. Bender, S., et al., *Reduced H3K27me3 and DNA hypomethylation are major drivers of gene expression in K27M mutant pediatric high-grade gliomas.* Cancer Cell, 2013. 24(5): p. 660-72.

15. Schwartzentruber, J., et al., *Driver mutations in histone H3.3 and chromatin remodelling genes in paediatric glioblastoma.* Nature, 2012. 482(7384): p. 226-31.

16. Artico, M., et al., *Supratentorial glioblastoma in children: a series of 27 surgically treated cases.* Childs Nerv Syst, 1993. 9(1): p. 7-9.

17. Paugh, B.S., et al., *Novel oncogenic PDGFRA mutations in pediatric high-grade gliomas.* Cancer Res, 2013. 73(20): p. 6219-29.

18. Raymond, E., et al., *Phase II study of imatinib in patients with recurrent gliomas of various histologies: a European Organisation for Research and Treatment of Cancer Brain Tumor Group Study.* J Clin Oncol, 2008. 26(28): p. 4659-65.

19. Nakamura, M., et al., *Loss of heterozygosity on chromosome 19 in secondary glioblastomas.* J Neuropathol Exp Neurol, 2000. 59(6): p. 539-43.

20. Nikitovic, M., et al., *Pediatric glioblastoma: a single institution experience.* Childs Nerv Syst, 2016. 32(1): p. 97-103.

21. Das, K.K., et al., *Pediatric glioblastoma: clinico-radiological profile and factors affecting the outcome.* Childs Nerv Syst, 2012. 28(12): p. 2055-62.

22. Mallick, S., et al., *Outcomes of pediatric glioblastoma treated with adjuvant chemoradiation with temozolomide and correlation with prognostic factors.* Indian J Med Paediatr Oncol, 2015. 36(2): p. 99-104.

23. Fallai, C. and P. Olmi, *Hyperfractionated and accelerated radiation therapy in central nervous system tumors (malignant gliomas, pediatric tumors, and brain metastases).* Radiother Oncol, 1997. 43(3): p. 235-46.

24. Finlay, J.L., et al., *Randomized phase III trial in childhood high-grade astrocytoma comparing vincristine, lomustine, and prednisone with the eight-drugs-in-1-day regimen. Childrens Cancer Group.* J Clin Oncol, 1995. 13(1): p. 112-23.

25. Wolff, J.E., et al., *Intensive chemotherapy improves survival in pediatric high-grade glioma after gross total resection: results of the HIT-GBM-C protocol.* Cancer, 2010. 116(3): p. 705-12.

26. Narayana, A., et al., *Bevacizumab in recurrent high-grade pediatric gliomas.* Neuro Oncol, 2010. 12(9): p. 985-90.

27. Gururangan, S., et al., *Lack of efficacy of bevacizumab plus irinotecan in children with recurrent malignant glioma and diffuse brainstem glioma: a Pediatric Brain Tumor Consortium study.* J Clin Oncol, 2010. 28(18): p. 3069-75.

28. Singh, S.K., et al., *Identification of human brain tumour initiating cells.* Nature, 2004. 432(7015): p. 396-401.

29. Igarashi, K., et al., *A patient-derived orthotopic xenograft (PDOX) mouse model of a cisplatinum-resistant osteosarcoma lung metastasis that was sensitive to temozolomide and trabectedin: implications for precision oncology.* Oncotarget, 2017. 8(37): p. 62111-62119.

30. Shervington, A. and C. Lu, *Expression of multidrug resistance genes in normal and cancer stem cells.* Cancer Invest, 2008. 26(5): p. 535-42.

31. Wahl, G.M. and B.T. Spike, *Cell state plasticity, stem cells, EMT, and the generation of intra-tumoral heterogeneity.* NPJ Breast Cancer, 2017. 3: p. 14.

32. Stupp, R., et al., *NovoTTF-100A versus physician's choice chemotherapy in recurrent glioblastoma: a randomised phase III trial of a novel treatment modality.* Eur J Cancer, 2012. 48(14): p. 2192-202.

33. Fabian, D., et al., *Treatment of Glioblastoma (GBM) with the Addition of Tumor-Treating Fields (TTF): A Review.* Cancers (Basel), 2019. 11(2).

34. DiMasi, J.A., et al., *Clinical approval success rates for investigational cancer drugs.* Clin Pharmacol Ther, 2013. 94(3): p. 329-35.

35. Kola, I. and J. Landis, *Can the pharmaceutical industry reduce attrition rates?* Nat Rev Drug Discov, 2004. 3(8): p. 711-5.

36. Rosfjord, E., et al., *Advances in patient-derived tumor xenografts: from target identification to predicting clinical response rates in oncology.* Biochem Pharmacol, 2014. 91(2): p. 135-43.

37. Morton, C.L. and P.J. Houghton, *Establishment of human tumor xenografts in immunodeficient mice.* Nat Protoc, 2007. 2(2): p. 247-50.

38. Cao, X., et al., *Defective lymphoid development in mice lacking expression of the common cytokine receptor gamma chain.* Immunity, 1995. 2(3): p. 223-38.

39. Williams, S.A., et al., *Patient-derived xenografts, the cancer stem cell paradigm, and cancer pathobiology in the 21st century.* Lab Invest, 2013. 93(9): p. 970-82.

40. Hoffman, R.M., *Patient-Derived Orthotopic Xenograft (PDOX) Models of Melanoma.* Int J Mol Sci, 2017. 18(9).

41. Hoffman, R.M., *Patient-derived orthotopic xenografts: better mimic of metastasis than subcutaneous xenografts.* Nat Rev Cancer, 2015. 15(8): p. 451-2.

42. Tentler, J.J., et al., *Patient-derived tumour xenografts as models for oncology drug development.* Nat Rev Clin Oncol, 2012. 9(6): p. 338-50.

43. Jung, J., H.S. Seol, and S. Chang, *The Generation and Application of Patient-Derived Xenograft Model for Cancer Research.* Cancer Res Treat, 2018. 50(1): p. 1-10.

44. Hanahan, D. and R.A. Weinberg, *Hallmarks of cancer: the next generation.* Cell, 2011. 144(5): p. 646-74.

45. Hoelder, S., P.A. Clarke, and P. Workman, *Discovery of small molecule cancer drugs: successes, challenges and opportunities.* Mol Oncol, 2012. 6(2): p. 155-76.

46. Wang, I.M., et al., *Systems biology approach for new target and biomarker identification.* Curr Top Microbiol Immunol, 2013. 363: p. 169-99.

47. Cheng, F., et al., *Personal Mutanomes Meet Modern Oncology Drug Discovery and Precision Health.* Pharmacol Rev, 2019. 71(1): p. 1-19.

48. Goda, K., Z. Bacso, and G. Szabo, *Multidrug resistance through the spectacle of P-glycoprotein.* Curr Cancer Drug Targets, 2009. 9(3): p. 281-97.

49. Zhou, J. and Y. Zhang, *Cancer stem cells: Models, mechanisms and implications for improved treatment.* Cell Cycle, 2008. 7(10): p. 1360-70.

50. Morrison, R., et al., *Targeting the mechanisms of resistance to chemotherapy and radiotherapy with the cancer stem cell hypothesis.* J Oncol, 2011. 2011: p. 941876.

51. Hammerman, P.S., P.A. Janne, and B.E. Johnson, *Resistance to Epidermal Growth Factor Receptor Tyrosine Kinase Inhibitors in Non-Small Cell Lung Cancer.* Clin Cancer Res, 2009. 15(24): p. 7502-7509.

52. Sequist, L.V., et al., *Genotypic and histological evolution of lung cancers acquiring resistance to EGFR inhibitors.* Sci Transl Med, 2011. 3(75): p. 75ra26.

53. Meads, M.B., R.A. Gatenby, and W.S. Dalton, *Environment-mediated drug resistance: a major contributor to minimal residual disease.* Nat Rev Cancer, 2009. 9(9): p. 665-74.

54. Ilie, M., et al., *Setting up a wide panel of patient-derived tumor xenografts of non-small cell lung cancer by improving the preanalytical steps.* Cancer Med, 2015. 4(2): p. 201-11.

55. Hidalgo, M., et al., *Patient-derived xenograft models: an emerging platform for translational cancer research.* Cancer Discov, 2014. 4(9): p. 998-1013.

56. Xin, H., et al., *Establishment and characterization of 7 novel hepatocellular carcinoma cell lines from patient-derived tumor xenografts.* PLoS One, 2014. 9(1): p. e85308.

57. Yu, L., et al., *A clinically relevant orthotopic xenograft model of ependymoma that maintains the genomic signature of the primary tumor and preserves cancer stem cells in vivo.* Neuro Oncol, 2010. 12(6): p. 580-94.

58. Bao, S., et al., *Glioma stem cells promote radioresistance by preferential activation of the DNA damage response.* Nature, 2006. 444(7120): p. 756-60.

59. Zhao, X., et al., *Global gene expression profiling confirms the molecular fidelity of primary tumor-based orthotopic xenograft mouse models of medulloblastoma.* Neuro Oncol, 2012. 14(5): p. 574-83.

60. Hughes, J.P., et al., *Principles of early drug discovery.* Br J Pharmacol, 2011. 162(6): p. 1239-49.

61. Bleicher, K.H., et al., *Hit and lead generation: beyond high-throughput screening.* Nat Rev Drug Discov, 2003. 2(5): p. 369-78.

62. Mayr, L.M. and D. Bojanic, *Novel trends in high-throughput screening.* Curr Opin Pharmacol, 2009. 9(5): p. 580-8.

63. Mayr, L.M. and P. Fuerst, *The future of high-throughput screening.* J Biomol Screen, 2008. 13(6): p. 443-8.

64. Klumpp, M., et al., *Readout technologies for highly miniaturized kinase assays applicable to high-throughput screening in a 1536-well format.* J Biomol Screen, 2006. 11(6): p. 617-33.

65. Guo, M.T., et al., *Droplet microfluidics for high-throughput biological assays.* Lab Chip, 2012. 12(12): p. 2146-55.

66. Malo, N., et al., *Statistical practice in high-throughput screening data analysis.* Nat Biotechnol, 2006. 24(2): p. 167-75.

67. Macarron, R., et al., *Impact of high-throughput screening in biomedical research.* Nat Rev Drug Discov, 2011. 10(3): p. 188-95.

68. Dorr, P., et al., *Maraviroc (UK-427,857), a potent, orally bioavailable, and selective small-molecule inhibitor of chemokine receptor CCR5 with broad-spectrum anti-human*

immunodeficiency virus type 1 activity. Antimicrob Agents Chemother, 2005. 49(11): p. 4721-32.

69. Lemm, J.A., et al., *Identification of hepatitis C virus NS5A inhibitors.* J Virol, 2010. 84(1): p. 482-91.

70. Gao, M., et al., *Chemical genetics strategy identifies an HCV NS5A inhibitor with a potent clinical effect.* Nature, 2010. 465(7294): p. 96-100.

71. Cawkill, D. and S.S. Eaglestone, *Evolution of cell-based reagent provision.* Drug Discov Today, 2007. 12(19-20): p. 820-5.

72. Zaman, G.J., et al., *Cryopreserved cells facilitate cell-based drug discovery.* Drug Discov Today, 2007. 12(13-14): p. 521-6.

73. Houston, J.G., et al., *Case study: impact of technology investment on lead discovery at Bristol-Myers Squibb, 1998-2006.* Drug Discov Today, 2008. 13(1-2): p. 44-51.

74. Kunapuli, P., et al., *Application of division arrest technology to cell-based HTS: comparison with frozen and fresh cells.* Assay Drug Dev Technol, 2005. 3(1): p. 17-26.

75. Digan, M.E., et al., *Evaluation of division-arrested cells for cell-based high-throughput screening and profiling.* J Biomol Screen, 2005. 10(6): p. 615-23.

76. Heilker, R., et al., *Confocal fluorescence microscopy for high-throughput screening of G-protein coupled receptors.* Curr Med Chem, 2005. 12(22): p. 2551-9.

77. McArthur, H., *An overview of HER-targeted therapy with lapatinib in breast cancer.* Adv Ther, 2009. 26(3): p. 263-71.

78. Rossi, A., et al., *Drug resistance of BRAF-mutant melanoma: Review of up-to-date mechanisms of action and promising targeted agents.* Eur J Pharmacol, 2019: p. 172621.

79. Park, S.J., et al., *Acquisition of a BCR-ABL1 transcript in a patient with disease progression from MDS with fibrosis to AML with myelodysplasia-related changes.* Ann Clin Lab Sci, 2011. 41(4): p. 379-84.

80. Bacher, U., et al., *Subclones with the t(9;22)/BCR-ABL1 rearrangement occur in AML and seem to cooperate with distinct genetic alterations.* Br J Haematol, 2011. 152(6): p. 713-20.

81. Padma, V.V., *An overview of targeted cancer therapy.* Biomedicine (Taipei), 2015. 5(4): p. 19.

82. Haghgoo, S.M., et al., *Pharmacogenomics and targeted therapy of cancer: Focusing on non-small cell lung cancer.* Eur J Pharmacol, 2015. 754: p. 82-91.

83. Eifert, C. and R.S. Powers, *From cancer genomes to oncogenic drivers, tumour dependencies and therapeutic targets.* Nat Rev Cancer, 2012. 12(8): p. 572-8.

84. Holohan, C., et al., *Cancer drug resistance: an evolving paradigm.* Nat Rev Cancer, 2013. 13(10): p. 714-26.

85. Flaherty, K.T., et al., *Combined BRAF and MEK inhibition in melanoma with BRAF V600 mutations.* N Engl J Med, 2012. 367(18): p. 1694-703.

86. Antonelli, G., et al., *Molecular-targeted therapy for elderly patients with advanced non-small cell lung cancer.* Oncol Lett, 2016. 11(1): p. 3-8.

87. Broniscer, A., et al., *Phase I and pharmacokinetic studies of erlotinib administered concurrently with radiotherapy for children, adolescents, and young adults with high-grade glioma.* Clin Cancer Res, 2009. 15(2): p. 701-7.

88. Liu, Z., et al., *Intravenous injection of oncolytic picornavirus SVV-001 prolongs animal survival in a panel of primary tumor-based orthotopic xenograft mouse models of pediatric glioma.* Neuro Oncol, 2013. 15(9): p. 1173-85.

89. Shu, Q., et al., *Direct orthotopic transplantation of fresh surgical specimen preserves CD133+ tumor cells in clinically relevant mouse models of medulloblastoma and glioma.* Stem Cells, 2008. 26(6): p. 1414-24.

90. Chaudhuri, L., et al., *CHK1 and WEE1 inhibition combine synergistically to enhance therapeutic efficacy in acute myeloid leukemia ex vivo.* Haematologica, 2014. 99(4): p. 688-96.

91. Chila, R., et al., *Combined inhibition of Chk1 and Wee1 as a new therapeutic strategy for mantle cell lymphoma.* Oncotarget, 2015. 6(5): p. 3394-408.

92. Guertin, A.D., et al., *Unique functions of CHK1 and WEE1 underlie synergistic anti-tumor activity upon pharmacologic inhibition.* Cancer Cell Int, 2012. 12(1): p. 45.

93. Magnussen, G.I., et al., *Combined inhibition of the cell cycle related proteins Wee1 and Chk1/2 induces synergistic anti-cancer effect in melanoma.* BMC Cancer, 2015. 15: p. 462.

94. McConkey, D.J., M. White, and W. Yan, *HDAC inhibitor modulation of proteotoxicity as a therapeutic approach in cancer.* Adv Cancer Res, 2012. 116: p. 131-63.

95. Bose, P., Y. Dai, and S. Grant, *Histone deacetylase inhibitor (HDACI) mechanisms of action: emerging insights.* Pharmacol Ther, 2014. 143(3): p. 323-36.

96. Boyault, C., et al., *HDAC6 controls major cell response pathways to cytotoxic accumulation of protein aggregates.* Genes Dev, 2007. 21(17): p. 2172-81.

97. Bleau, A.M., et al., *PTEN/PI3K/Akt pathway regulates the side population phenotype and ABCG2 activity in glioma tumor stem-like cells.* Cell Stem Cell, 2009. 4(3): p. 226-35.

98. Pei, Y., et al., *HDAC and PI3K Antagonists Cooperate to Inhibit Growth of MYC-Driven Medulloblastoma.* Cancer Cell, 2016. 29(3): p. 311-23.

99. Cheng, L., et al., *L1CAM regulates DNA damage checkpoint response of glioblastoma stem cells through NBS1.* EMBO J, 2011. 30(5): p. 800-13.

100. Wang, R., et al., *Reciprocal regulation of BMF and BIRC5 (Survivin) linked to Eomes overexpression in colorectal cancer.* Cancer Lett, 2016. 381(2): p. 341-8.

101. Carew, J.S., F.J. Giles, and S.T. Nawrocki, *Histone deacetylase inhibitors: mechanisms of cell death and promise in combination cancer therapy.* Cancer Lett, 2008. 269(1): p. 7-17.

102. Sorensen, C.S. and R.G. Syljuasen, *Safeguarding genome integrity: the checkpoint kinases ATR, CHK1 and WEE1 restrain CDK activity during normal DNA replication.* Nucleic Acids Res, 2012. 40(2): p. 477-86.

103. Toledo, L., K.J. Neelsen, and J. Lukas, *Replication Catastrophe: When a Checkpoint Fails because of Exhaustion.* Mol Cell, 2017. 66(6): p. 735-749.

104. Carrassa, L., et al., *Combined inhibition of Chk1 and Wee1: in vitro synergistic effect translates to tumor growth inhibition in vivo.* Cell Cycle, 2012. 11(13): p. 2507-17.

105. Davies, K.D., et al., *Chk1 inhibition and Wee1 inhibition combine synergistically to impede cellular proliferation.* Cancer Biol Ther, 2011. 12(9): p. 788-96.

106. Hauge, S., et al., *Combined inhibition of Wee1 and Chk1 gives synergistic DNA damage in S-phase due to distinct regulation of CDK activity and CDC45 loading.* Oncotarget, 2017. 8(7): p. 10966-10979.

107. Ronco, C., et al., *ATM, ATR, CHK1, CHK2 and WEE1 inhibitors in cancer and cancer stem cells.* Medchemcomm, 2017. 8(2): p. 295-319.

108. Zhao, H., J.L. Watkins, and H. Piwnica-Worms, *Disruption of the checkpoint kinase 1/cell division cycle 25A pathway abrogates ionizing radiation-induced S and G2 checkpoints.* Proc Natl Acad Sci U S A, 2002. 99(23): p. 14795-800.

109. Sorensen, C.S., et al., *Chk1 regulates the S phase checkpoint by coupling the physiological turnover and ionizing radiation-induced accelerated proteolysis of Cdc25A.* Cancer Cell, 2003. 3(3): p. 247-58.

110. Friedel, A.M., B.L. Pike, and S.M. Gasser, *ATR/Mec1: coordinating fork stability and repair.* Curr Opin Cell Biol, 2009. 21(2): p. 237-44.

111. Petermann, E., et al., *Chk1 requirement for high global rates of replication fork progression during normal vertebrate S phase.* Mol Cell Biol, 2006. 26(8): p. 3319-26.

112. Petermann, E., M. Woodcock, and T. Helleday, *Chk1 promotes replication fork progression by controlling replication initiation.* Proc Natl Acad Sci U S A, 2010. 107(37): p. 16090-5.

113. Fasulo, B., et al., *Chk1 and Wee1 kinases coordinate DNA replication, chromosome condensation, and anaphase entry.* Mol Biol Cell, 2012. 23(6): p. 1047-57.

114. Heald, R., M. McLoughlin, and F. McKeon, *Human wee1 maintains mitotic timing by protecting the nucleus from cytoplasmically activated Cdc2 kinase.* Cell, 1993. 74(3): p. 463-74.

115. Parker, L.L. and H. Piwnica-Worms, *Inactivation of the p34cdc2-cyclin B complex by the human WEE1 tyrosine kinase.* Science, 1992. 257(5078): p. 1955-7.

116. Tse, A.N., et al., *90-kDa heat shock protein inhibition abrogates the topoisomerase I poison-induced G2/M checkpoint in p53-null tumor cells by depleting Chk1 and Wee1*. Mol Pharmacol, 2009. 75(1): p. 124-33.

117. De Witt Hamer, P.C., et al., *WEE1 kinase targeting combined with DNA-damaging cancer therapy catalyzes mitotic catastrophe.* Clin Cancer Res, 2011. 17(13): p. 4200-7.

118. Hirai, H., et al., *MK-1775, a small molecule Wee1 inhibitor, enhances anti-tumor efficacy of various DNA-damaging agents, including 5-fluorouracil.* Cancer Biol Ther, 2010. 9(7): p. 514-22.

119. Dai, Y. and S. Grant, *New insights into checkpoint kinase 1 in the DNA damage response signaling network.* Clin Cancer Res, 2010. 16(2): p. 376-83.

120. Oliva, C.R., et al., *Identification of Small Molecule Inhibitors of Human Cytochrome c Oxidase That Target Chemoresistant Glioma Cells*. J Biol Chem, 2016. 291(46): p. 24188-24199.